MODELING OF RISER-SEABED-WATER INTERACTION AT TOUCH DOWN ZONE USING COMPUTATIONAL FLUID DYNAMICS APPROACH

by

© Anup Fouzder

A Thesis submitted to the

School of Graduate Studies

In partial fulfillment of the requirements for the degree of

Masters in Engineering

Faculty of Engineering and Applied Science

Memorial University of Newfoundland

April, 2015

St. John's Newfoundland Canada

ABSTRACT

Steel catenary risers (SCR) are widely used in deepwater oil and gas production. Due to environmental loading the riser may be subject to six degrees of motion; however, in the touchdown zone (TDZ), the vertical penetration into the seabed and uplift are two of the main components. The riser-seabed-water interaction near the touchdown zone is one of the main concerns in fatigue life design of SCR. During upward displacement, suction develops under the riser and a trench might be formed when it separates from the seabed near the touchdown point (TDP). In subsequent downward movement, the riser penetrates through this trench to the seabed. Therefore, modeling of suction and trench formation is very important. In most of the existing models these factors are incorporated using empirical relationships. It is also recognized that the available finite element (FE) modeling techniques for this large deformation problem are computationally very expensive, although the penetration resistance can be simulated.

In the present study, numerical modeling of riser-seabed-water interaction at the TDZ is conducted using ANSYS CFX software to evaluate the response of the riser during its penetration and uplift. A new model for undrained shear strength of soft clay is proposed that is applicable to a wide range of shear strain rates. The models for the effects of strain rate and strength degradation on undrained shear strength are incorporated properly in ANSYS CFX and simulations are performed for one penetration-uplift cycle. The CFX model developed in this study using the subdomain approach is computationally very efficient. It is found that the suction under the riser is the main source of uplift resistance for shallow embedments. The parametric study shows that the maximum uplift resistance and depth of trench depend on uplift velocity and undrained shear strength of clay.

ACKNOLEDGEMENTS

I wish to express my foremost gratitude to my thesis supervisor Dr. Bipul Hawlader, Associate Professor, Memorial University of Newfoundland, for his time, involvement, constant guidance and advice.

I would also like to express my sincerest thank to my co-supervisor Dr. Arash Zakeri, BP, America, for his support and guidance. His several enlightening ideas encouraged me to learn ANSYS CFX which finally became an efficient numerical modeling tool for riser-seabed-water interaction analysis.

I would not have been able to undertake this work without the financial support from C-CORE, MITACS, NSERC and Memorial University.

I wish to extend my warmest thanks to Sujan Dutta for helping me with his wide range of numerical modeling experience in pipelines in soft clay seabed.

I also wish to extend my sincere thanks to my colleagues at C-CORE, especially Dr. Rodney McAffee, Dr. Ryan Phillips and Gerry Piercy for their encouragement to finish my thesis work.

I deeply appreciate Krishna Roy, Shikha Roy and Juran Goyali for their endless mental support and encouragement to complete my thesis. I owe my loving thanks to my wife, Sima Roy, my daughter Sreya and my mom. Without their encouragements, sacrifices and understanding, it would have been impossible for me to finish this work.

Table of Contents

List of Tables

List of Figures

List of Symbols

Symbol	Descriptions
s_u	mobilized undrained shear strength
s_{uN}	undrained shear strength used for normalization
s_{u0}	initial s_u before remoulding at $\dot{\gamma}_{\text{ref}}$
s_{um}	s_{u0} at mudline
$s_{u0(i)}$	s_{u0} at the invert of the riser
v	penetration and uplift velocity
I_p	plasticity index
y'	depth of soil element
γ_w	unit weight of water
f_1	strain rate effect on undrained shear strength
f_2	softening effect on undrained shear strength
$\dot{\gamma}$	shear strain rate
τ	shear stress
τ_y	yield stress, equal to s_{uc}
K	clay property (viscous)
n	clay property (exponent)
ω	rotation speed of vane
ω_{ref}	reference rotation speed of vane
β	material constant for power law

c_1	material property for modified Herschel-Bulkley model
f_{20}	f_2 at inner face of zone-II
R_x	radial distance
k	strength gradient
μ	dynamic viscosity of clay
μ_w	dynamic viscosity of water
S_t	remolded sensitivity of soil
N_{pu}	normalized penetration and uplift resistance
$\hat{w}$	normalized penetration
F	penetration or uplift resistance
D_e	effective pipe diameter
L	length of riser section
q_u	ultimate bearing capacity
N_p	normalized resistance
γ'	submerged unit weight of soil
γ_{sat}	saturated unit weight
D_f	depth of foundation below seabed
Q_u	ultimate bearing load
B	bearing width
D	diameter of pipe
D_e	effective diameter of pipe

L	length of riser/pipe
w	embedment of pipe invert
t_b	breakout time
γ	shape factor
P	force per unit length
y	vertical displacement of pipe
P_u	ultimate penetration resistance
P_{u_suc}	ultimate suction force
f_{suc}	suction model parameter
K_C, k_V, k_T	dimensionless empirical factor
k_F, n_F	empirical constant
Δ_B	vertical displacement of riser from the max penetration to the distance where the riser separate from the seabed
k_{DC}, k_{DV}, k_{DT}	empirical constant
k_D, n_D	empirical constant
m	mass
a	acceleration
F_{grv}	gravitational force
F_{press}	pressure force
F_{visc}	viscous force
α	friction coefficient

αs_{u0}	max undrained shear resistance at the pipe-soil interface in FE model
s_{u_int}	shear strength of one row of clay elements just outside the riser
$\nabla\tau$	shear strength gradient
α_1, $\beta_{1,}$ $\alpha_{2,}\beta_2$	material constant

Chapter 1

Introduction

1.1 General

As hydrocarbon resources on land are drying up due to increasing demand of energy worldwide and therefore offshore oil and gas became the alternative sources to meet the higher energy demand. Meanwhile, many shallow waters offshore oil and gas fields have been already used or ready to be immediate use. As a result, deep and ultra-deep water oil and gas exploration have been expanded in the recent years. While in shallow water fixed platform could be used, in deepwater floating production system (FPS) is only the economic choice. Risers are used for transportation of hydrocarbon products from the sub-sea wellheads, templates or pipelines to fixed or floating offshore platforms. One of the most widely used risers in deepwater is the Steel Catenary Risers (SCR). The SCR is a steel pipe suspended almost vertically from the FPS, curving in a catenary shape, and becomes almost horizontal near the seabed. The point at which SCR first touches the seabed is known as touchdown point (TDP) (Fig. 1.1). Due to environmental loading such as wind, current and wave might cause six degrees of motion of the FPS (heave, surge, sway, yaw, roll and pitch), which induce a complex motion of the riser at the TDP (Hu, 2010). The riser experiences high stresses and greatest fatigue damages at the TDP due to repeated loading from the motion of the FPS. The fatigue life of the riser is significantly influenced by riser-seabed-water interaction in the touchdown zone (TDZ) as shown in Fig. 1.1.

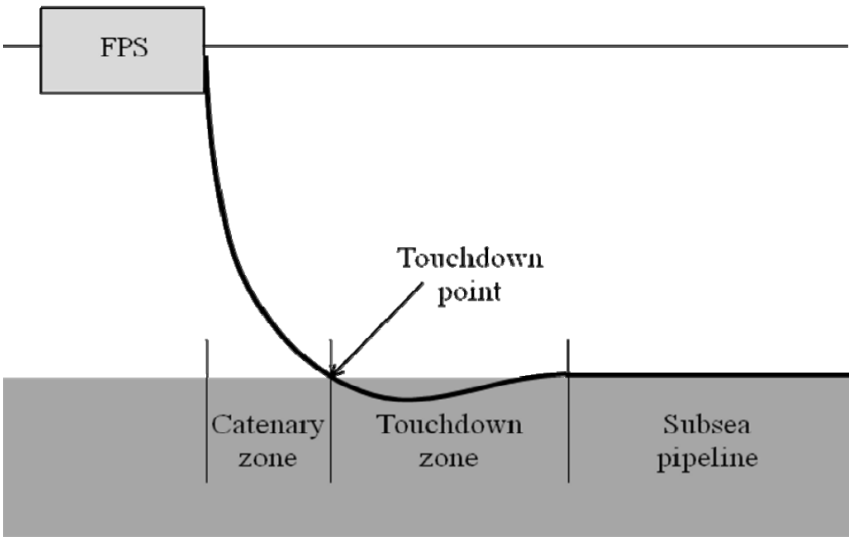

Figure 1.1: Typical SCR configuration (after Hu 2010)

In the current design, seabed is modeled as a rigid surface or using a set of springs connected to the riser (Fig. 1.2a). The load displacement behaviour of the spring has been defined using a set of empirical equations which has been proposed from the trend of two-dimensional experimental (Fig. 1.2b) results. However, experimental results show that the load displacement response under repeated loading in the touchdown zone is not so simple rather it is significantly influenced by various factors such as suction, trench formation, shear strength degradation and water flow. Numerical modeling could be used for better insights into the mechanisms. A number of numerical modeling techniques have been developed in the past to simulate penetration behaviour. However, for uplift behaviour empirical models are used.

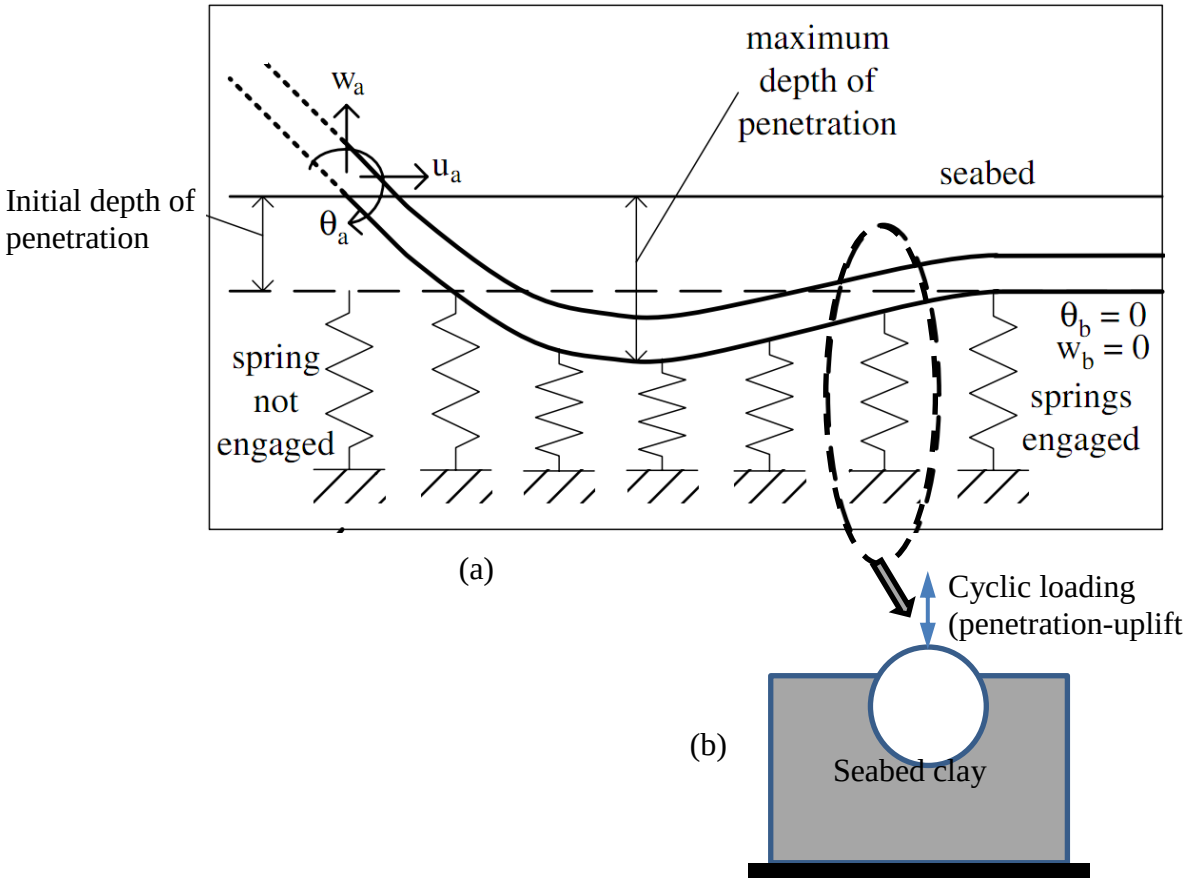

Figure 1.2:Current design approach: (a) riser-spring model at touchdown zone, (b) typical 2-D experiment for spring behaviour (modified from Hodder and Byrne 2010)

1.2 Objectives of this thesis

The purpose of this study is to examine the mechanisms involved in vertical penetration and uplifting of a section of riser in soft clay seabed. The main objective of this study is to develop a computationally efficient numerical modeling technique that can:

- investigate the soil failure mechanisms during penetration (loading) and uplift(unloading);

- identify the parameters affecting the penetration and uplift resistance;
- evaluate the trench formation after departure of the riser from seabed;
- quantify water effects on penetration and uplift response;
- quantify the suction under the riser during uplift;
- quantify the role of suction behind the riser at intermediate embedment;
- investigate the effects of strain rate and strength degradation due to remoulding on uplift resistance.

1.3 Organization of the thesis

The thesis is organized in the following way.

Chapter1 contains the introductory information including the scope, objective and major contribution of this study.

Chapter2 covers the literature review. Critical review of previous studies primarily on penetration and uplift behaviour of a section of riser is presented in this chapter, which is the focus of the present study.

Chapter 3 presents the numerical simulation of penetration behaviour of a section of riser using ANSYS CFX. The development of CFX models, their performance and comparison with available model test results are presented in this chapter.

Chapter 4 describes mainly the uplift behaviour. The increase in undrained shear strength with strain rate is discussed. Based on comprehensive CFX modeling, the role of suction on uplift resistance and trench formation mechanisms are examined. A parametric study is also presented in this chapter to show the effects of soil parameters on uplift behaviour.

Chapter 5 provides the summary and conclusions of the present study. Some limitations and recommendations for further study are also presented in this chapter.

1.4 Major contributions

Large deformation finite element (LDFE) modeling has been used in previous studies to simulate the penetration behaviour; however, it is computationally very expensive. Moreover, LDFE cannot simulate the suction and role of water in riser-seabed-water interaction properly. Therefore, an alternative numerical modeling technique based on computational fluid dynamics approach is considered in the present study. Numerical analyses are carried out using the ANSYS CFX 13 software. CFX does not have any direct option to define the undrained shear strength of soft clay; therefore, a technique has been proposed to implement the undrained shear strength of soft clay in CFX. During penetration and uplift, the soil around the riser might experience higher strain rates than that of typical geotechnical engineering problems. Therefore, a new model for undrained shear strength is proposed that is valid for a wide range of strain rates. In addition, a simplified model is proposed for degradation of shear strength due to remoulding (softening). The soil model, combining both strain rate and softening, is properly implemented in CFX and analysis is performed for uniform and linearly increasing initial undrained shear strength profiles of the seabed.

Chapter 2

Literature Review

2.1Introduction

In deepwater oil and gas projects, steel catenary risers (SCR)are widely used that connects seabed systems to the floating production systems (FPS) which are generally subjected to various types of motion (surge, sway, heave, yaw, roll and pitch) due to environmental loadings such as wind, wave and current (Hu, 2010). During its lifetime, a SCR experiences many different types of cyclic loadings due to small to high waves, long period storms and slow drift motions. The fatigue life of SCR is one of the critical components of the design. The fatigue life of the riser near the touchdown point depends on riser-seabed-water interaction in the touchdown zone. The soil near the mudline in deepwater is generally soft clay (Thethi and Moros 2001). As the displacement rate during penetration and uplift of the riser in the touchdown zone is sufficiently high, the undrained shear strength governs the response in most of the cases. In structural design and fatigue life calculations, the load-displacement response of soil around the riser needs to be defined. In the current design practice, the seabed is simply characterized as linear/nonlinear springs or rigid surfaces. However, the seabed response to the load from the riser is way more complex than simple spring model.

The aim of the present study is to model numerically the riser-seabed-water interaction which could be used to develop improved load-displacement curves during penetration and uplift. Although a complex six degrees of motion is possible, only the vertical

penetration and uplift behaviour is modeled in this study. Based on the focus on the present study, the literature review presented in this chapter is organized in the following ways. First, the penetration behaviour is presented in the Section 2.2. As the penetration of other cylindrical objects (e.g. surface laid pipelines and T-bar) is similar to the penetration of riser, previous studies on penetration of these objects are also discussed in this section in addition to the studies on riser penetration. In the second part of the literature review (Section 2.3) the uplift behaviour is discussed. As the risers are subjected to many cycles of penetration and uplift, the mathematical models in the form of *P*-y (load-deflection) curves proposed in the past are discussed in the Section 2.3. For other issues related to the design of riser including an overview of FPS motion, its effects to the touchdown zone, current design practice and limitations could be found in previous studies (e.g. Bridge 2005; Bai and Bai 2005, Hu 2010).

2.2Penetration of pipeline/riser into seabed

With increase in demand of deepwater oil and gas development, considerable research works have been dedicated to understand the mechanisms involved in penetration of riser or surface laid pipelines into the seabed. Mainly three different techniques have been used in the past for modeling vertical penetration of surface laid pipeline/riser into the clay seabed: (i) theoretical modelling, (ii) physical modeling and (iii) numerical modeling.

2.2.1 Theoretical modeling

Assuming the pipeline as an infinitely long strip footing, some early researchers (e.g. Small et al., 1971) calculated penetration resistance using simple model similar to

Terzaghi's bearing capacity equation for shallow foundations in undrained condition (Terzaghi 1943).

$$q_u = N_c s_u + \gamma' D_f \quad (2.1)$$

Where q_u is the ultimate bearing capacity, N_c is the bearing capacity factor, s_u is the undrained shear strength of soil, γ' is the submerged unit weight of soil and D_f is the depth of the foundation below seabed. The value of N_c is 5.14 for undrained loading condition.

It is also recognized that, unlike the bottom of the strip footing, pipe surface is curved and therefore the shape of the failure surfaces could be different from those of the shallow foundations as shown in Fig. 2.1. Based on plasticity solution or upper and lower bound solutions, different values of N_c have been proposed for smooth and rough pipeline soil interface conditions.

Small et al. (1971) and Bostrom et al. (1998) assumed that a surface laid offshore pipe starts to sink if its submerged weight exceeds the bearing capacity of soil. Based on this assumption, Small et al. (1971) extended the concept of bearing capacity of shallow foundation to circular pipe section embedded into the seabed as the following equation:

$$Q_u = N_c s_u B \quad (2.2)$$

Where, Q_u is the ultimate bearing load, B is the bearing width (Figs. 2.1b & c). They also proposed a model for the formation of soil wedge underneath the pipe and soil failure mechanism as shown in Fig 2.1. Depending upon depth of embedment two possible scenarios was identified: CASE 1 for shallow embedments (i.e. the centre of the pipeline is at or above the mudline, Fig. 2.1b) and CASE 2 for deep embedment (i.e. the centre of

the pipeline is below the mudline, Fig. 2.1c). In both cases the failure pattern is very similar to the failure of soil under a shallow foundation.

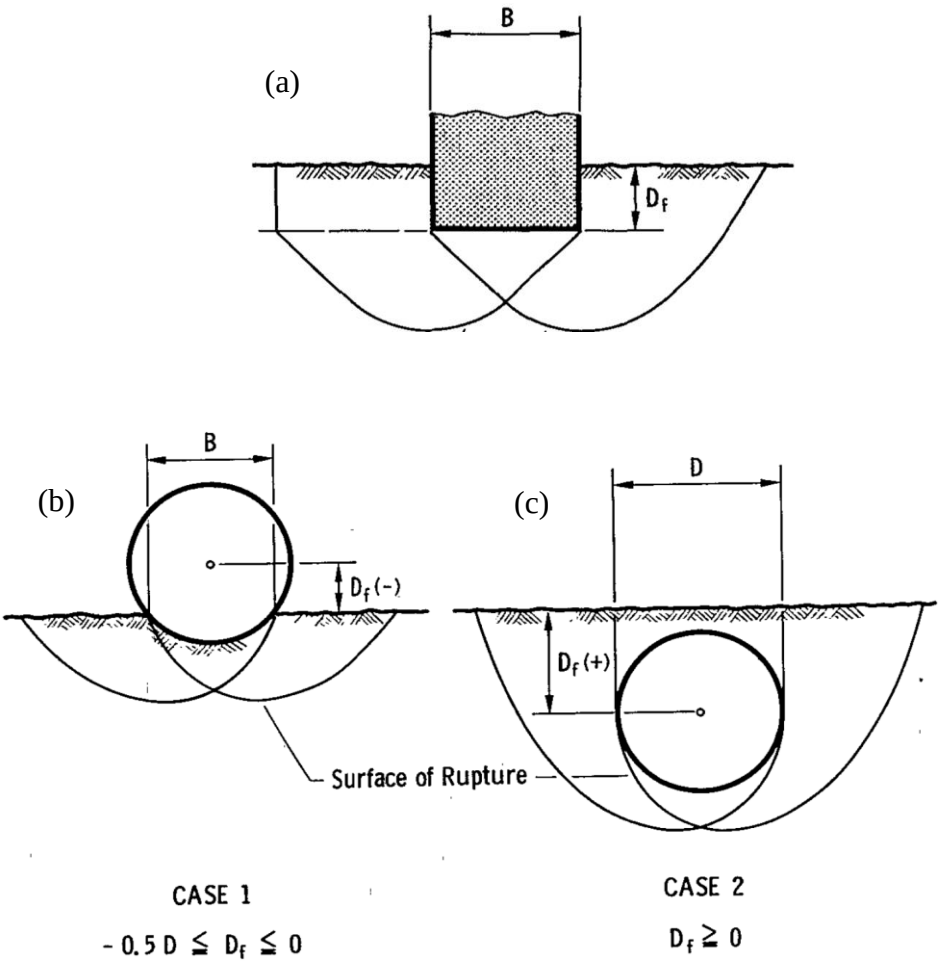

Figure 2.1: Failure modes: (a) strip footing (b) shallow embedded offshore pipeline, (c) deep embedded offshore pipeline (Small et al. 1971)

Figure 2.2 shows the normalized penetration resistance with depth of embedment, in which the upper and lower lines represent the values based on general and local shear failure modes. As shown in Fig. 2.2that the maximum vertical resistance is mobilized at D_f=4D, where D_f is the depth of the centre of the pipe from mudline and D is the diameter of the pipe. It is to be noted here that berms will be formed in both sides of the pipe when

it is pushed in the seabed. However, Small et al. (1971) did not consider the effects of berm on penetration resistance. Moreover, their solution is valid only for uniform undrained shear strength profiles. However, Davis and Booker (1973) showed that conventional slip surface failure overestimate the bearing capacity when undrained shear strength increases with depth. Moreover, pipe roughness also has a significant influence on vertical resistance.

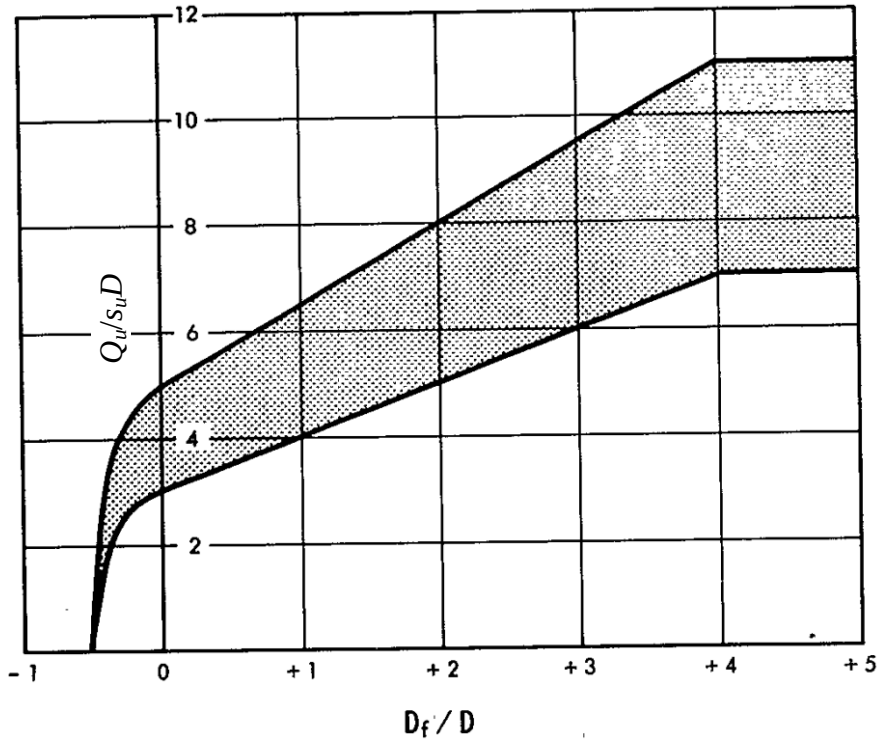

Figure 2.2: Penetration resistance with depth of embedment (Small et al. 1971)

Based on the failure mechanism developed by Randolph and Houlsby (1984), Murff et al. (1989) developed upper and lower bound plasticity solutions for partially embedded pipelines in cohesive soil for both smooth and rough pipeline-soil interface conditions. Two sets of analyses were conducted. In the first set the effects of berm were neglected while in the second set these were considered. The later gives higher penetration

resistance. For example, at pipe embedment of 0.2*D*, the penetration resistance increased by 10-15% when the effects of berm were considered. The maximum depth of embedment of their study was 0.5*D*. Aubeny et al. (2005) extended the upper bound solution of Randolph and Houslby (1984) for embedments greater than 0.5*D* and the analyses were performed for both uniform and varying undrained shear strength profiles.

Dunlap et al. (1990) derived an empirical equation from experimental results to estimate penetration resistance for monotonic loading.

$$w = \frac{0.01573}{D^{0.7822}}\left(\frac{F}{s_u (v/D)^n}\right)^{1.7822} \tag{2.3}$$

Where w is the embedment of pipe invert in inch, $D$is the diameter of the pipe in inch, F is the applied force in lbs, s_u is the undrained shear strength in lbs/ft^2, v is the penetration speed in inch/s, and n is a dimensionless constant.

Similarly, Verley and Lund (1995) proposed an empirical equation by fitting all the experimental results available in the literature to estimate penetration resistance through dimensionless analysis. However, Cathie et al. (2005) showed a wide variation among the proposed models available in the literature at that time and also between experimental results (Fig. 2.3).

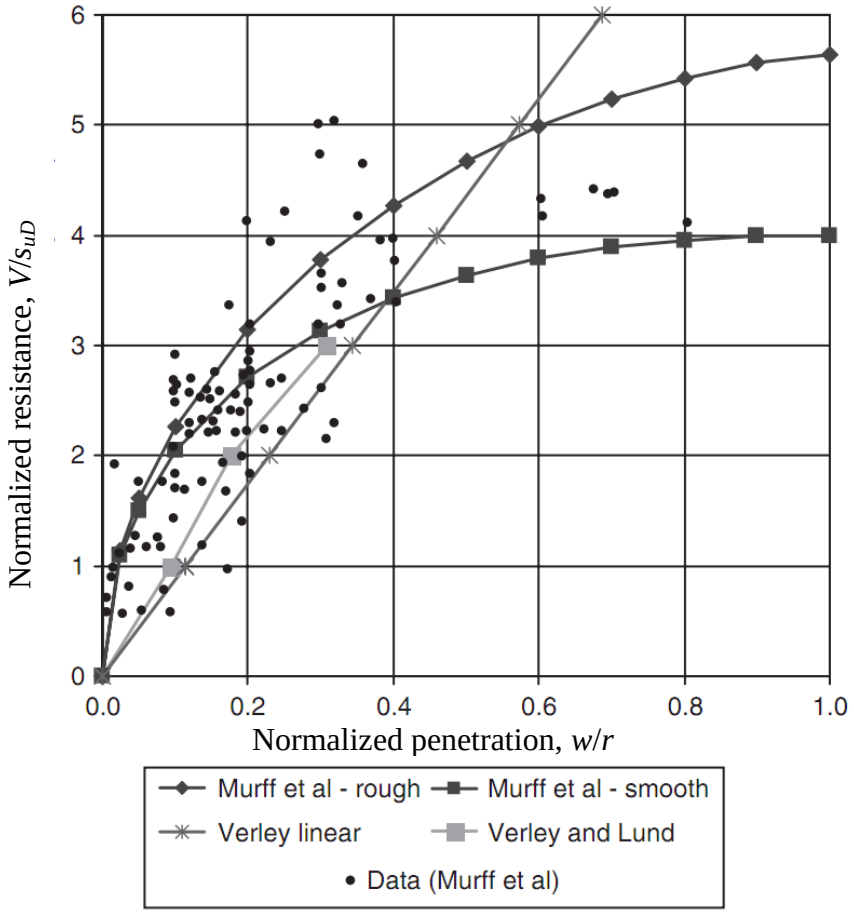

Figure 2.3: Comparison between various models (Cathie et al., 2005)

2.2.2 Physical modeling

Small- to large-scale experiments were conducted in the past for modeling vertical penetration of offshore pipelines. Dutta (2012) provided a brief summary of these experiments (Table 2.1).Except for only one (SINTEF 1986b), most of these experiments were conducted on soft clay seabed.

Cheuk et al. (2007) showed the performance of tow empirical models (Verley and Lund 1995; and Murff et al. 1989) by comparing their large-scale tests results in kaolin (JIP) and West African (WA) clays as shown in Fig. 2.4.

Table 2.1: Summary of small- to large-scale test for vertical penetration (after Dutta 2012).

References	Summary
Lyons, C.G.(1973)	D =0.41m; s_u=2 kPa
SINTEF (1986a) (for PIPESTAB)	D =1.0(0.5) m; s_u=1 kPa
SINTEF (1986b) (for PIPESTAB)	D =1.0 (0.5) m; s_u=70 kPa
SINTEF (1987) (for AGA)	D =1.0(0.5) m ;s_u=1.4 kPa
Morris et al. (1988)	D =0.15 m; s_u=1 kPa
Dunlap et al. (1990)	D =0.15 m; s_u=1.4 kPa
Brennodden (1991)	D =0.5m; s_u=1-2 kPa
TAMU (1992) (for AGA)	D =0.324m ;S_u=1-8 kPa

*D=Pipe diameter, s_u = Soil undrained shear strength

In addition to 1g laboratory tests, centrifuge tests were also conducted to understand the mechanisms involved in vertical penetration. Dingle et al. (2008) conducted centrifuge tests using a 0.8 m diameter pipe section in prototype scale. The pipe was pushed into the clay seabed having linearly increasing undrained shear strength profile to 0.45D. The comparison presented in Figure 2.5 shows that the empirical model proposed by Murff et al. (2007) underestimates the penetration resistance. FE results in Fig. 2.5 show that interface behaviour significantly influences the penetration resistance. In this case, centrifuge test gives higher penetration resistance than that of empirical model and FE

analyses which might be due to increase in undrained shear strength with strain rate and berm effects.

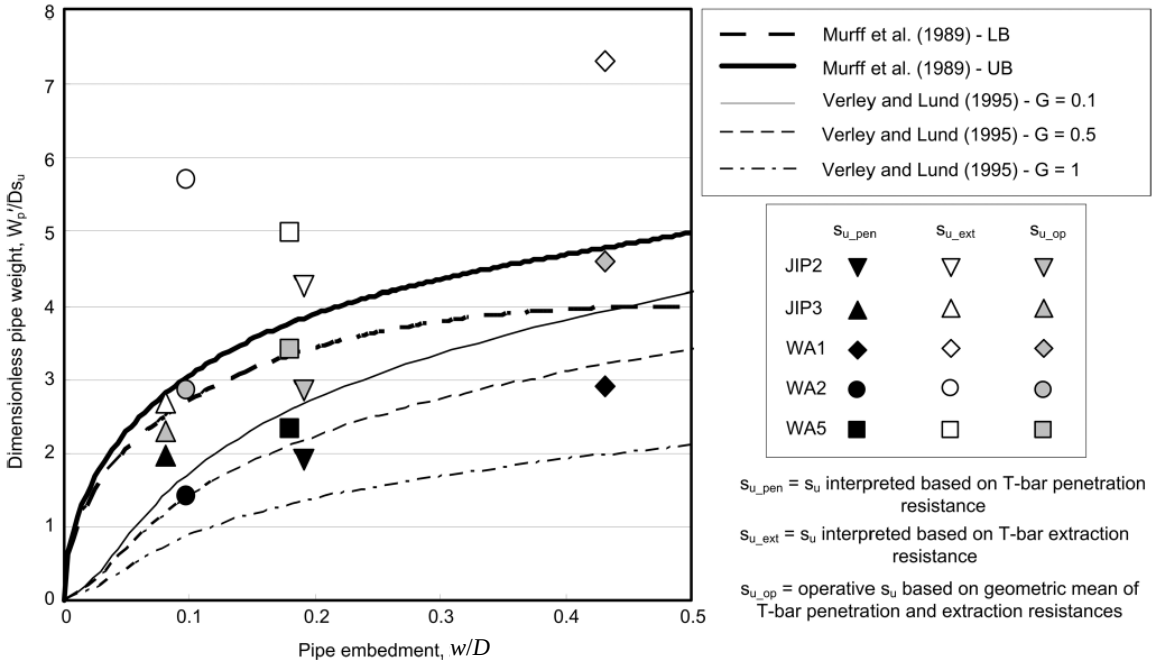

Figure 2.4: Comparison between mathematical model and large scale test results (Cheuk et al. 2007)

Recognizing the fact that a section of riser might penetrate several diameters into the seabed, Hu (2010) conducted a number of centrifuge tests for deeper pipe penetration (up to three pipe diameters). Tests were conducted in a soft clay seabed with linearly increasing undrained shear strength profile. The main focus of his study was to model cyclic vertical penetration and uplift response of steel catenary riser at the touchdown zone.

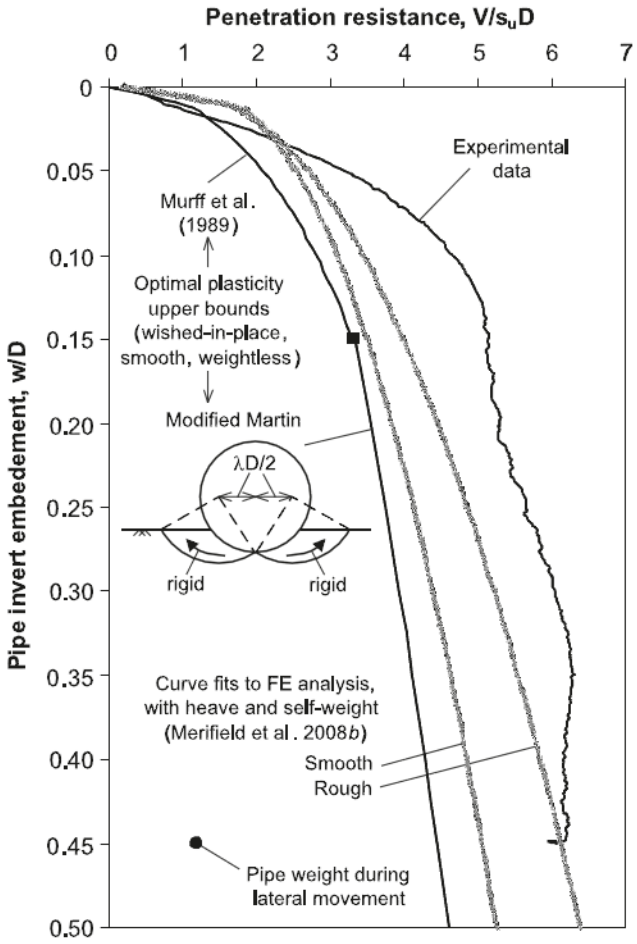

Figure 2.5: Comparison between empirical, FE and centrifuge test results (Dingle et al., 2008)

2.2.3 Numerical modeling

For numerical modeling, mainly three different techniques have been used: (i) small-strain FE modeling, (ii) large-strain FE modeling and (iii) finite difference modeling. Among them, very limited studies used the finite difference approach (e.g. Morrow and Bransby 2010). A number of studies used the small-strain FE technique in Lagrangian

framework (Aubeny et al., 2005; Bransby et al., 2008; Zhao et al., 2010; Martin and White, 2012). However, recognizing the fact pipeline/riser penetration into the seabed is a large deformation problem, large deformation FE (LDFE) modeling techniques have been developed in the past (e.g. Barbosa- Cruz and Randolph, 2005, Bransby et al., 2008, Merifield et al., 2009, Wang et al. 2010, Tho et al., 2011, Dutta et al. 2014). Among them remeshing and interpolation techniques with small strain (RITSS) developed at the University of Western Australia is one of the well-used techniques. In recent studies, the Coupled Eulerian Lagrangian (CEL) approach in Abaqus FE software has been successfully used by some researchers (Tho et al., 2011, Dutta et al. 2014). A summary of the numerical tools developed in the past is shown in Table 2.2.

The FE modeling in Lagrangian framework cannot handle large deformation because of excessive mesh distortion and convergence issues (Woodworth Lynas et al., 1996). Therefore, some researchers conducted FE analysis of pre-embedded "wished in place (WIP)" pipe configurations in which the pipe is initially placed at the desired depth and then displaced further down to calculate penetration resistance (e.g. Aubeny et al., 2005; Bransby et al., 2008). Some researchers used the Arbitrary Lagrangian Eulerian (ALE) method which could reduce numerical issues related to mesh distortion to a certain degree (e.g. Merifield et al., 2009).

Table 2.2: Development of numerical modeling techniques (after Dutta et al. 2014)

Numerical Technique	Soil model (s_u)	References
Small strain FE analysis using Abaqus	von-Mises, uniform , linearly increasing with depth	*,1Aubeny et al.(2005)
	Tresca, uniform	*,1Bransby et al.(2008); †,1Merifield et al.(2008)
	Linear Drucker- Prager (D-P) elasto-plasticity model, uniform	*,1 Zhao et al.(2010)
FE analysis using OxLim	Tresca, uniform, linearly increasing with depth	†,1 Martin and White (2012)
Finite difference technique FLAC 6.0	Tresca, linearly increasing with depth	*,1 Morrow and Bransby (2010)
Large strain analysis using nonlinear geometry option in Abaqus	Tresca, uniform	*,2Bransby et al.(2008)
Arbitrary Eulerian	Tresca, uniform	†,2Merifield et al.(2009)

Numerical Technique	Soil model (s_u)	References
Lagrangian (ALE) using Abaqus		
Large deformation FE analysis using RITSS technique	Tresca, uniform , linearly increasing with depth	*,2Barbosa-Cruz and Randolph (2005)
	Tresca, linearly increasing with depth, strain softening and rate effects.	†,2Wang et al. (2010); *,2Chatterjee et al. (2012a); 2 Chatterjee et al. (2012b)
Coupled Eulerian Lagrangian technique using Abaqus	Tresca, uniform	*,2Tho et al.(2012)
	von-Mises, linearly increasing with depth	*,2 Shi et al. (2011)
	von-Mises, linearly increasing with depth, strain softening and rate effects	*,2Dutta et al. (2012 a, b); †,2Dutta et al. (2012 c); Dutta (2013)

* Analyses performed only for vertical penetration

†Analyses performed for both vertical and lateral movement

1 Wished in place (WIP)

2 Pushed in place (PIP)

The RITSS technique could be used to avoid mesh tangling/convergence issues (Hu and Randolph, 1998; Barbosa-Cruz and Randolph, 2005). Finally, the CEL approach available

in Abaqus FE software can also model large deformation behaviour (Pike et al., 2010; Tho et al., 2012, Dutta et al. 2012a). Tho et al. (2012) conducted FE analyses without considering the effects of strain rate and softening, although it has been recognized by other researchers that these two factors might significantly influence the undrained shear strength of soil and thereby penetration resistance (Wang et al., 2010; Chatterjee et al., 2012a). Dutta et al. (2014) implemented these two effects using user subroutines and conducted FE analyses using Abaqus CEL and showed that it can successfully simulate the penetration behaviour of shallow embedment process.

While the above mentioned numerical techniques could simulate the penetration behaviour of partially embedded pipelines, the following issues need to be highlighted.

a) Computational time

One of the main issues in large deformation FE analysis is the computational time. For example, Barbosa-Cruz and Randolph (2005) mentioned that the simulation of penetration of a pipe in plane strain condition using RITSS required 1 to 30 days depending upon mesh density using a personal computer having 2.81 GHz Intel processor and 2.0 GB RAM. The computational time for 10 simulations was 111 days. Similar experience of computational time was reported for the analysis using Abaqus CEL (Dutta, personal communication). Therefore, if someone wants to simulate many cycles, LDFE techniques may not be feasible or at least extremely high speed computer is required.

b) Role of water in the cavity behind the pipe

When a pipeline penetrates to an intermediate depth, water might be trapped in the cavity behind the pipe as shown in Fig. 2.6. The LDFE cannot model the role of water

as it simply model the cavity as a void. In other words, in previous studies the cavity is simply assumed as open drainage condition where water can flow easily and the soil is modeled using submerged unit weight.

If the cavity is hydraulically isolated, suction (negative pressure) will be developed in the water behind the pipe. Unfortunately, none of the previous LDFE modeling technique could simulate this or at least not reported.

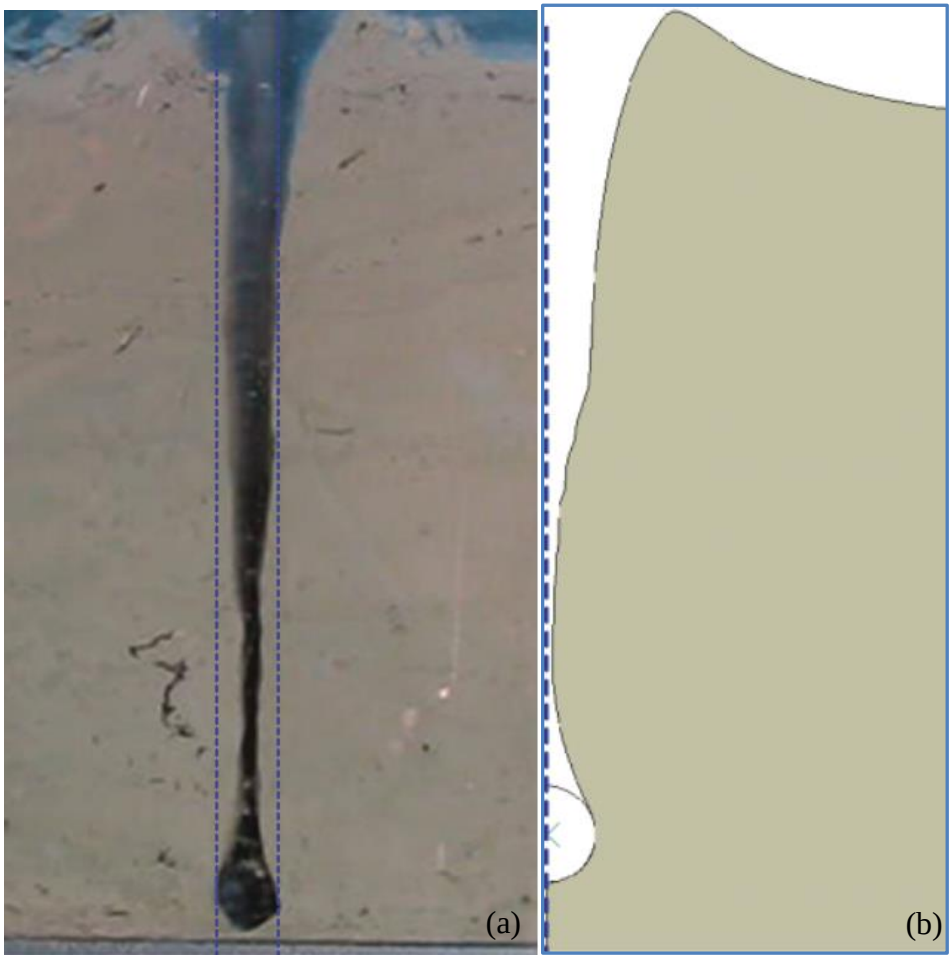

Figure 2.6: Deformed shape at intermediate penetration: a) Laboratory test after Puech et al. (2010), (b) FE simulation using Abaqus CEL after Tho et al. (2012)

In the present study, the above two factors are taken into consideration and an alternative numerical modeling tool in ANSYS CFX is developed.

2.3 Uplift

In riser-seabed-water interaction near the touchdown zone, the uplift behaviour is equally important in addition to penetration behaviour. However, comparatively lower numbers of studies on uplift behaviour are available in the literature. During upward movement suction may be developed under the riser and a trench might be formed when it separates from the seabed especially near the touchdown point (TDP). In the subsequent movement, the riser penetrates through this trench. Therefore, the uplift resistance depends on suction under the riser.

2.3.1 Uplift mechanisms

Most of the theories for uplift resistance have been developed for horizontal plate anchors. To understand the uplift behavior of an anchor, Merifield et al. (2001a) performed numerical modeling using the limit theorem of Sloan (1988) and Sloan and Kleeman (1995). Analyses were performed for plain strain strip anchor in uniform and linearly increasing undrained shear strength profiles. Upper and lower bound breakout resistances (i.e. the maximum uplift force) were obtained from numerical analysis. Although the maximum uplift force could be obtained, it does not provide any information of the development of uplift force with upward displacement of the anchor. Moreover, the suction under the anchor was not simulated.

Dickin (1994) pointed out that pipelines and anchors exhibits similar behavior for peak uplift resistance, although some other issues such as mobilized displacement at failure is different for SCR/pipelines.

Pipe laying contractors reported that the required uplift force for pipe retrieval is greater than the self-weight of the pipe Foda (1983). This greater uplift force is due to the suction under the pipe. Foda (1983) proposed the following empirical equation to determine the time to break out an object from seabed while applying a constant load.

$$t_b = \gamma s_u F^{-1.5} \qquad 2.4$$

Where, t_b is the break out time in second, γ is the shape factor of the plate in $N^{1/2}$-s-m^2 and F is the pullout force (N).

Audibert et al (1984) stated that the uplift resistance of a buried pipeline can be calculated assuming it as reverse bearing capacity problem and proposed an equation similar to bearing capacity equation as:

$$q_u = s_u N_{cv} D \qquad (2.5)$$

Where, N_{cv} represents vertical bearing capacity factor.

The reverse bearing capacity type failure mechanisms were simulated for uplifting of a pipe section by Martin and White (2012) who conducted numerical investigation using the finite element limit analysis code OxLim developed at Oxford University. They conducted FE analyses for 'wished-in-place' pipe configuration assuming full (unlimited) and no interface tensions. For no tension condition, zero (for smooth) and small (for rough) uplift resistance is calculated for shallow embedments (e.g. less than half a

diameter of the pipe) because the suction under the pipe is not modeled. The formation of trench due to uplift was not examined in their study.

2.3.2Experimental studies

Bostrom et al. (1998) conducted an experimental investigation of pipeline-soil interaction for penetration and uplift as encountered in the touchdown section of SCR. A small pipe section was rigidly attached to an actuator for penetration and subsequent uplift through a clay seabed. Figure 2.7 shows the variation of vertical force (penetration and uplift) for two tests. They also conducted numerical modeling using this force-displacement behaviour and showed that soil suction increases 37% bending moment during quasi-static loading.

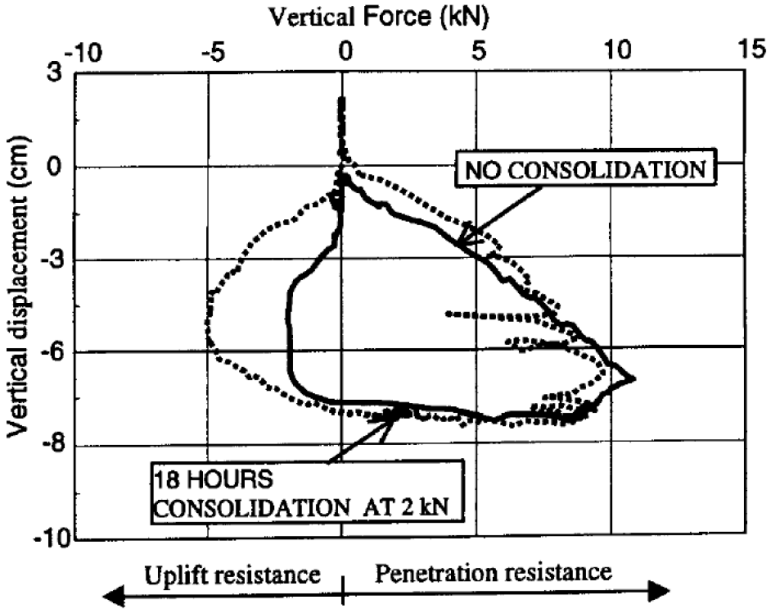

Figure 2.7: Force displacement curves (Bostrom et al. 1998)

Figure 2.8 shows a 1g model test results conducted by Aubeny et al. (2008). Cyclic tests were conducted with 25mm diameter and 125mm long pipe section in a 220 mm thick

consolidated test bed having almost uniform undrained shear strength of 3.7 kPa. Figure2.8 shows that the uplift resistance curves are not similar to the penetration resistance curves. At a given depth, the uplift resistance is lower that the penetration resistance. During upward displacement, significant uplift force acts on the pipe; however, at one stage it starts to decrease quickly and reduces to zero but the invert of the pipe is still at a depth below the original mudline (i.e. creates a trench).

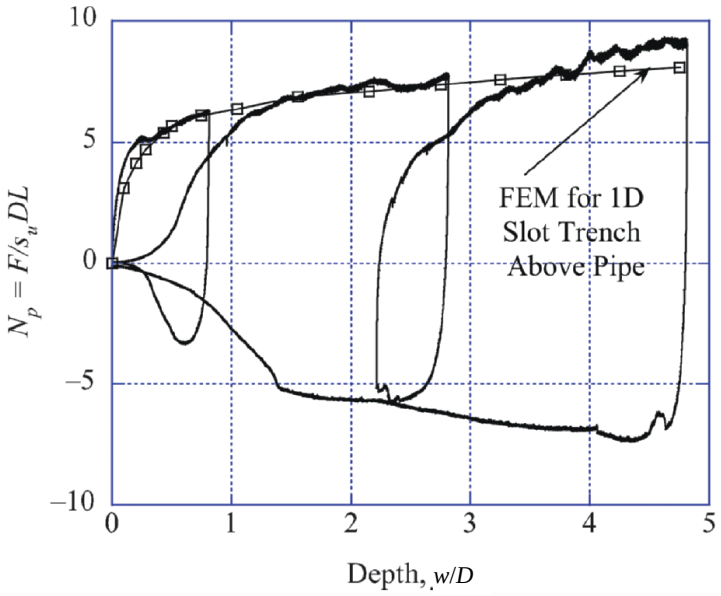

Figure 2.8: Normalized force-displacement curve. (Aubeny et al. 2008)

Cheuk et al. (2007) conducted a number of centrifuge model tests using lumpy clay backfill material. The pipe was placed on a stiff over consolidated clay bed and the then covered with a lumpy clay backfill and consolidated for a varying period of time with a targeted cover height of the pipe of 3.5*D*. The pipe was then pulled up at two different speeds (slow 0.16D /hr and fast 8.1D /hr). Figure2.9 shows the measured uplift forces in prototype scale (subtracting buoyant weight) with dimensionless pipe displacements. The

uplift resistance increases with rate of upward displacement. Moreover, with increase in consolidation time the uplift resistance increases.

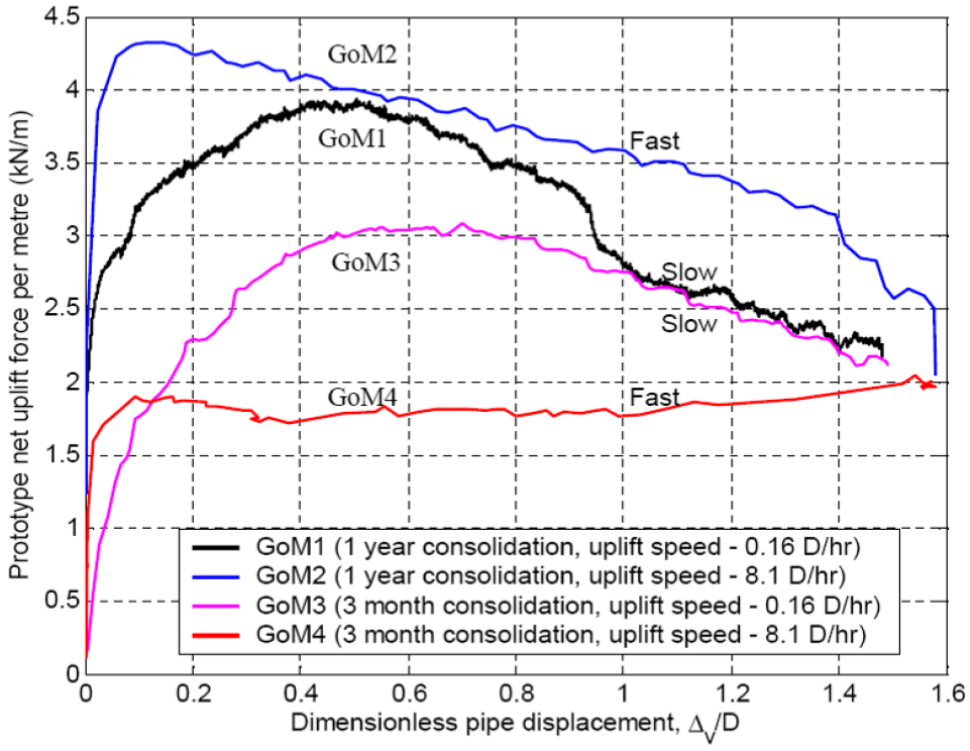

Figure 2.9: Influence of uplift speed and consolidation on uplift resistance. (Cheuk et al. 2007)

The rate of movement of the riser into the seabed or from the seabed has a significant effect on vertical resistance. Langford et al (2008) conducted a series of large-scale cyclic model tests in re-constituted high plasticity marine clay from the Gulf of Guinea. The model pipe was rough coated having dimensions of 1300mm in length and 174 mm in diameter. Tests were conducted at different speeds. The undrained shear strength of the clay seabed increases linearly with depth. The first 3 penetration tests (1, 2 and 3) were

conducted at a displacement rate of 0.05mm/s while the test 4 was conducted at 0.5mm/s. Figure 2.10 shows that the penetration resistance in test 4 is higher than that of other 3 tests because of higher displacement rate.

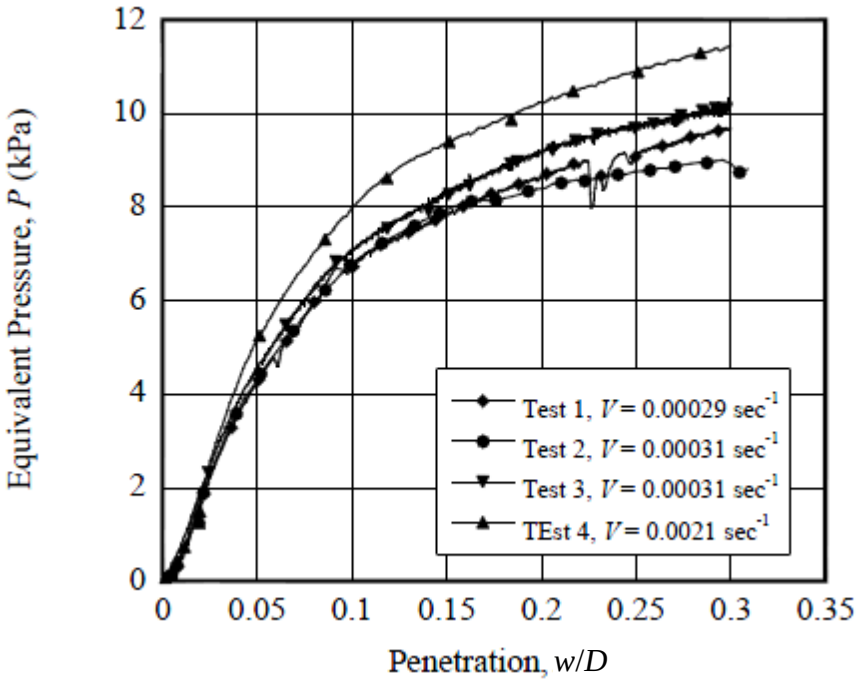

Figure 2.10: Initial penetration resistance vs. penetration depth (Langford et al 2008)

Figure 2.11 shows the cyclic response. The uplift resistance is more sensitive to the rate of displacement than penetration resistance. The maximum uplift resistance inTest4 (conducted at 0.5 mm/s) is almost twice the maximum uplift resistance in Test1 (conducted at 0.05 mm/s). However, the maximum penetration resistance in Test 4 is approximately 15% higher than the maximum penetration resistance in Test 1.

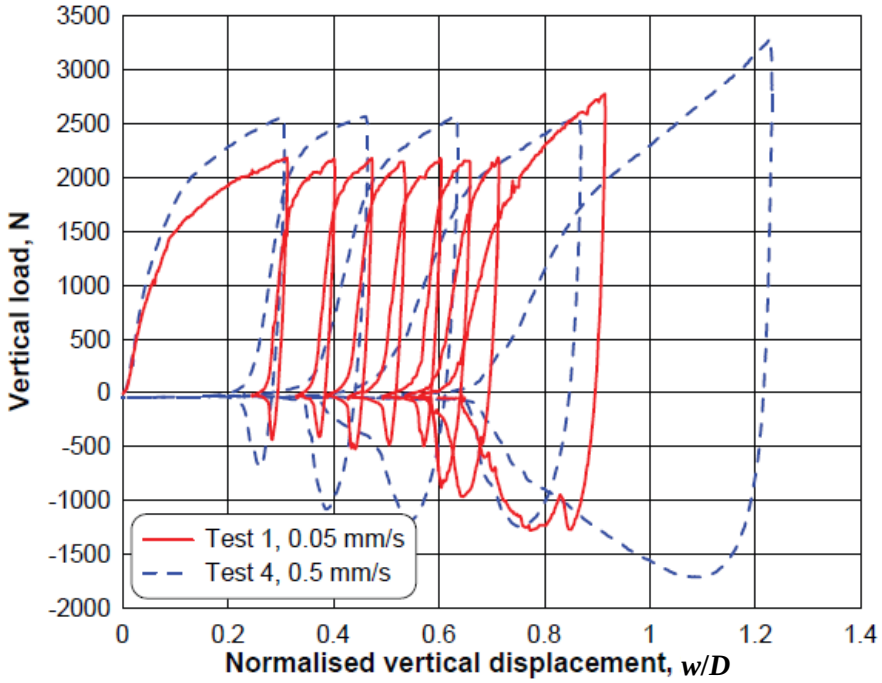

Figure 2.11: Effect of displacement rate in cyclic loading (Langford et al 2008)

A large number of laboratory tests were conducted in the CARISIMA-JIP during 1999–2002 to develop a riser-seabed interaction model. Tests were conducted using Onsøy clay collected from the south-eastern part of Norway. The undrained shear strength of the model seabed was 1.5 kPa at the mudline and linearly increased to 4 kPa at a depth of 200mm. In two phases, more than 40 tests were performed at different pullout velocities and consolidation time. Figure 2.12 schematically show the summary of all the test results, which shows that uplift resistance increases with pullout velocity (Har 2007 and Giertsen et. al. 2004). Very similar results were obtained in the STRIDE (Steel Risers in Deepwater Environments) JIP two-dimensional small-scale model tests.

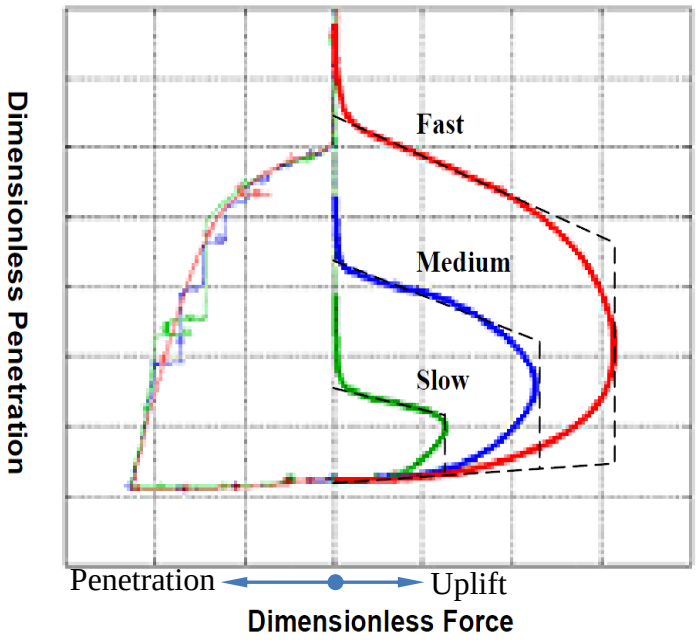

Figure 2.12: Effects of displacement rate on uplift resistance (After Har, C.G. 2007)

In order to understand three-dimensional response, large-scale field and laboratory tests (e.g. Bridge et al. 2003; Hodder and Byrne 2010; Wang et al. 2014), reduced-scale centrifuge tests (e.g. Elliott et al. 2013a & b, 2014; Hu 2010) and small-scale laboratory tests (e.g. Bridge 2005; Aubeny et al. 2008; Langford et al. 2008a & b) were conducted in the past to understand this behaviour.

In summary, small-scale two-dimensional model tests show that the uplift resistance significantly depends on pullout velocity and soil shear strength (magnitude, consolidation time and variation with depth). Reverse bearing capacity type of failure cannot explain the uplift behaviour properly, especially at shallow embedments, and suction under the riser plays a significant role.

2.3.3 Trench formation

The mechanisms of trench formation in the touchdown zone due to cyclic displacements of the riser are very complex. Displacement of soil, erosion, flow of water/slurry along the trench, pumping and scouring are some of the causes of trench formation. Bridge (2005) reported trench shapes of a number of sites as the one shown in Figs. 2.13(a). That full-scale test also showed similar type of trench formation (Fig. 2.13(b)). To date no theoretical model or numerical analyses are available which could explain trench formation mechanisms properly. In the present study, an attempt has been taken to simulate trench formation due to riser-seabed-water interaction during loading unloading at the touchdown zone.

2.3.4 P-y curves

In the current design practice, the riser-seabed interaction in the TDZ is modeled using the *P-y* curves, where *P* represents the force per unit length and *y* represents the vertical displacement. Based on model test results (e.g. Dunlap et al. 1990; Bridge 2005), Aubeny and Biscontin (2008, 2009) proposed a conceptual *P-y* curve model as shown in Fig. 2.14. This idealized seabed model has the following major components: (i) the backbone curve, (ii) elastic unloading, (iii) suction, (iv) full separation and (v) reloading. The backbone curve (0-1) represents the penetration of the riser into the virgin soil and can be defined by $P=N_p s_u D$, where N_p is a bearing capacity factor. Based on small strain finite element modeling of "wished in place" pipes, (Aubeny et al. 2005) proposed an empirical relation $N_p = a(w/D)^b$, where a and b are fitting parameters and w is the depth of embedment of the invert of the pipe. Aubeny and Biscontin (2009) further modified this equation using

initial width of the trench. It is shown that the depth and width of the trench has a significant effect on penetration resistance.

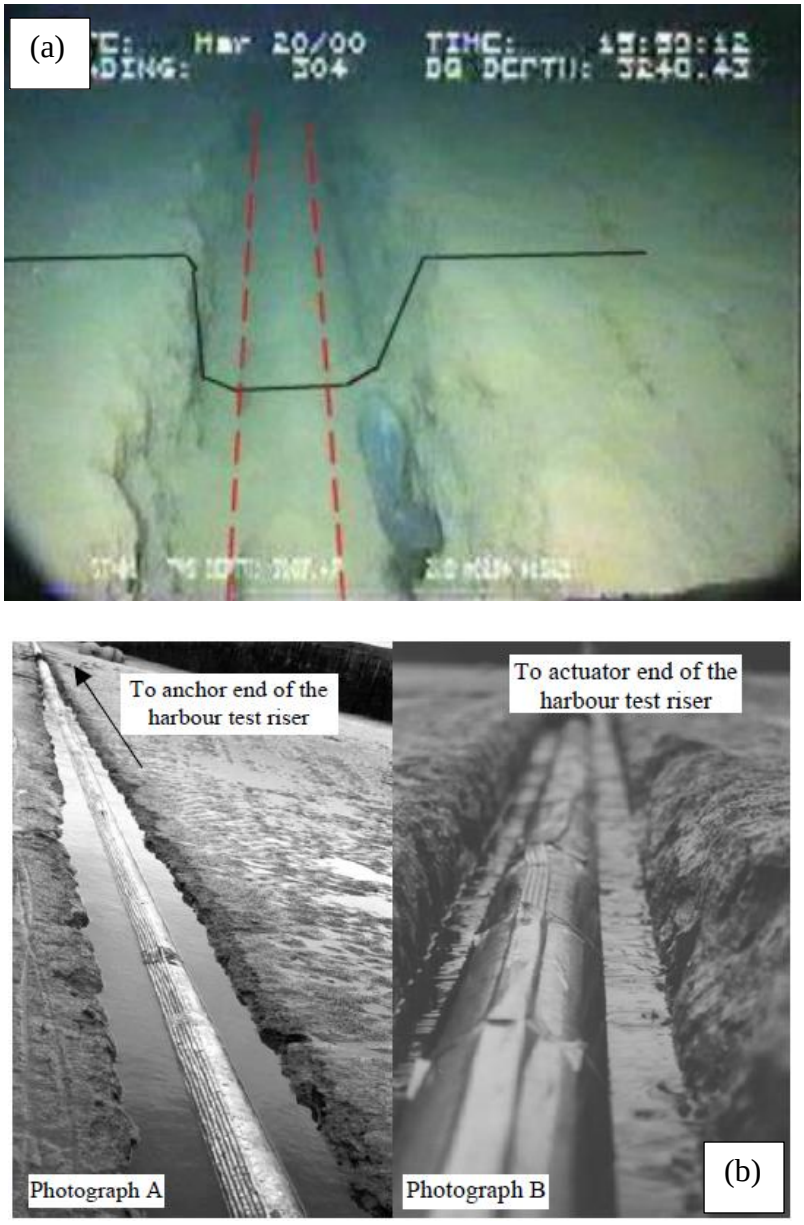

Figure 2.13: Observed trench shapes: (a) Allegheny site (b) full-scale test (Bridge et al. 2003)

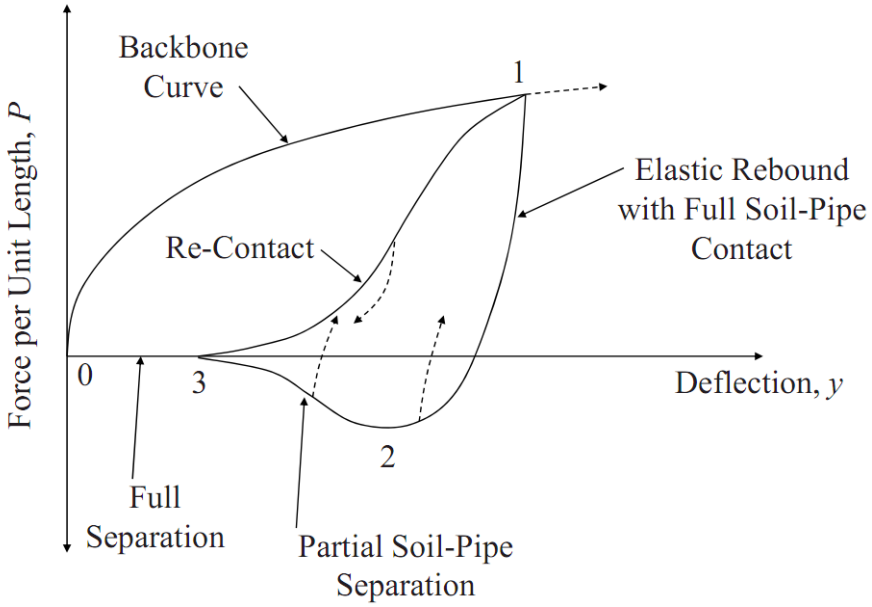

Figure 2.14: P-y curve model for rise-seabed interaction (after Aubeny and Biscontin, 2009)

Another important component of the *P-y* model is the unloading (uplift), which is represented by 1-2-3-0 in Fig. 2.14. The initial elastic rebound reduces the resistance quickly to P=0 followed by negative P (uplift resistance), which mainly depends upon suction under the riser for shallow embedments. The maximum uplift force is developed at point 2 and then gradually decreases to 0 at point 3 where full separation of the riser from the seabed is occurred. The path 3-0 represents the travel of the riser in water. Upon reloading, the *P-y* curve follows the path 0-3-1 instead of 0-1 because of the trench formed by previous loading-unloading cycle.

The suction under the riser significantly affects its fatigue life (Thethi and Moros 2001). Quantification of suction is a challenging task. Based on field observation and model test results empirical factors have been proposed in the past. The ultimate suction force

(P_{u_suc}) is expressed as a function of ultimate penetration resistance P_u using a model parameter f_{suc} as P_{u_suc}=-$f_{suc}P_u$. The value of f_{suc} depends on many factors such as rate of upward movement of the risers, soil strength, flow of water under the riser and others. The value of f_{suc} could vary widely between 0 and 1.0. Another empirical factor known as "suction decay factor" is used to define the upward displacement of the riser over which suction could sustain.

Another nonlinear mathematical model (Fig. 2.15) proposed by Randolph and Quiggin (2009) is in fact an improved version of Aubeny and Biscontin (2009) model with some additional features. In the Fig. 2.15 penetration represents by z instead of y. In this model, the initial penetration resistance increases with depth and asymptotically approaches the ultimate penetration resistance (P_u). Similarly, with upward displacement, the uplift resistance curve asymptotically approaches the ultimate suction resistance curve ($P_{u\text{-}suc}$). The displacement from which suction decay initiates (segment 4 of the uplift curve) is defined by another factor. Suction decay could bring the uplift resistance to zero. In subsequent loading it will follow the re-penetration curve and again reaches asymptotically the P_u curve. The re-penetration curve is also defined by some empirical factors.

Based on extensive laboratory experiment results in various conditions, Bridge et al. (2004) proposed an empirical model to calculate soil suction during uplift (Fig. 2.16). According to their model, the ratio between the maximum suction and ultimate penetration resistance (f_{suc}) can be calculated as

$$f_{suc} = -k_C k_V k_T \tag{2.6}$$

Where k_C, k_V and k_T are dimensionless empirical factors. The constant k_V is related to v/D as $k_V = k_F(v/D)^{n_F}$, where k_F are n_F are two empirical constants.

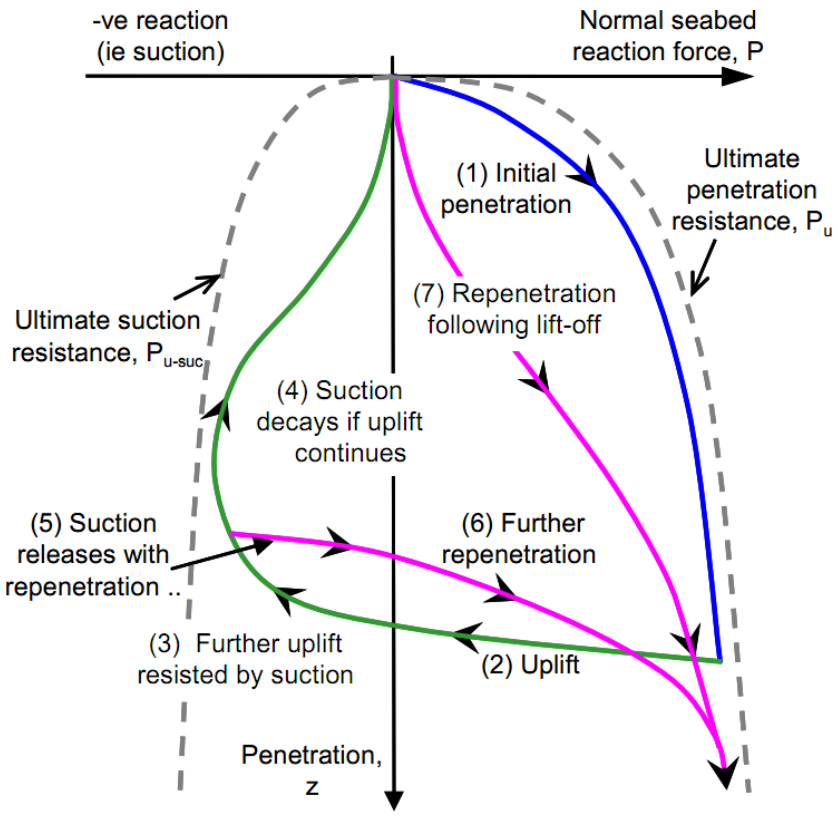

Figure 2.15: P-y curve for different modes (after Randolph and Quiggin, 2009)

Bridge et al. (2004) also provided a model for breakout displacement Δ_B (the vertical displacement of the riser from the maximum penetration to the point where the riser separates from the seabed).

$$\frac{\Delta_B}{D} = k_{DC}k_{DV}k_{DT} \qquad (2.7)$$

Where k_{DC}, k_{DV} and k_{DT} are empirical constants. Moreover, $k_{DV} = k_D(v)^{n_D}$, where k_D are n_D are two empirical constants.

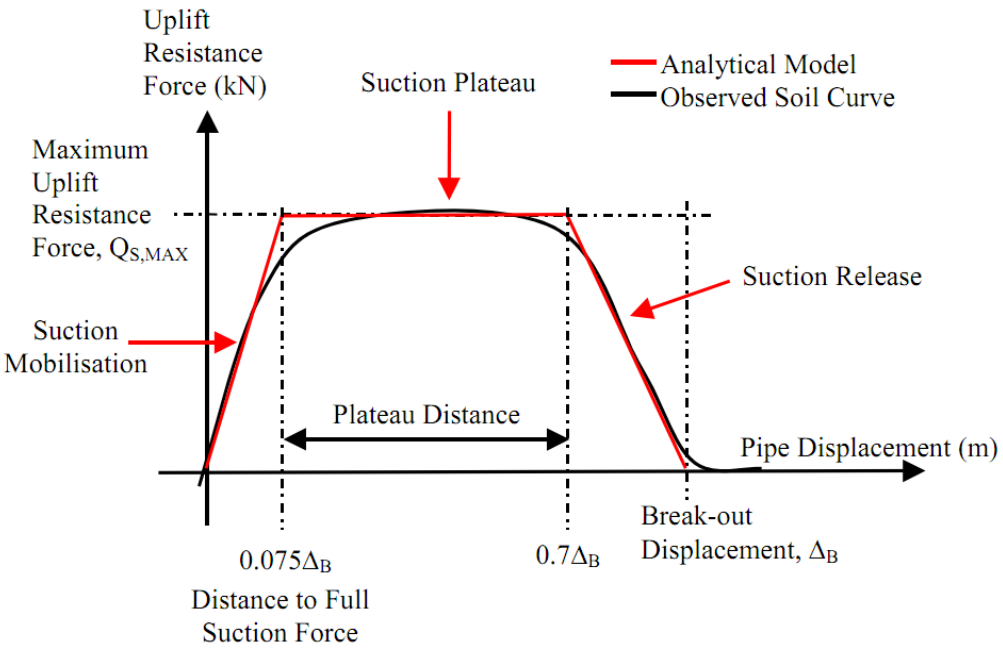

Figure 2.16: Proposed uplift curve from experimental results (after Bridge 2004)

In summary, although simple, the proposed *P-y* curve models require a number of empirical factors.

2.4 Chapter summary

Both penetration and uplift behaviour are equally important in the design of riser fatigue life near the touchdown zone. Available LDFE model can simulate the penetration behaviour for shallow or deep embedment conditions; however, at the intermediate depth the water in the cavity behind the riser might be trapped which could influence

penetration resistance. Moreover, the existing LDFE modeling techniques currently available in the literature are computationally very expensive. One of the major limitations of the current LDFE modeling tools is that they cannot simulate the suction. To the best knowledge of the author, there is no numerical model available in the literature for simulation of suction in riser-seabed-water interaction. Currently, *P-y* curves are used in the design, which are based on a number of empirical factors.

In order to overcome some of the above limitations, a numerical technique has been developed in the present study for riser-seabed-water interaction. The penetration behaviour is presented in Chapter 3 and mainly the uplift behaviour discussed in Chapter 4.

Chapter 3

Modeling of Penetration of Steel Catenary Riser in Soft Clay Seabed

3.1 Introduction

Steel Catenary Risers (SCRs) are frequently used in offshore to connect floating production facilities to the seabed well systems. Typically the diameter of SCR varies between 150 mm and 600 mm (Hu et al. 2011). The surface waves and current could cause vertical motion of the riser of several diameters near the touchdown point (TDP), which could be even higher in storm events. Proper modeling of cyclic motion of the riser near the TDP and its interaction with the seabed and water is very important in the design, because the region near the TDP is a fatigue hotspot. The fatigue life of a steel catenary riser depends on seabed properties at the touchdown zone (TDZ) as well as motion characteristics. In the current industry practice, the seabed response is idealized using linear/nonlinear soil springs or rigid surfaces. Empirical equations have been proposed in the past to model the seabed taking into account of various complex mechanisms, including trench configuration, nonlinearity of soil stiffness, degradation of soil shear strength, and suction effects (Aubeny et al. 2005; Randolph and Quiggin, 2009). While these methods attempt to capture the processes involved in riser-seabed-water interaction, significant uncertainties still remain in modeling of this intrinsically complex problem. Moreover, the uncertainties from other sources such as vortex induced vibration could further complicate the process. Because of these uncertainties, the design codes (e.g. DNV 2010) recommend design fatigue factor of 6.0 and as high as 10 for critical

components. The design fatigue factor has no actual theoretical basis, but has been established from experience to maintain low risk of failure (Li and Low 2012).The main objective of the research presented in this chapter is to develop an advanced computationally efficient numerical tool to simulate the penetration behaviour of a section of riser.

3.2Previous studies

Large-scale field tests and small-scale laboratory model tests were performed in the past to understand the complex mechanism of riser-seabed-water. In the STRIDE JIP (Steel Risers in Deepwater Environments Joint Industry Project), full-scale tests were conducted over a period of three months at a harbor location in the west of England (Bridge et al. 2003). Large-scale indoor tests (e.g. Hodder and Byrne 2010; Wang et al. 2014) are also available in the literature. A series of small-scale laboratory tests were conducted under the Catenary Riser-Soil Interaction Model for Global Riser Analysis (CARISIMA) JIP using clay from a site in Onsøy, Norway. Similar tests were conducted in the STRIDE JIP, and it was shown that the results are consistent with CARISIMA test results (Bridge 2005). The STRIDE and CARISIMA test results provide some valuable insight into the riser-seabed-water interaction mechanism, such as penetration resistance, suction mobilization during uplift, suction plateau, suction release and effect of soil consolidation (Bridge and Willis 2002; Willis and West 2001).

To understand load-displacement mechanisms, Dunlap et al. (1990) conducted a series of small-scale laboratory tests in soft sediment having undrained shear strength (s_{u0}) of 1.0-1.5 kPa using a 1.52 m×152 mm (length×diameter) model pipe section. Aubeny et al.

(2008) investigated the cyclic response by conducting tests in kaolin clay seabed of s_{u0}≈3.7 kPa using a 125 mm length and 25 mm diameter model pipe section. Langford and Aubeny (2008) conducted tests in a high plastic clay of linearly increasing s_{u0} profile using a rough coated 1,300 mm×174 mm pipe section.

Besides 1g laboratory tests, centrifuge tests were also conducted in the past.Hu (2010) presented centrifuge modeling of penetration and uplift behavior of riser sections in Malaysia kaolin clay of varying over consolidation ratio (OCR) of 1, 3 and 5, where the tests were conducted with 600 and 1,000 mm diameter (D) pipe sections in prototype scale. While some other centrifuge tests (e.g. Dingle et al. 2008) provides penetration behavior of shallowly embedded pipelines, Hu (2010) shows the response for wider range of embedments (3D). In the above centrifuge tests, only a section of the riser is modeled. However, at C-CORE and Memorial University, centrifuge modeling of a full length riser (108 m in prototype) was performed using a novel experimental facility developed at C-CORE supported by offshore industry (Elliott et al. 2013a, b, 2014).

Currently, the riser-seabed interaction in the TDZ is modeled using the *P-y* curves, where P represents the force per unit length and y represents the vertical displacement. Based on model test results (e.g. Dunlap et al. 1990; Bridge 2005), Aubeny and Biscontin (2008, 2009) proposed a conceptual *P-y* curve model. The nonlinear mathematical model proposed by Randolph and Quiggin (2009) is in fact an improved version of Aubeny and Biscontin (2008) model with some additional features. One of the main components of these models is the backbone curve. Based on small strain FE modeling of pipes in "wished in place" configuration, Aubeny et al. (2005) proposed an empirical relation for

penetration resistance, which has been further modified, incorporating the effects of initial width of the trench, in Aubeny and Biscontin (2009).

3.3 Problem definition

In the CFX modeling, a section of a riser of diameter D is placed in water above the mudline at a distance y_w as shown in Fig. 3.1. The riser is then displaced vertically downward at a velocity v. To eliminate buoyancy effect of water, the weight of the riser is assumed to be equal to the weight of the riser section filled with seawater. During the initial displacement through water, the resistance is simply governed by the flow of water around the riser. However, when the bottom of the riser is moved close to the mudline the response is govern by riser-seabed-water interaction. The penetration of the riser in the soft clay seabed is relatively fast and therefore undrained condition governs the behavior. Two types of variation of undrained shear strength (s_{u0}) are used in this paper: (i) uniform s_{u0}, (ii) linearly increasing s_{u0}, which is defined as $s_{u0} = s_{um} + ky'$ where s_{um} is the undrained shear strength of clay at the mudline, k is the strength gradient and y' is the depth of the soil element from the mudline (Fig. 3.1). The depth of penetration (w) represents the depth of the invert of the riser from the mudline.

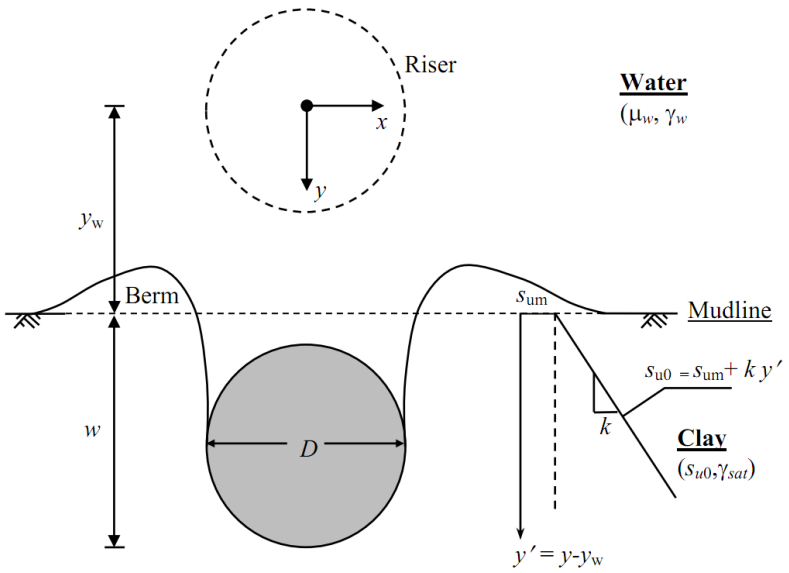

Figure 3.1: Problem definition

3.4 CFD simulation

The general purpose ANSYS CFX 13.0 software is used in this study for CFD simulation. Note that the CFD approach has been used in previous studies for modeling debris flows, glide blocks and out-runner blocks (e.g. De Blasio et al. 2004 a & b, 2005; Gauer et al. 2005 & 2006; Harbitz et al. 2003; Zakeri 2009; Zakeri et al. 2009a; Zakeri and Hawlader 2013). In ANSYS CFX, the domain is discretized into three-dimensional mesh. The governing equations are solved adopting a solution methodology based on finite volume, which are constructed using the discretized mesh. The force-displacement behaviour is modeled using the Navier-Stokes equations, which has been developed applying Newton's Law (F=ma) to fluid elements. Here F is the force, m is the mass and a is the acceleration. The forcing term (F) is the sum of gravitational force (F_{grv}), pressure force (F_{press}) and viscous force (F_{visc}). The gravitational force F_{grv} (=mg) is same as it is in solid

mechanics, where g is the gravitational acceleration. The last two (F_{press} and F_{visc}) are the reaction forces to the motion, which are analogous to the normal and frictional resistance in solid mechanics. The parameters required in CFX to calculate F_{grv} and F_{press} are given by density of soil and water, and the boundary conditions including the displacement of the riser. The coefficient of dynamic viscosity (μ) is used to calculate F_{visc}. The definition of μ, as a function of undrained shear strength, is discussed in the following sections.

3.4.1 CFX model setup

Figure 3.2 shows the domains used in CFX simulation. The riser (D=350 mm) is modeled as an impermeable wall. The CFX allows only three-dimensional modeling, and therefore the analyses are performed for one element of 10 mm in the out of plane direction. The following three CFX modeling techniques are first developed to identify an appropriate modeling approach.

Model-I: In this case, the center of the riser is placed at one diameter above the mudline in water and then displaced downward. As shown in Fig. 3.2(a), the upper 2.35 m (=6.7D) of the domain is water and the lower 4.65 m (=13.3D) is clay. The right vertical boundary is placed at 3 m (=8.6D) from the center of the riser. The boundaries are placed at sufficiently large distance from the riser and therefore no boundary effects are observed on penetration/uplift resistance and soil displacement. Taking the advantage of symmetry, only the right half of the domain is modeled.

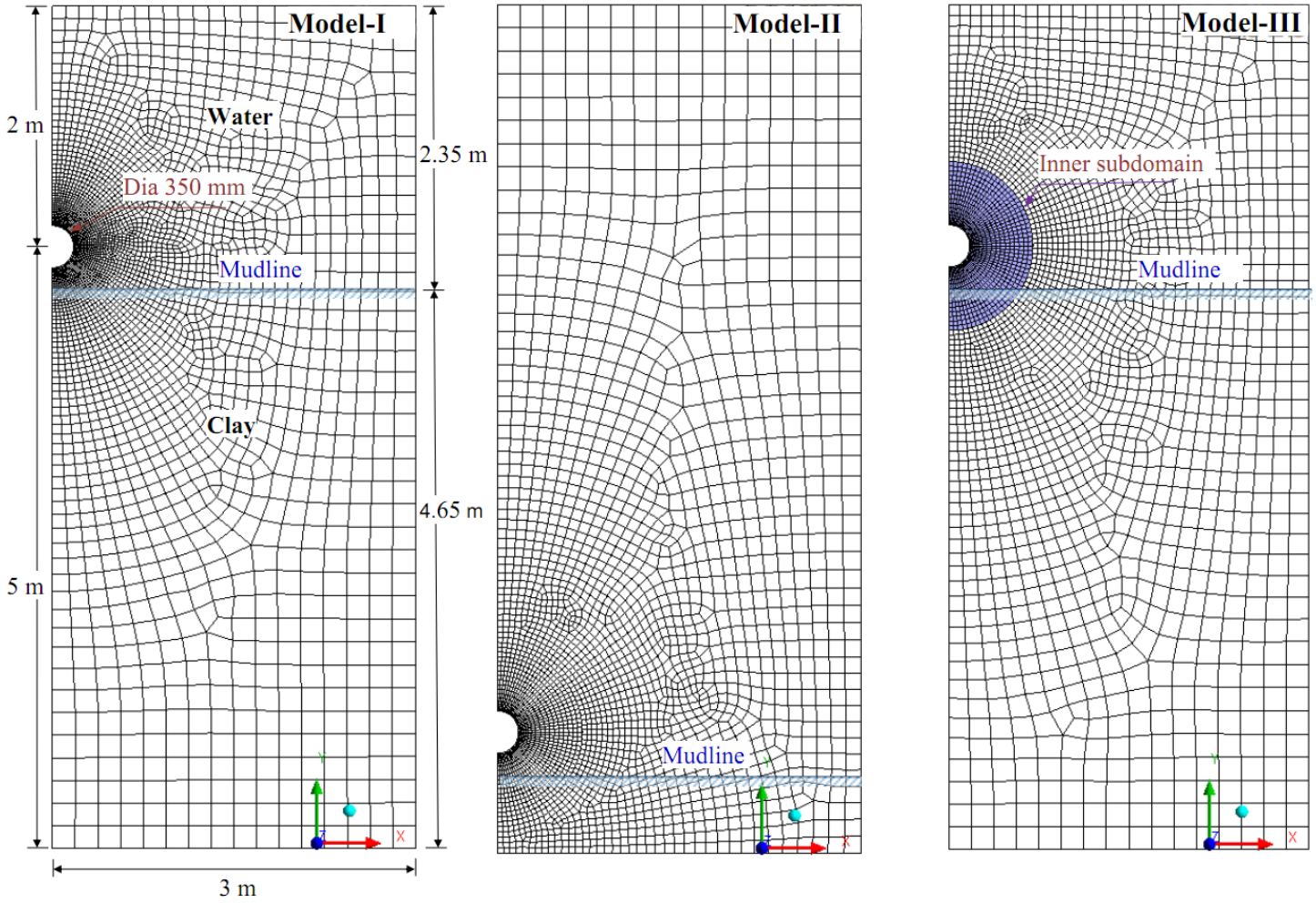

Figure 3.2: CFX models

Clay and water are modeled using homogeneous multiphase Eulerian materials. The interface between clay and water that represents the mudline is defined by a step function through CFX Command Language (CCL) — a declarative language in CFX for enhanced simulation without writing external FORTRAN routines. The clay and water in the domain are defined initially using the volume fraction tool. In the elements above the mudline, the volume fraction of water is set to 1 and the volume fraction of clay is 0. On the other hand, in the elements below the mudline, the volume fraction of water is 0 and volume fraction of clay is 1.

The bottom and all the vertical faces are defined as walls, which are solid impermeable boundaries to fluid flow. No-slip boundary condition is applied to the bottom wall and riser surface, and therefore the velocity of the Eulerian material (soil/water) next to these walls is zero. Free-slip boundary condition is applied on the right vertical wall. On the other three vertical faces, symmetry plane boundary conditions are applied, which implies that the flow of Eulerian material (soil/water) on one side of the plane is a mirror image of the flow on the opposite side. “Unspecified mesh motion” option in CFX is used for the vertical walls. This setting allows the mesh node on these walls to move in the vertical direction preserving the quality of mesh during the displacement of the riser. The top of the water is defined as an opening to allow water to flow in and out of the domain.

The mesh is formed using the options available in CFX. Very fine mesh is used near the riser and the size of the elements is increased with distance from the riser. The maximum dimension of the mesh just outside the riser surface is 10 mm. The riser is displaced vertically downward at a given velocity specifying the motion of the nodes on riser wall.

Model-II: In this case, the riser is kept at a fixed location as shown in Fig. 3.2(b) and the clay is moved upward. The bottom boundary is defined as an inlet while the other boundary conditions are same as in Model-I. The clay is entered through the inlet at a constant velocity (v). As the clay is modeled in undrained condition (no volume change), the top surface of the clay (mudline) moves upward at constant velocity v until it touches the riser. When the riser obstructs the flow of soil, the flow pattern changes and a berm forms near the pipe. However, the velocity of top soil surface far from the riser, such as the points near the right wall, is still same as the flow velocity in the inlet. That means, the relative velocity between the riser and soil surface far from it in Model-II is same as in Model-I.

Model -III: This approach can be considered as a "subdomain approach." The Model-III is same as Model-I, except for an inner subdomain shown by the shaded zone near the riser in Fig. 3.2(c). No mesh deformation is allowed in the subdomain, and therefore the shape and size of the mesh does not change with displacement of the riser. However, the Eulerian materials (clay and water) can flow through the mesh both in subdomain and outside the subdomain. The radial thickness of the subdomain of 1.5D is used because the velocity of soil elements outside this zone during penetration is not significant as shown later. As the modeling of the zone near the riser is very critical, the inclusion of the subdomain increases the robustness of simulation significantly, which is discussed further in the following sections. In this case, the riser and the subdomain are displaced vertically at a constant speed specifying the motion of the nodes using CCL expressions. No additional interface conditions, such as no-slip or free-slip conditions, are applied to the interface between the subdomain and surrounding soil/water. This allows inward and

outward flow of soil and water through this interface maintaining same fluid flux in both side of the interface.

3.4.2 Undrained shear strength in CFX

Based on fluid mechanics approach, the dynamic viscosity (μ) of soft clay can be defined as $\mu = \tau / \dot{\gamma}$, where τ is shear stress and $\dot{\gamma}$ is shear strain rate. Following geotechnical notations, the symbol τ is replaced by s_{u0}. Comprehensive discussions on estimation of shear strength of soft clays in deepwater are available in Lunne and Andersen (2007) and Lunne et al. (2011). It is known that the undrained shear strength increases with strain rate; however, it is not considered in this chapter. The effects of strain rate on s_{u0}could be found elsewhere (Dutta et al. 2014; Zakeri and Hawlader 2013). In CFX analyses, the value of $\dot{\gamma}$ for each element is obtained at every time step, and then μ is assigned using CCL expressions.

Generally in FE modeling, the maximum undrained shear resistance at the pipe-soil interface is defined as αs_{u0}, where α is a coefficient that varies between 0 (smooth/frictionless) and 1 (rough). As it depends on many factors, analyses have been performed in the past for different values of α. For example, Wang et al. (2010) used α=0.5 while some other researchers (e.g. Tho et al. 2012) modeled for smooth condition (α=0). In CFX, different values of α cannot be defined directly. Therefore, the shear strength of one row of clay elements just outside the riser (s_{u_int}) is defined as $s_{u\_int}=f_2 s_{u0}$ with $0 \le f_2 \le 1.0$. Note that, f_2=0 approximately represents the smooth condition as the soil near the riser cannot sustain any shear stress.

3.4.3 Penetration resistance

The geometry and soil parameters used in the analyses are listed in Table 3.1. The penetration resistance (N_p) is presented in normalized form as $N_p=F/s_{uN}D_eL$, where F is the penetration resistance, s_{uN} is the undrained shear strength used for normalization, D_e is the effective diameter and L is the length of riser section (=10 mm). The undrained shear strength depends on mode of shearing (e.g. triaxial or simple shear), depth (linear s_{u0}), and strain rate. One should interpret N_p value carefully because s_{uN} at different conditions has been used in previous studies (e.g. Langford and Aubeny 2008; Zhu and Randolph 2010; Wang et al. 2010; Bridge 2005). In the present study, considering triaxial compression as the standard test of reference, s_{u0}at the invert of the riser ($s_{u0(i)}$) in triaxial compression condition is used for s_{uN}. Using Tresca hexagon in the deviatoric plane it can be shown that $s_{uN}=\frac{2}{\sqrt{3}}s_{u0(i)}$ (Smith and Griffiths 2004; Sousa et al. 2011; Tho et al. 2013). For uniform s_{u0} profile $s_{u0(i)}=s_{u0}$ and for linearly increasing s_{u0} profile the value of $s_{u0(i)}$ increases with depth of penetration. It is to be noted here that some researchers (e.g. White et al. 2010; Tho et al. 2011) reported a corrected value of N_p by subtracting the influence of soil buoyancy on penetration resistance. However, the normalized penetration resistance presented in the following sections is without any correction of buoyancy.

Following the concept of Gui and Bolton (1998) and assuming that the failure is occurred at a distance of half of the element size from the outer surface of the riser, the value of D_e can be calculated as 360 mm (=350 mm+2×10 mm/2) for 10 mm element size just outside the riser. If D (=350 mm) is used instead of D_e, the normalized penetration resistance will

be increased by only 2.8%. In this study D_e is used. The depth of penetration is normalized as $\hat{w} = w/D_e$.

Table 3.1: Geometry and Material Parameters used in CFX analysis

Parameters	Values
Diameter of riser, D (mm)	350
Length of riser section, L (mm)	10
Soil parameters	
a) Uniform shear strength, s_{u0}	
Undrained shear strength, s_{u0} (kPa)	3.7 (2.3,5)
Saturated unit weight, γ_{sat} (kN/m^3)	16.31
Coefficient f_2	1.0 (0.01,0.2,0.5)
b) Linearly increasing shear strength ($s_{u0} = s_{um} + ky'$)	
Mudline shear strength, s_{um} (kPa)	2.3(1.0,3.7)
Shear strength gradient, k (kPa/m)	2.0 (0,1,3)
Coefficient f_2	0.01(0.2,0.5,1.0)
Saturated unit weight, γ_{sat} (kN/m^3)	16.31
Note: Numbers in parenthesis in right column show the values used in the parametric study	

Figure 3.3 shows the N_p vs $\hat{w}$ curves obtained from three CFX models (I, II, and III in Fig. 3.2) for the following parameters: s_{u0}=3.7 kPa (uniform), γ_{sat}=16.31 kN/m^3, f_2=1 and v=60 mm/s. The value of N_p is zero until the riser touches the mudline at $\hat{w}$=0. In all three models (I to III) the penetration resistance increases with depth of penetration. The value of N_p at $\hat{w}$=5D is 10.45. If we subtract the buoyancy effect of approximately equal to $\gamma' A_s/s_{u0}D$, the value of N_p will reduce to 9.97. The plasticity limit analysis (Randolph and Houlsby 1984; Martin and Randolph 2006) shows that the value of N_p for deep embedments and rough pipe-soil interface condition is 11.94, which is higher than the calculated value because fully deep failure mechanism is not developed at $\hat{w}$=5D, rather it is in the transition stage as shown later.

For all three cases, very similar N_p vs $\hat{w}$ curves are obtained for these conditions. However, in Model-I significant mesh distortion occurs at large penetration. Although the analysis could be performed for this particular condition, numerical issues are encountered for other conditions presented in the following sections and therefore the Model-II and III are developed.

Unlike Model-I, numerical errors due to mesh distortion are not encountered in Model-II. However, one disadvantage with this model is that the presentation of the results, such as instantaneous velocity vectors of soil, is difficult because soil is moved instead of the riser. In addition, one of the main objectives of the present research program is to model the suction under the riser when it moves upward during cyclic motion, which could not be simulated using the Model-II.

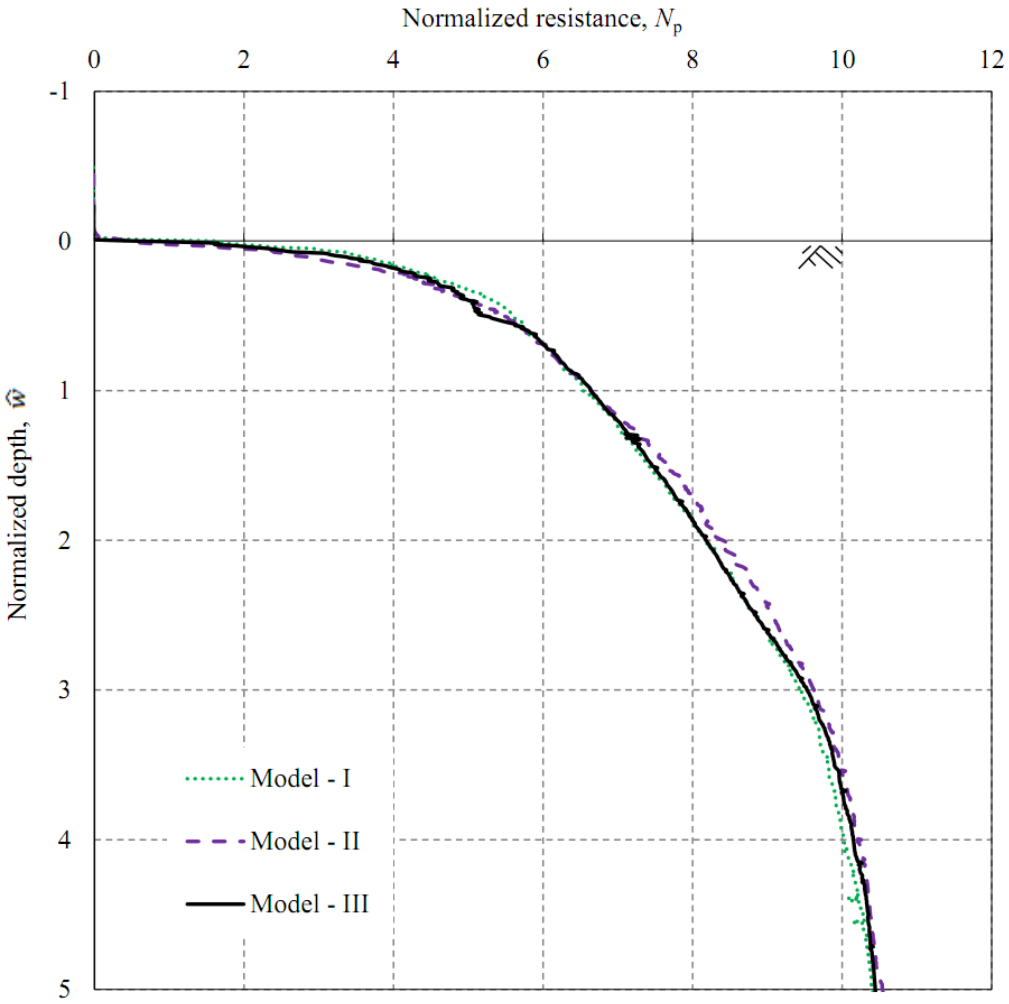

Figure 3.3: Penetration resistance for three models (f2 =1.0; su0 = 3.7 kPa)

Some mesh distortion occurs outside the subdomain in Model-III; however, it does not have significant influence on simulation. In this case, non-deformable subdomain mesh moves with the riser at same velocity, and Eulerian materials (clay and water) flow through it. Numerical issues due to mesh distortion near the riser also could be avoided. Another advantage is that the value of f_2 could be precisely assigned to the first row of the soil elements near the riser surface because the size of the mesh does not change with

riser displacement. Considering these advantages, the Model-III is used in the following CFX analyses.

Figure 3.4 shows the negative pressure in the Eulerian materials (clay and water) calculated by CFX. The solid lines show the clay-water interface. For w=2.0D, the suction (absolute values of negative pressure) is developed in a small zone just above the springline of the riser. At this depth of penetration, there is a wide space above the riser between clay-water interface and symmetry plane. Water can flow easily through this space during penetration. With increase in penetration depth, the width of the trench above the riser becomes narrow as shown in Fig. 3.4(c and d). For this penetration speed (60 mm/s), sufficient water cannot flow through this narrow space and therefore considerable suction develops above the riser as shown in Figs. 3.4c and 3.4d with shaded zones. As CEL cannot simulate this suction, N_p from CEL is less than the values obtained from CFX for $\hat{w}$>3.0.

In a recent study, Tho et al. (2012) showed the influence of size and shape of the trench or soil cavity on penetration resistance. They also recognized the importance of the boundary conditions at the trench wall or cavity which are related to drainage of water through the trench. Two extreme idealized scenarios identified are: (i) open drainage, where the water in the cavity can easily drain away and (ii) closed drainage, where the water in the cavity is hydraulically isolated. They performed FE analyses using Abaqus CEL for an open drainage condition by modeling the trench as void and therefore the trench walls are stress-free.

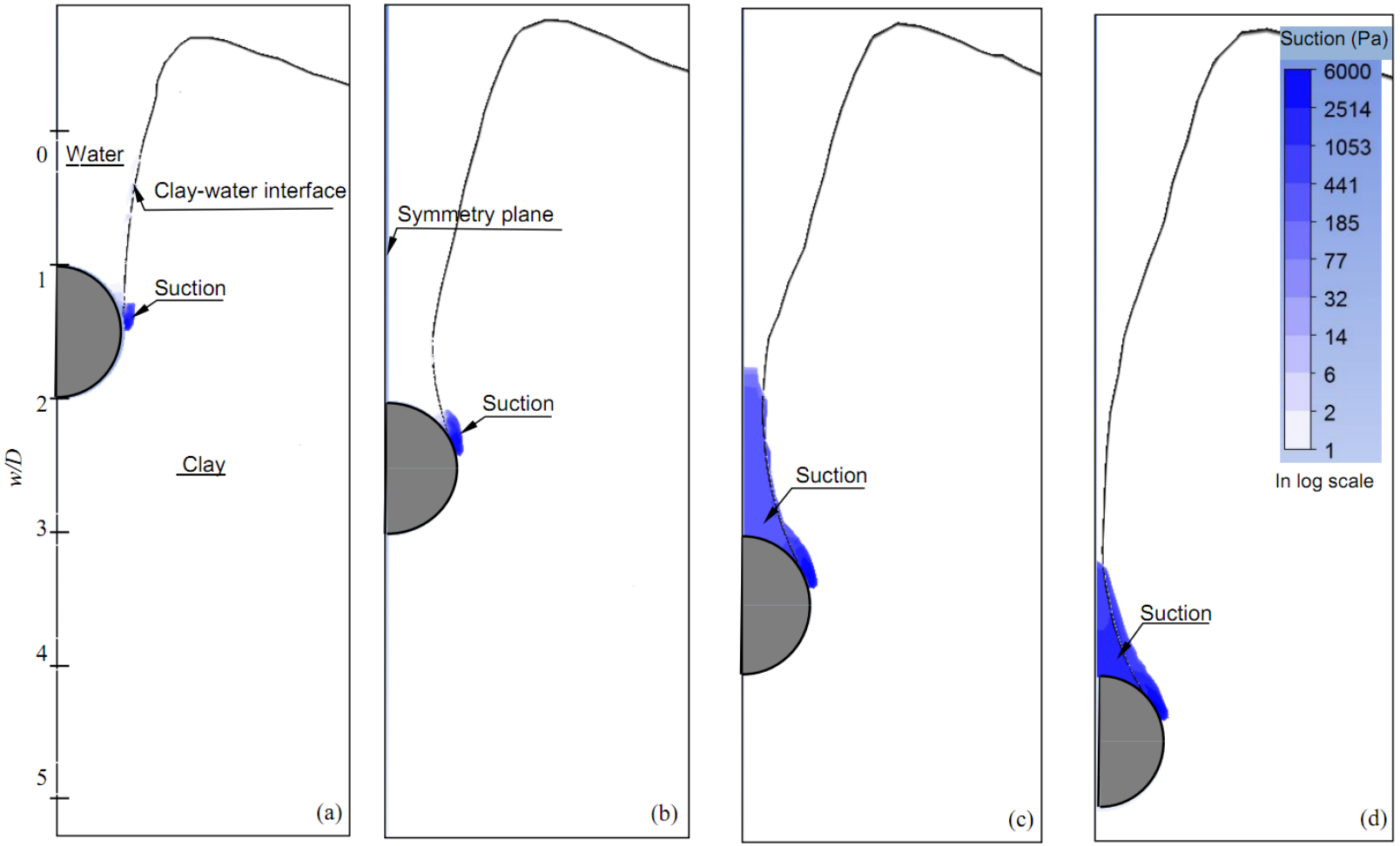

Figure 3.4: Suction at different pipe penetration depth (a) 2*D* (b) 3*D* (c) 4*D* (d) 5*D*

In Abaqus CEL analysis, the trench walls are stress-free and a void space represents the trench. In contrast, the trench is filled with water in CFX modeling. The stress on the clay-water interface is not always zero. The CFX calculates the stress that depends mainly on trench shape and penetration speed. For example, Fig. 3.4(a) shows that at w=2D the stress on the clay-water interface of the trench is negligible. However, at w=5D a considerable stress acts on trench wall due to suction in water above the crown. Therefore, it can be concluded that CFX can simulate the stress condition on the trench wall which could not be done using Abaqus CEL.

The suction above the riser also has some effects on trench formation and instantaneous velocities of clay. Figure 3.5 shows the shape of the trench and instantaneous velocity vectors obtained from CFX analysis. At a large $\hat{w}$ (e.g. $\hat{w}$=3 or 5) the suction in water pulls the clay particles towards the crown of the riser that enhances formation of circular shaped instantaneous velocity vectors in CFX. In CFX simulation, the suction above the crown could also promote the backflow mechanism and speed up the closure of trench walls. The CFX simulation of clay velocity vectors even at large $\hat{w}$ is consistent with centrifuge test results of Hu (2010).

The CFX analysis shown in Fig. 3.3 takes only 104 minutes with a 3.2 GHz Intel Core i5 processor and 8 GB RAM. A same analysis is performed using Abaqus CEL (not shown here), which takes approximately23hourson the same computer (i.e. CFX is 13 times faster than CEL). One of the main advantages of the CFX Model-III is that the finer mesh near the riser moves at same velocity of the riser. However, in CEL the mesh is fixed which cannot be moved. The difference between solution techniques of these two numerical programs is also the cause of significant variation in computational time. It is

to be noted here that RITSS technique developed at the University of Western Australia is also computationally intensive and takes several days to analyze this type of problem (Barbosa-Cruz and Randolph 2005). In summary, the present CFX modeling is computationally very efficient as compared to other large deformation FE analyses.

3.5 Parametric study

As shown in previous sections, CFX can successfully simulate the penetration resistance. Moreover, the proposed CFX Model-III is computationally very efficient. This model is used for a parametric study.

3.5.1 Uniform s_{u0}

In the parametric study for uniform s_{u0}, the following parameters are kept constant: D=350 mm, γ_{sat}=16.31 kN/m^3, and v=60 mm/s, while the value of f_2 and $s_{u0}$are varied.

a)Effects of f_2 - uniform s_{u0}

Figure 3.6 shows the variation of N_p with $\hat{w}$ for four different values of f_2 (0.01, 0.2, 0.5 and 1.0) and s_{u0}=3.7 kPa. The penetration resistance increases with f_2. At shallow depths, these results are comparable with previous studies (e.g. Wang et al. 2010: ideal soil without rate and softening effects). At $\hat{w}$=5, N_p=9.33 and 10.45 for f_2=0.01 and 1.0, respectively. Note that, at this $\hat{w}$ the suction in the cavity above the riser increases the magnitude of N_p.

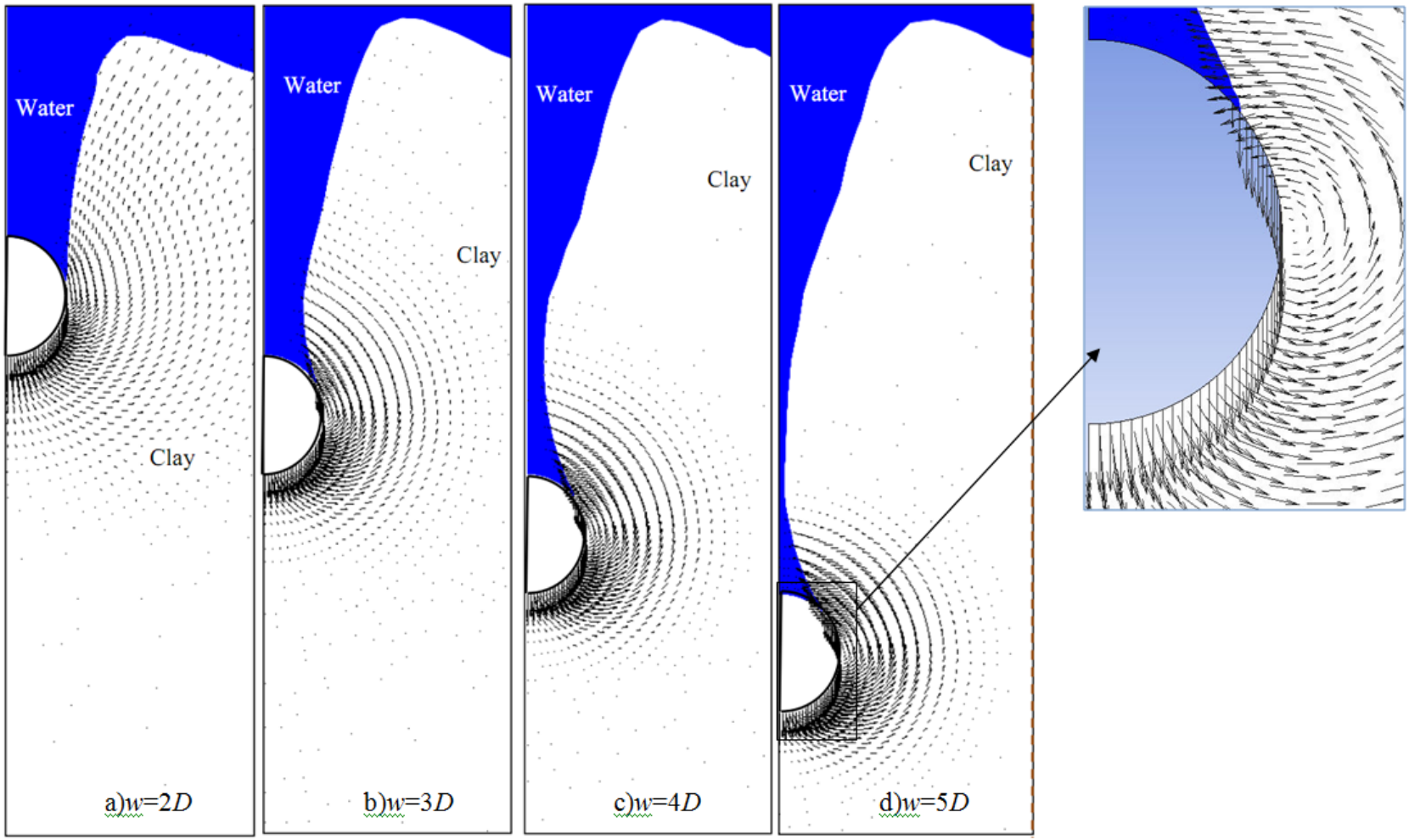

Figure 3.5: Velocity vectors and trench formation at different penetration depths

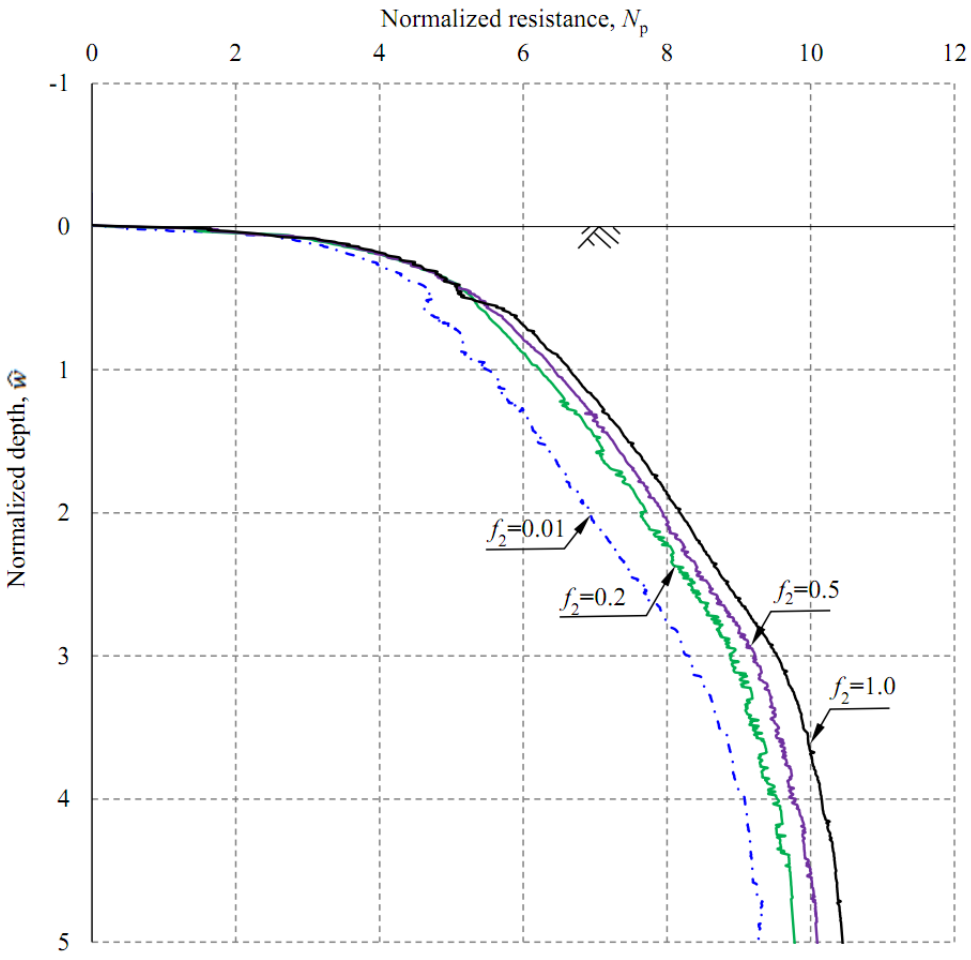

Figure 3.6: Effects of f_2 on pipe penetration resistance for s_{u0}= 3.7 kPa

b) Effects of s_{u0}

Figure 3.7 shows the variation of N_p for three different values of uniform s_{u0}. The magnitude of N_p increases with decrease in s_{u0}. Martin and White (2012) conducted FE analyses of pipes in wished in place configuration and showed that N_p increases with a normalized parameter $\gamma' D/s_{u0}$. The values of $\gamma' D/s_{u0}$ for the analysis presented in Fig. 3.7 are 1.0 and 0.46 for s_{u0}= 2.3 and 5 kPa, respectively. At $\hat{w}$=5, N_p=10.94 and 9.69 for s_{u0}= 2.3 and 5 kPa, respectively. Although the analyses of Martin and White (2012) are for

some idealized conditions (full tension/no tension and smooth/rough), the calculated N_p in their study are comparable with the present study.

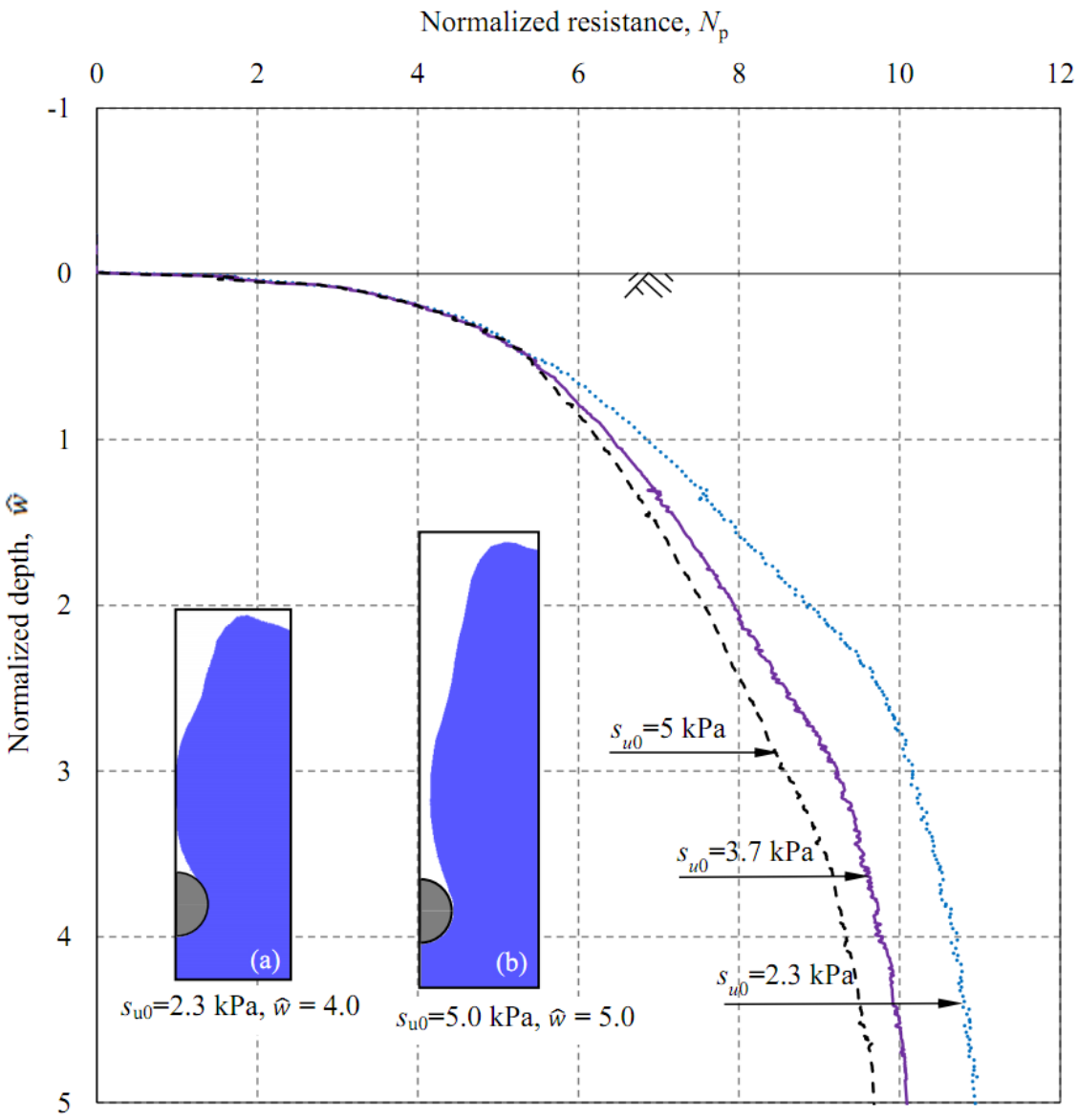

Figure 3.7: Effects of soil undrained shear strength on pipe penetration resistance for f_2 = 0.5

The insets of Fig. 3.7 show the shape of the trench for two penetration depths and s_{u0}. As shown in inset-a that for a low s_{u0}=2.3 kPa the wall of the trench touches the symmetry plane at $\hat{w}$=4 that results in almost a closed drainage condition for the water in the cavity just above the crown. Further penetration results in suction in this cavity and increases N_p. On the other hand, for s_{u0}=5 kPa there is still a wide space between the trench wall and symmetry plane even at $\hat{w}$=5 (inset-b in Fig. 3.7). In other words, the shape of the trench at the intermediate depths also influences N_p.

3.5.2 Linearly increasing s_{u0}

The analyses presented in the previous sections are for uniform s_{u0}. In deepwater, linear increase of s_{u0} with depth has been reported by many researchers (e.g. Puech et al. 2010; Jeanjean 2002; Dingle et al. 2008).The linearly increasing s_{u0} profile is defined as $s_{u0} = s_{um} + ky'$ (Fig. 3.1). The parameters used in the "base case" analyses for linearly increasing shear strength profile are: D=350 mm, v=60 mm/s, s_{um}=2.3 kPa, k=2.0 kPa/m, f_2=0.01 and γ'=6.5 kN/m^3. In the parametric study, only one parameter is varied while the other parameters are same as above unless otherwise mentioned.

In this study, a special technique in CFX has been developed such that the soil elements carry the initial value of s_{u0} although they move through the mesh. The parallel contours in Fig. 3.8(a) show that s_{u0}increases linearly with depth before penetration of the riser in the seabed. Fig. 3.8(b) shows the s_{u0} contours at w=5D, which are no longer parallel lines. The displaced soil elements carry the initial value of s_{u0}. For example, the soil elements just below the riser are pushed down from a higher location but still carry s_{u0} at original

locations. In summary, s_{u0} is properly carried by the displaced clay elements during the progress of analysis.

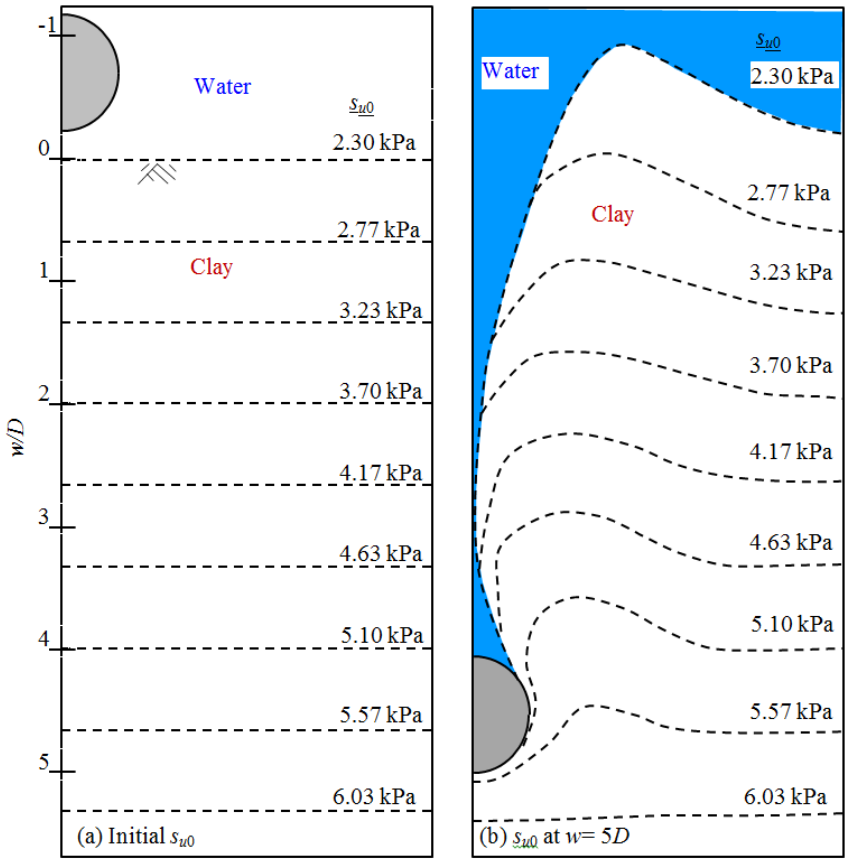

Figure 3.8: Contour of initial shear strength s_{u0}: (a) before penetration (b) at w= 5D

Figure 3.9 shows the comparison of N_p from CFX simulation for the base case of linearly increasing s_{u0} profile. In the inset of Fig. 3.9, the zone of suction (negative pressure) is shown for three different w (2.5D, 4D and 5D). Considerable suction is developed above the riser at large embedments (e.g. w=4D to 5D) that increases the penetration resistance. The effects of suction on N_p are discussed in detail in the previous sections for uniform s_{u0}.

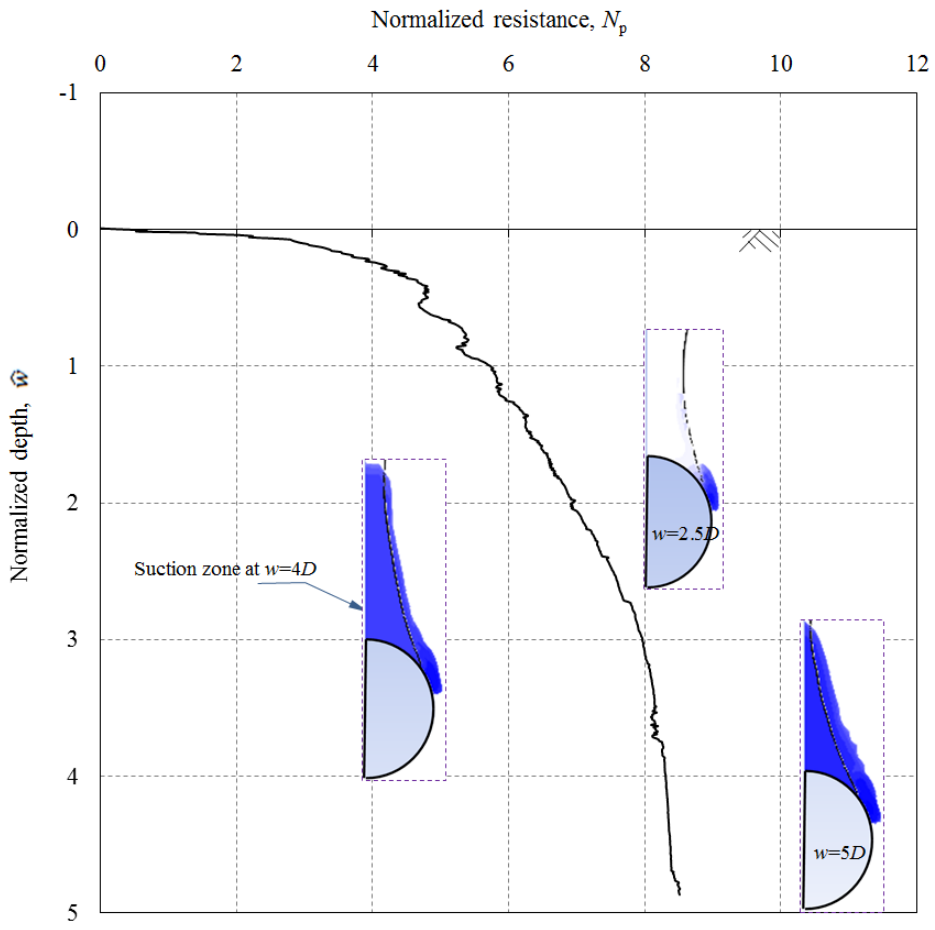

Figure 3.9: Penetration resistance for base case linearly increasing shear strength profile (s_{u0} = 2.3 + 2.0y′ kPa with f_2 = 0.01)

a) Effects of f_2

The effects of f_2 on N_p for linearly increasing s_{u0}profile are shown in Fig. 3.10. The normalized penetration resistance increases with increase in f_2. At $\hat{w}$=5, N_p=8.5 and 9.4 for f_2=0.01 and 1.0, respectively.

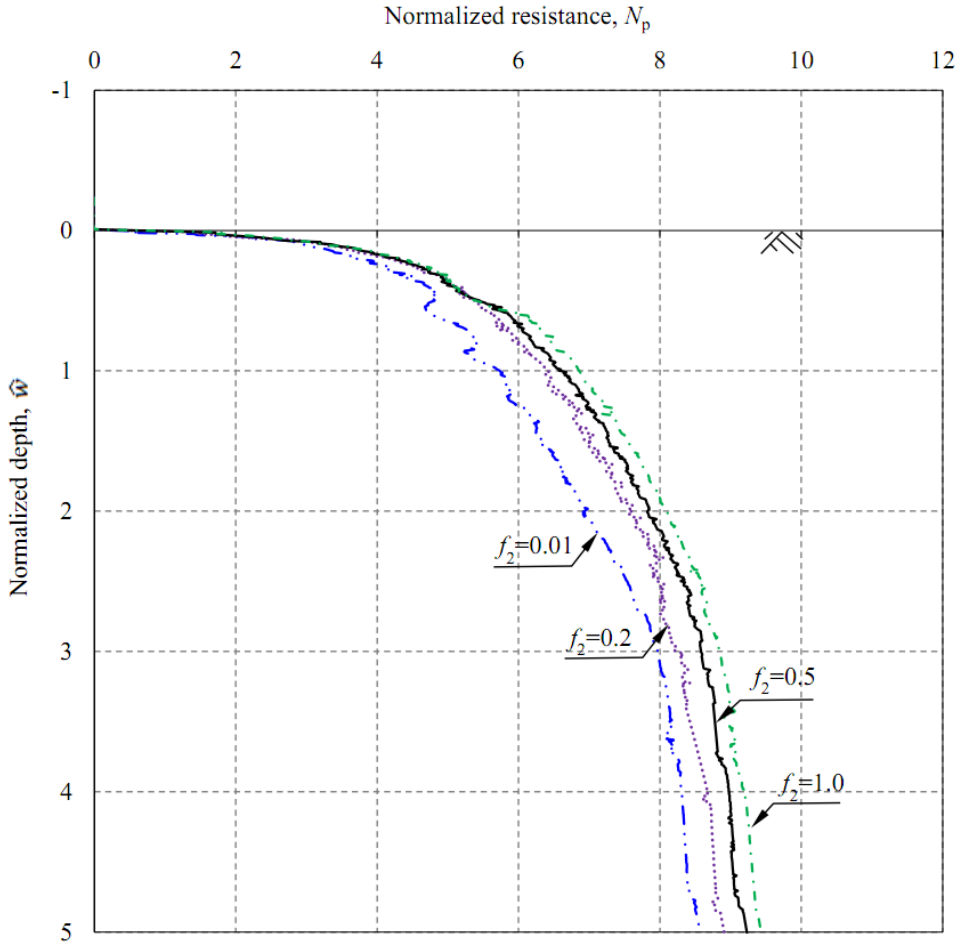

Figure 3.10: Effects of f_2 on penetration resistance for linearly increasing shear strength profile

b) Effects of s_{um}

The mudline shear strength might vary from zero to several kPa (e.g. s_{um}=2.0 kPa in Langford and Aubeny 2008; s_{um}=3.7 kPa in Aubeny et al. 2008; s_{um}=0 in Hu 2010; s_{um}=4.3 kPa in Clukey et al. 2011). Figure 3.11 shows the variation of N_p for three different values of s_{um} (=1.0 2.3, 3.7 kPa) with f_2=0.5. As shown in this figure that with increase in s_{um} the normalized penetration resistance decreases. The insets of this figure show the shape of the trench. When s_{um}=3.7 kPa, the trench is open even at $\hat{w}$=5 (see

inset-b). However, the face of the trench touches the symmetry plane for a low s_{um}=1.0 kPa at $\hat{w}$=3 as shown in the inset-a. The water in the cavity above the crown is hydraulically isolated and therefore suction will develop during further penetration, which also contributes to the higher N_p for s_{um}=1.0 kPa.

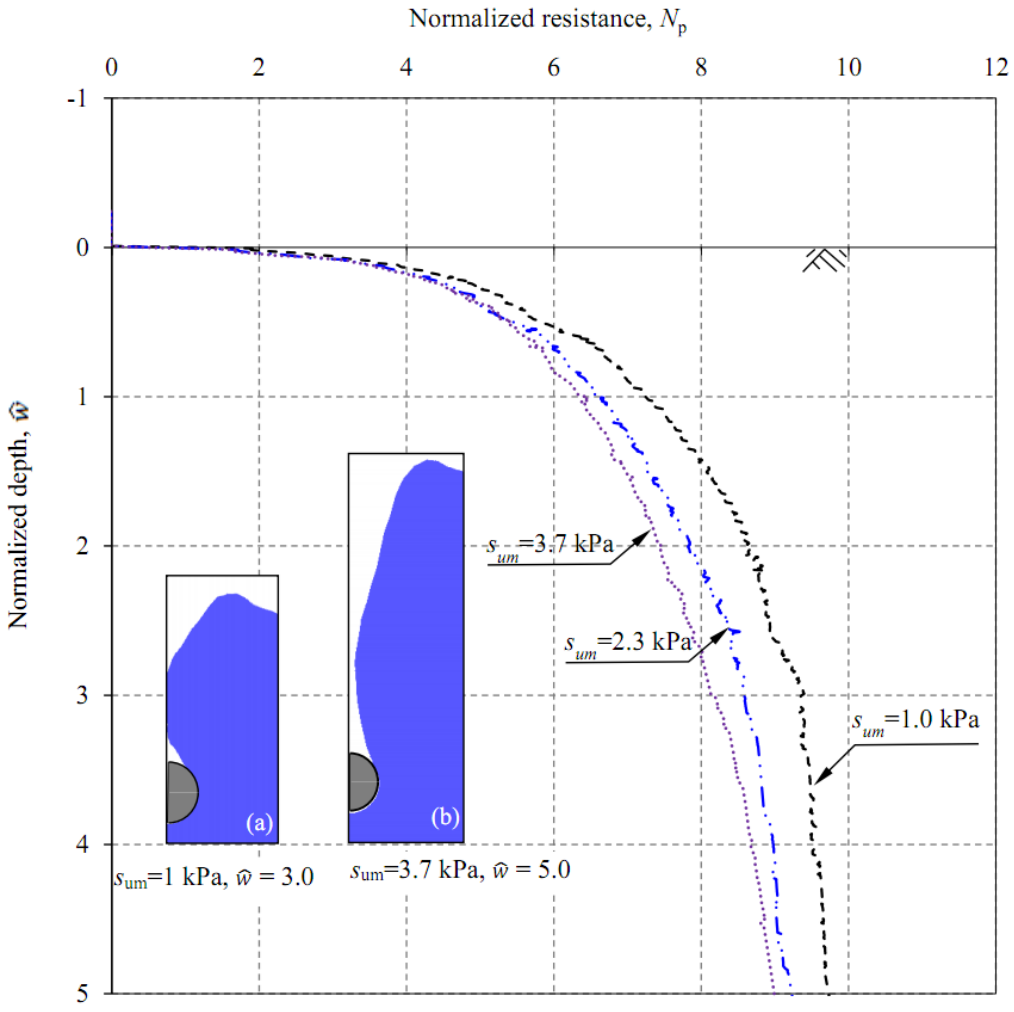

Figure 3.11: Effects of mudline shear strength on pipe penetration resistance (f_2 = 0.5; k = 2 kPa)

c) Effects of shear strength gradient, k

The shear strength gradient (k) could vary widely in deepwater offshore clays (e.g. Fugro 1999; Jeanjean 2002). Model tests were also conducted in the past for a wide range of k. For example, Aubeny et al. (2008) conducted model tests in kaolin clay of uniform s_{u0} (k=0) of 3.7 kPa, while Langford and Aubeny (2008) conducted a series of model tests using a high plastic marine clay from the Gulf of Guinea with k=13 kPa/m and s_{um}=2.0 kPa (i.e. s_{u0}=2.0+13y' in kPa). Similarly, Hu (2010) conducted centrifuge modeling varying k between 1.39 and 5.19.

Figure 3.12 shows the variation of N_p for four different values of k. The other soil parameters used in these analyses are s_{um}=2.3 kPa/m and f_2=0.5. Very small variation in N_p is obtained up to $\hat{w}$=0.75. This is consistent with the small strain FE analyses of Aubeny et al. (2005), who showed that at shallow embedment (w≤0.5) the normalized penetration resistances fall into a very narrow range for uniform and linearly increasing s_{u0}. For $\hat{w} \geq 0.75$, the higher the value of k the lower the N_p. This trend is also similar to previous studies (Morrow and Bransby 2010; Martin and White 2012), although their analyses are for different soil properties and riser-soil interface conditions.

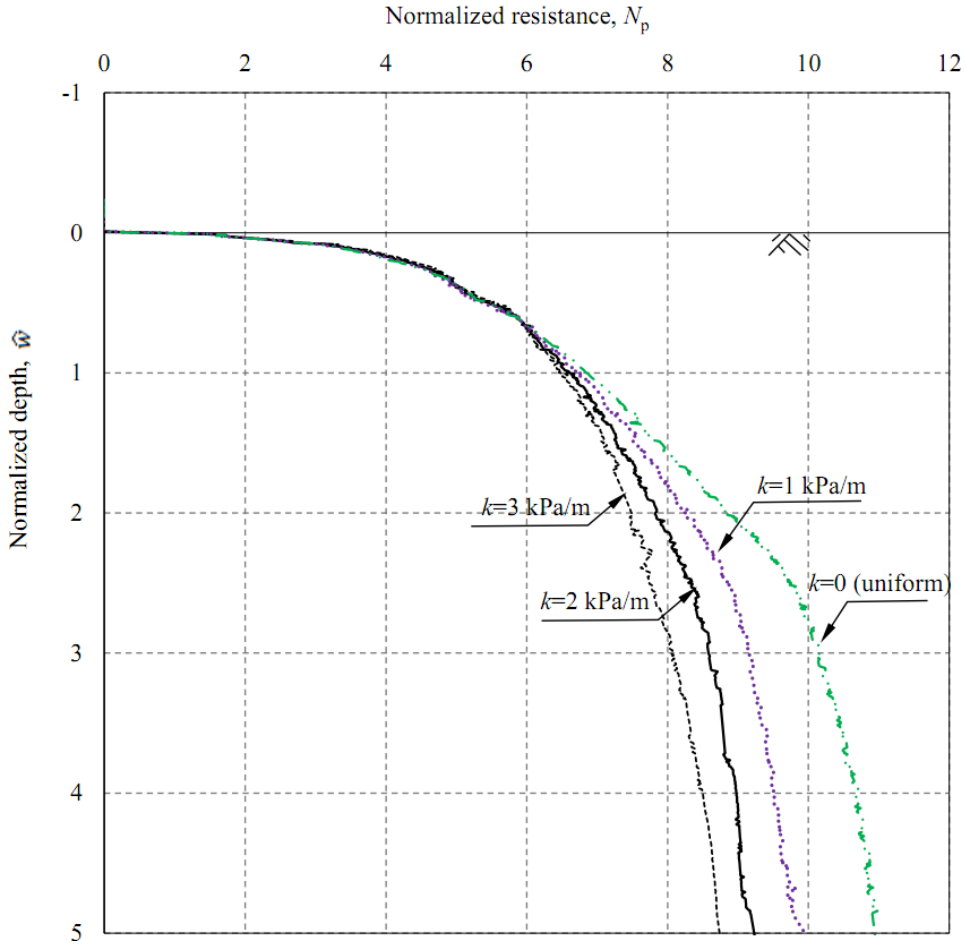

Figure 3.12: Effects of shear strength gradient on penetration resistance (f_2 = 0.5; s_{um} = 2.3 kPa)

3.6 Chapter summary

The penetration of steel catenary riser and other cylindrical objects, such as offshore pipelines or T-bar penetrometer, in soft clay seabed is of practical importance in many deepwater oil and gas development. Finite element (FE) analyses of these large deformation problems are computationally very expensive. Water can also play a significant role through development of suction behind the riser. Keeping in mind two critical issues, namely the computational cost and modeling of suction, a numerical

modeling technique is developed using the computational fluid dynamics (CFD) approach. The CFD modeling is performed using ANSYS CFX 13.0 software. Among the three different types of CFX models developed in the present study, the 'subdomain' modeling techniques is found to be more efficient. It is shown that CFX can successfully simulate the penetration of riser or pipeline in soft clay seabed. The main advantages of the present CFX modeling over existing large deformation finite element modeling are: (i) the CFX can simulate suction and (ii) the CFX modeling with a subdomain is computationally very efficient.

Chapter 4

Modeling of Suction and Trench Formation at the Touchdown Zone

4.1Introduction

Steel catenary risers (SCR) are pipes that connect the seabed systems to the flexible floating production systems (FPS) such as Floating Production Storage and Offloading vessels (FPSO), semi-submersible and SPARs, which are widely used in deepwater oil and gas production. The SCR are usually suspended from FPS to the seabed in catenary shape. The riser-seabed-water interaction near the touchdown zone significantly influences the design of SCR, because this is one of the places of high stress concentration and possible fatigue damage. In conventional analysis, the seabed is modeled using simple linear springs with or without damping. Large-scale field and indoor tests (e.g. Bridge et al. 2003; Hodder and Byrne 2010; Wang et al. 2014), reduced-scale centrifuge tests (e.g. Elliott et al. 2013a & b, 2014; Hu 2010) and small-scale laboratory tests (e.g. Bridge 2005; Aubeny et al. 2008; Langford et al. 2008a & b) were conducted in the past to understand this behaviour.

The vertical penetration and uplift of the riser are two of the main loading phenomena at the touchdown zone. The vertical penetration of a cylindrical body, such as a section of riser, pipeline or a T-bar penetrometer, has been examined by many researchers. Previous research on modeling of vertical penetration of pipelines can be categorized into three groups: (i) theoretical modeling based on bearing capacity equations, upper and lower bound plasticity models and slip-line field theory (e.g. Small et al. 1972; Murff et al.

1989; Aubeny et al. 2005; Zhao et al. 2009), (ii) small and large-scale physical modeling, (Dunlap et al. 1990;SINTEF 1986a, b; 1987; AGA/PRC 1992; Cheuk et al. 2007; Cardoso et al. 2010; Dingle et al. 2008; Hu 2010; White and Dingle 2011) and (iii) numerical analyses. The numerical analyses are performed using small strain FE modeling techniques in Lagrangian framework (Aubeny et al. 2005; Bransby et al. 2008; Zhao et al. 2010; Martin and White 2012), finite difference approach (Morrow and Bransby 2010), and also recently introduced large deformation FE modeling techniques (Barbosa-Cruz and Randolph 2005; Merifield et al. 2009; Wang et al. 2010; Shi et al. 2011; Tho et al. 2012; Chatterjee et al. 2012). The penetration behaviour is discussed in Chapter 3 and is not repeated here.

Similar to vertical penetration, physical modeling was also conducted in the past for uplift (e.g. Bridge 2005; Hu 2010; Giertsen et al. 2004). The numerical modeling of uplift is very limited. Most of the theories and numerical models for uplift are developed from modeling of horizontal plate anchors (Merrifield et al. 2001, 2003; Thorne et al. 2004). Martin and White (2012) conducted FE analyses of 'wished-in-place' pipes embedded in clay at different depths for full (unlimited) and no interface tensions. For no tension condition, zero (for smooth) and small (for rough) uplift resistance was calculated for shallow embedments (e.g. less than half a diameter of the pipe) because the suction under the pipe is not modeled. The formation of trench due to uplift was not examined in this study. Significant soil strength degradation occurs if the riser separates from the seabed (breakout) during unloading leaving a trench near the mudline, because in the subsequent penetration, the riser moves through the trench to the clay underneath (Clukey et al. 2007). Hu (2010) examined this effect through centrifuge modeling and showed that the

water entrainment during re-penetration increases the degradation of soil strength. Therefore, numerical simulation of the motion of the riser through water to the seabed better represents the condition in this zone, instead of cycling only in clay or clay and void.

In this chapter the discussion is mainly focused on uplift resistance, although both penetration and uplift are numerically simulated. This chapter is organized in the following way. First, the observed response in model tests is presented. Second, the CFX modeling including the fundamental concepts related to riser-seabed-water interaction analyses are discussed. Third, as the shear strength of soil significantly influences the force-displacement behaviour, the modeling of soil and its implementation in CFX are discussed. Fourth, the performance of the present numerical model is shown by comparing the results with available empirical models based on experimental results and also with FE analysis. Finally, a parametric study is conducted to show the effects of various parameters.

4.2 Two-dimensional model test results

A series of model tests were conducted under the Catenary Riser-Soil Interaction Model for Global Riser Analysis (CARISIMA I) Joint Industry Project (JIP) using clay from a site in Onsøy, Norway, a marine clay with geotechnical properties similar to deepwater Gulf of Mexico clay (Marintek 2000a, b). To show the trend, the force-displacement curves for 3 uplift tests are shown in Fig. 4.1. In these tests, a 101.6 mm diameter and 406.4 mm long pipe section was pushed in the virgin clay seabed to 0.5D depth in undrained condition. The undrained shear strength of the seabed increases linearly from

an average value of 1.5 kPa at the mudline at a rate of 12.5 kPa per meter depth (Bridge 2005). After 12 hours consolidation under 100 N vertical load, the pipe was pulled upward at different speeds (v).

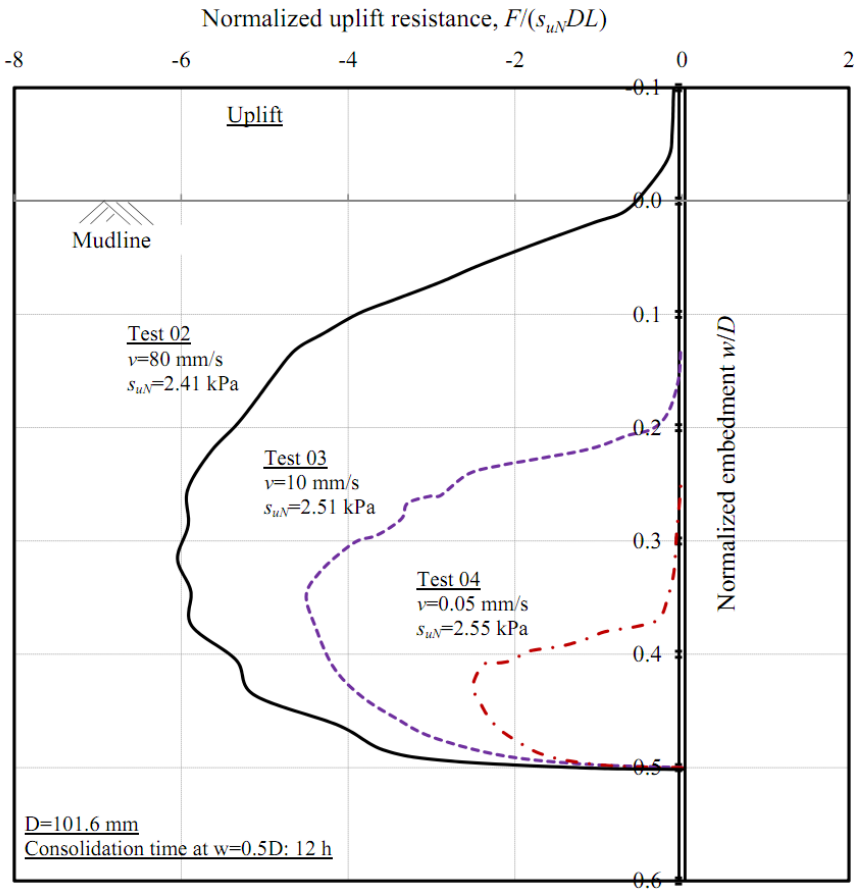

Figure 4.1: Uplift resistance in CARISIMA Phase-I test (Redrawn from Bridge, 2005)

The negative values of normalized resistance $F/(s_{uN}DL)$ in Fig. 4.1 represent the uplift resistance, where F is the vertical resistance, D and L are the diameter and length of the pipe section, respectively, and s_{uN} is the undrained shear strength of clay. During the vertical movement of the riser, the mobilized undrained shear strength (s_u) of a soil element depends on mode of shearing, strain rate, strength degradation and the location of

the soil element. As s_u is not constant, the penetration and uplift resistance have been normalized by s_u at different conditions in the past, which will be discussed in the following sections. The values of s_{uN} used in Fig. 4.1 are obtained from Bridge (2005). The use of different s_{uN} will not change the general trend of the curve although the magnitude of normalized resistance will be different. In the vertical axis of Fig. 4.1, w represents the depth of pipe invert. Figure 4.1 shows that the uplift resistance is significantly influenced by v. Upon upward displacement, the uplift resistance increases gradually, reaches to the maximum and then decreases. The maximum uplift resistance also increases with v. Moreover, the depth at which the pipe separates from the seabed depends on v. For example, the riser separates from soil, leaving a trench, at w/D=0.18 in Test 03, which is very different from Test 02 and Test 04. In Test 02, the uplift resistance is measured even above the mudline.

In the STRIDE (Steel Risers in Deepwater Environments) JIP, similar two-dimensional small-scale model tests were performed. The uplift tests were conducted in existing trenches, which were created by pushing a pipe to a depth of 0.5D. Tests were conducted in high plastic soft clay from the Watchet Harbour. Bridge (2005) presented a large number of test results and showed a very good comparison between CARISIMA and STRIDE 2-D test results.

In summary, the STRIDE-2D, CARISIMA, and other model tests (e.g. Aubeny et al. 2008; Langford and Aubeny 2008a & b) provide some valuable insight into the mechanism to develop a riser-seabed-water interaction model. Empirical models have been proposed in the past in the form of P-y curve based on model test results and field observation (Bridge et al. 2004; Aubeny and Biscontin 2009; Randolph and Quiggin

2009). These models are also used to calculate the response of riser (e.g. Nakhaee and Zhang 2010; Ting et al. 2011; Li and Low 2011; Shiri and Randolph 2010). Although these models are simple, a number of empirical parameters are required to define the *P*-*y* curve, especially for uplift as discussed in the following sections.

4.3 Problem definition

A riser section of diameter D is placed in water above the mudline at a distance y_w (Fig. 4.2), which is then displaced vertically at a velocity v. To eliminate buoyancy effect of water, the weight of the riser is assumed to be equal to the weight of the riser section filled with seawater. Two types of variation of initial undrained shear strength (s_{u0}) are considered in this study: (i) uniform s_{u0}, and (ii) linearly increasing s_{u0}. After penetration to the desired depth ($0.5D$), the riser is pulled up at a constant velocity v.

4.4 CFD simulation

The numerical simulations are performed using ANSYS CFX 13.0.

4.4.1 Fundamental concepts

In ANSYS CFX, the domain is first discretized into three-dimensional mesh. The governing equations are solved adopting a solution methodology based on finite volume, which are constructed using the discretized mesh. The force-displacement behaviour is modeled using the Navier-Stokes equations (also known as momentum equation), which has been developed applying Newton's Law ($F=ma$) to fluid elements. Here F is the force, m is the mass and a is the acceleration. The momentum equation is also

supplemented by the mass conservation equation. The forcing term (F) is the sum of gravitational force (F_{grv}), pressure force (F_{press}), viscous force (F_{visc}).

$$ma = F_{grv} + F_{press} + F_{visc} \quad (1)$$

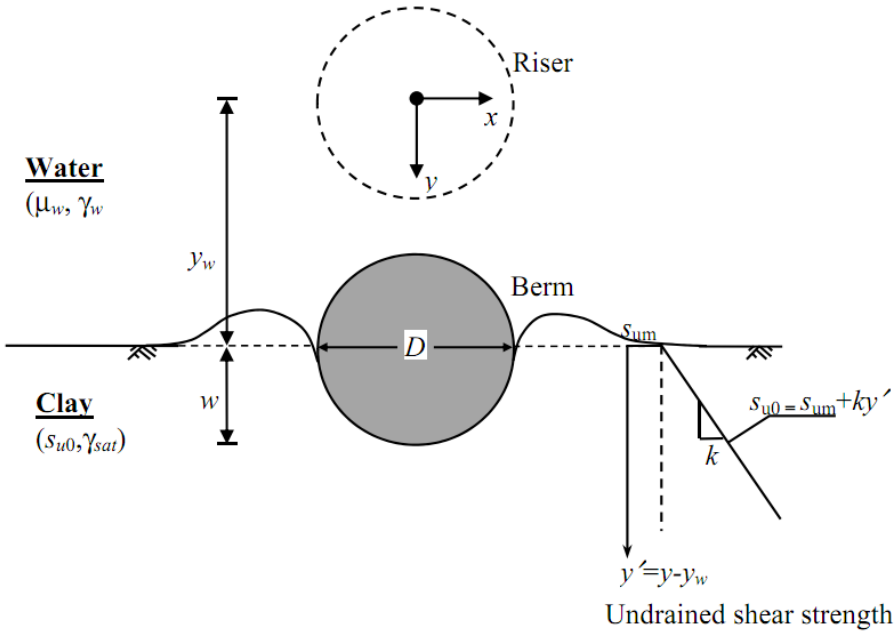

Figure 4.2: Problem definition

The gravitational force F_{grv} (=mg) is same as it is in solid mechanics, where g is the gravitational acceleration. Pressure (p) is the normal stress on the surface of the control volume, which is analogous to the normal stresses in solid mechanics. The pressure gradient ∇p is used to calculate F_{press} as $F_{press} = -\nabla p dV$. The pressure change may be caused by external sources such as movement of the riser. The viscous force F_{visc} is caused by the shear stress acting parallel to the surface. It is similar to frictional force in the solid mechanics. Similar to F_{press}, shear stress gradient ($\nabla\tau$) is used to calculate $F_{visc} = \nabla\tau dV$.

In this study, the parameters required in CFX to calculate F_{grv} and F_{press} are given by density of soil and water, and the boundary conditions including the displacement of the riser. The most critical component of the present CFX modeling is the definition of τ, which must be consistent with the undrained shear strength of clay (s_u). The CFX uses the coefficient of dynamic viscosity (μ) as an input parameter to calculate τ. The definition of μ as a function s_u are discussed in the following sections. In summary, assigning these input parameters properly, the force-displacement behaviour of the riser can be calculated.

4.4.2 CFX model setup

Figure 4.3 shows the CFX model setup. CFX allows only three-dimensional modeling, and therefore the analyses are performed for only one element of 10 mm in the out of plane direction. The riser (D=350 mm) is modeled as an impermeable wall. The center of the riser is placed in water at y_w=1.0D above the mudline. An inner subdomain, shown by the shaded zone near the riser, is created. No mesh deformation is allowed in the subdomain and therefore the shape and size of the mesh does not change with displacement of the riser. Moreover, it moves with the riser at same velocity. However, soil and water as Eulerian materials flow through the mesh both in subdomain and outside the subdomain. Based on previous studies (e.g. Dutta et al. 2014), the radial thickness of the subdomain of 1.5D is considered because the strains in the soil elements outside this zone are not very significant. This modeling approach increases the computational efficiency and robustness of the simulation significantly as discussed in Chapter 3. It has also some other advantages as discussed in the following sections.

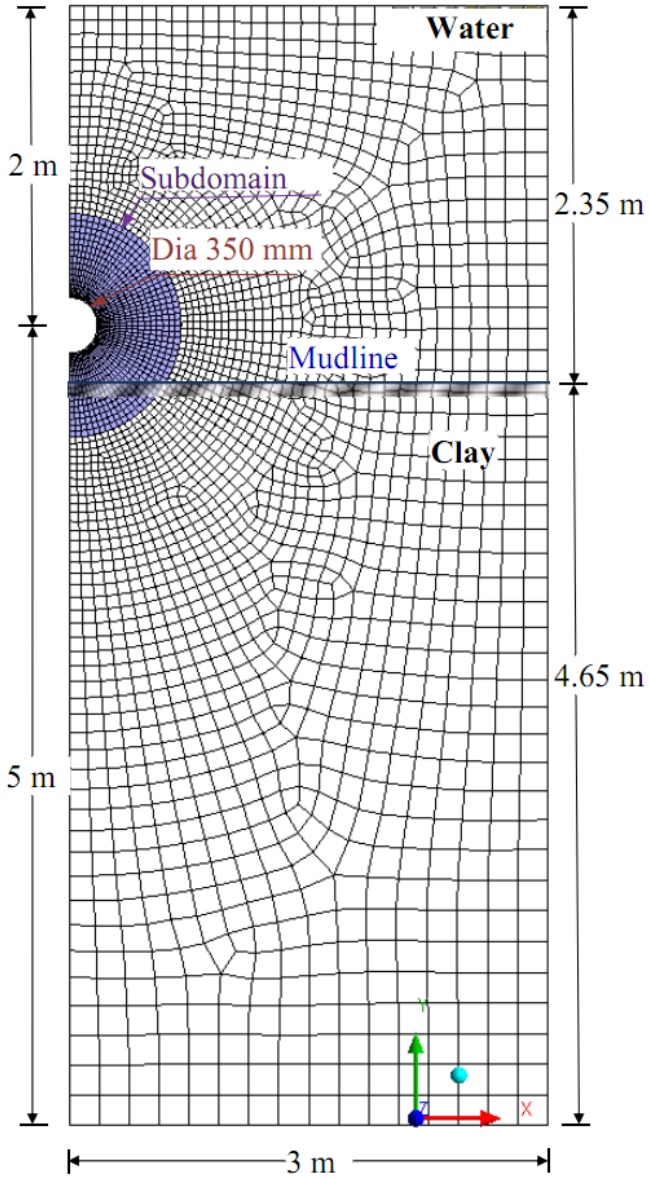

Figure 4.3: Development of CFX model in ANSYS

As shown in Fig. 4.3, the upper 2.35 m (=6.7*D*) of the domain is water and the lower 4.65 m (=13.3*D*) is clay. The right vertical boundary is placed at 3 m (=8.6*D*) from the center of the riser. The boundaries are placed at sufficiently large distance from the riser

and therefore no boundary effects are observed. Taking the advantage of symmetry, only the right half of the domain is modeled.

The bottom and all the vertical faces are defined as walls, which are solid impermeable boundaries to fluid flow. No-slip boundary condition is applied to the bottom wall and riser surface, and therefore the velocity of the Eulerian material (soil/water) next to these walls is zero. Free-slip boundary condition is applied on the right vertical wall. On the other three vertical faces, symmetry plane boundary conditions are applied, which implies that the flow of Eulerian material (soil/water) on one side of the plane is a mirror image of the flow on the opposite side. “Unspecified mesh motion” option in CFX is used for the vertical walls. This setting allows the mesh node on these walls to move in the vertical direction preserving the quality of mesh during the displacement of the riser. The top of the water is defined as an opening to allow water to flow in and out of the domain. If one wants to compare with typical FE modeling, the above boundary conditions represent rollers in vertical faces and hinges at the bottom. Vertical displacement (same as the displacement of the riser) is assigned for the interface between the subdomain and surrounding soil/water without giving any additional interface conditions such as no-slip or free-slip conditions. This allows inward and outward flow of soil and water through this interface maintaining same fluid flux in both side of the interface.

Both clay and water are modeled using homogeneous multiphase Eulerian materials. The interface between clay and water that represents the mudline is defined by a step function through CFX Command Language (CCL) — a declarative language in CFX for enhanced simulation without writing and linking separate external Fortran routines. The clay and water in the domain are defined using the volume fraction tool. In the elements above the

mudline, the volume fraction of water is set to 1 and the volume fraction of clay is 0. On the other hand, in the elements below the mudline the volume fraction of water is 0 and volume fraction of clay is 1.

The mesh is formed using the options available in the CFX. Very fine mesh is used near the riser and the size is increased with distance from the riser. The maximum dimension of the mesh just outside the riser surface is 10 mm. The riser is displaced vertically specifying the motion of the nodes on riser wall and subdomain. Mesh sensitivity analyses are performed with coarser and finer mesh than the one shown in Fig. 4.3. Based on these analyses the optimum mesh (Fig. 4.3) is selected for further analyses.

4.5 Modeling of soil

In deepwater, very soft clays of low s_{u0} and high plasticity index are generally encountered near the mudline (Fugro, 1999). The s_{u0}might be constant or increase linearly with depth. The linear variation of s_{u0} is defined as $s_{u0} = s_{um} + ky'$, where s_{um} is the undrained shear strength of clay at the mudline, k is the strength gradient and y' is the depth of the soil element (Fig. 4.2). Fugro (1999) reported typical values of s_{um} (1.2–2.6 kPa) and k (0.8–1.6 kPa/m) for deepwater clays in the Gulf of Mexico, West Europe and West Africa. Numerical analyses and laboratory tests for higher values of s_{um} up to 10 kPa and k of 13 kPa/m were also performed to show the effects of these parameters (e.g. Chatterjee et al. 2012; Langford and Aubeny 2008b). A comprehensive discussion on estimation of shear strength of soft clays in deepwater are available in Lunne and Andersen (2007) and Lunne et al. (2011).

The mobilized undrained shear strength (s_u) depends on rate of shearing. Also, the soil around the riser might experience significant plastic strain that could degrade the shear strength (e.g. Einav and Randolph 2005; Zhou and Randolph 2007). The effects of these two factors on s_u are incorporated as:

$$s_u = f_1 \times f_2 \times s_{u0} \quad (2)$$

where $f_1 = [s_u / s_{u0}]_{f_2=1}$ and $f_2 = [s_u / s_{u0}]_{f_1=1}$ are the effects of strain rate and softening, respectively.

4.6 Effect of shear strain rate

4.6.1 Geotechnical and fluid mechanics frameworks

There are two frameworks available in the literature to incorporate the effects of shear strain rate ($\dot{\gamma}$) on s_u, namely the geotechnical and fluid mechanics frameworks. In the geotechnical framework, the inverse hyperbolic, logarithmic and power law models are commonly used to capture the effects of $\dot{\gamma}$ (Einav and Randolph 2005; Lunne et al. 2011; Boukpeti et al. 2012a). These models show satisfactory performance for typical geotechnical engineering practice if appropriate values of model parameters are selected. Typical ranges of the model parameters are given by several authors based on experimental results (e.g. Boukpeti et al. 2012a; Lunne and Andersen 2007).

In the fluid mechanics approach, clay slurries or very soft clays are usually modeled using the Herschel-Bulkley model, in which the dynamic viscosity (μ) is defined as:

$$\mu = \frac{\tau}{\dot{\gamma}} = \frac{\tau_y + K(\dot{\gamma})^n}{\dot{\gamma}} \quad (3)$$

Where τ_y represents the minimum shear stress required for commencement of viscous flow (yield stress); *K* is the viscous property and the flow index (*n*) is a material property. As the geotechnical approach is used, the symbol τ_y is replaced by s_{uc}. Experimental evidences show that both *K* and τ_y increase exponentially with volumetric concentration of solid (C_{sv}) as $K = \alpha_1 e^{\beta_1 C_{sv}}$ and $\tau_y = \alpha_2 e^{\beta_2 C_{sv}}$ (O'Brien and Julien1988; Major and Pierson 1992), where α_1, β_1, α_2 and β_2 are material constants. That means, *K* can be assumed to be proportional to τ_y (or s_{uc}), for a given C_{sv}.

4.6.2 Laboratory test results

Because of faster penetration and pull-out, $\dot{\gamma}$ in soil near the touchdown zone could be significantly higher than $\dot{\gamma}$ in typical geotechnical laboratory tests, such as triaxial tests. Sheahan et al. (1996) conducted consolidated undrained triaxial tests and showed that the effects of $\dot{\gamma}$ on s_u increases at high strain rates. Biscontin and Pestana (2001) conducted vane shear tests at shear strain rates much higher than that used in common laboratory tests. From T-bar penetrometer and vane shear tests at various water contents, Boukpeti et al. (2012a) reported the effects for a wide range of $\dot{\gamma}$. To investigate the effects of high strain rates, Abelev and Valent (2013) conducted vane shear tests for a wide range of $\dot{\gamma}$ on sediments from the Gulf of Mexico. The undrained shear strengths reported in these studies are plotted in Fig. 4.4 in normalized form. In this figure, the data from Boukpeti et al. (2012a) are plotted in terms of $\dot{\gamma} / \dot{\gamma}_{ref}$, where $\dot{\gamma}_{ref} = 0.06\,\mathrm{s}^{-1}$. On the other hand the data from Biscontin and Pestana (2001) and Abelev and Valent (2013) are plotted in terms of ω/ω_{ref}, where ω is the angular rotation rate of the vane. The standard field vane shear tests

at ω=0.1°/s represent an approximate shear strain rate of 0.05 s^{-1} (Boukpeti et al. (2012a). Therefore, all data represent the effect of $\dot{\gamma}$ as they are normalized using reference values of similar range.

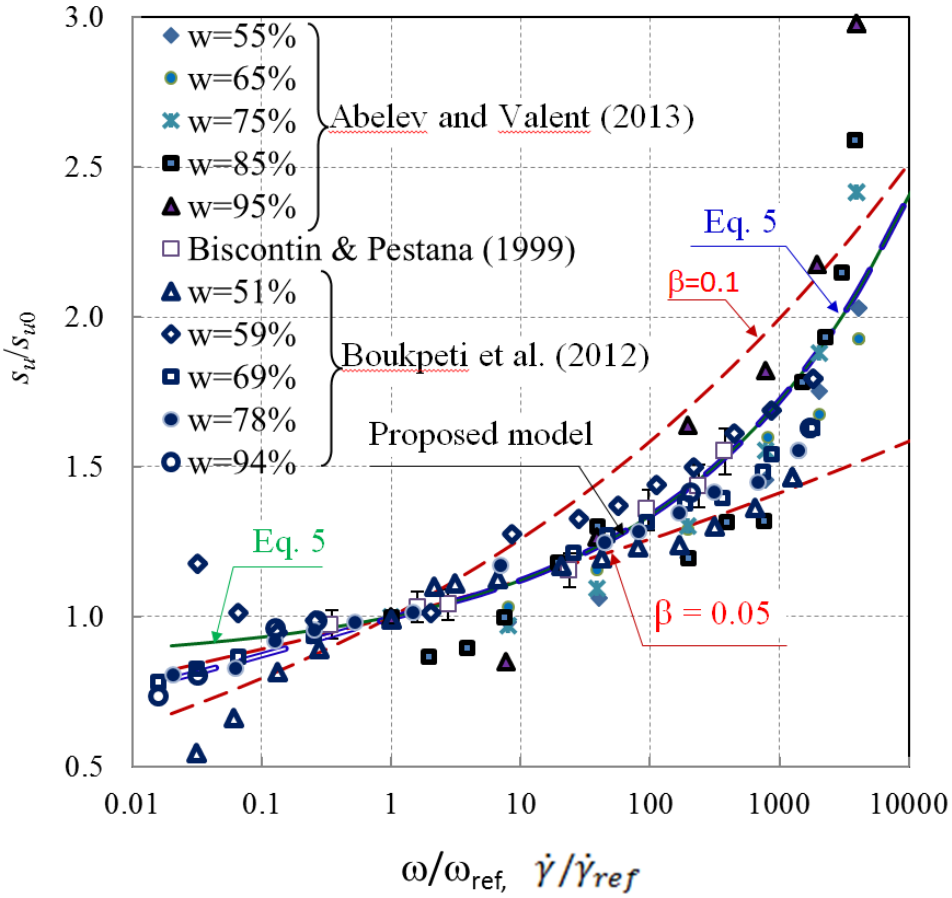

Figure 4.4: Strain rate effects on undrained shear strength

4.6.3 Power law model

One of the widely used model for strain rate effect is the power law model, $s_u / s_{u0} = (\omega / \omega_{ref})^{\beta} = (\dot{\gamma} / \dot{\gamma}_{ref})^{\beta}$, where β is a constant (0.05-0.1) (Boukpeti et al. 2012b). Two red dashed lines in Fig. 4.4 are drawn using the power law model with β=0.05 and

0.1. As shown, most of the data points are in between these two lines. However, a unique value of β cannot model properly the whole range of $\dot{\gamma}$. For example, consider Biscontin and Pestana (2001) tests data. The power law with β=0.05 can model properly the shear strength up to $\omega/\omega_{\text{ref}} = 20$. Above this strain rate, β=0.05 underestimates the shear strength, and to match the test results higher values of β is required. In other words, a constant value of β does not model the whole range of $\dot{\gamma}$ above $\dot{\gamma}_{ref}$. To fit these data, Abelev and Valent (2013) revised the power law with an additive term, which is similar to the Herschel-Bulkley model (Eq. 3).

4.6.4 Proposed unified model

A unified model is proposed in this study combining the power law and modified form of Herschel-Bulkley model. It is suggested to use the modified Herschel-Bulkley model at higher strain rates ($\geq \dot{\gamma}_{ref}$). As mentioned before, *K* can be assumed to be proportional to s_{uc}. Assuming $K = c_1 s_{uc}$, where c_1 is a material property, the variation of s_u with $\dot{\gamma}$ in a modified form of Herschel-Bulkley model can be written as:

$$s_u = s_{uc}(1 + c_1\dot{\gamma}^n) \tag{4}$$

Using the reference strain rate conditions ($s_u = s_{u0}$ at $\dot{\gamma} = \dot{\gamma}_{ref}$) it can be shown that $s_{uc} = s_{u0}/(1 + c_1\dot{\gamma}_{ref}^n)$. Now inserting s_{uc} in Eq. (4), the following expression is obtained.

$$\frac{s_u}{s_{u0}} = \frac{1 + c_1\dot{\gamma}^n}{1 + c_1\dot{\gamma}_{ref}^n} \tag{5}$$

Equation (5) represents the strain rate effects $f_1 = s_u/s_{u0}$ in Eq. (2) without any softening.

The undrained shear strength of clay in deepwater is usually obtained from T-bar, ball penetration, and vane shear tests. The operative shear strain rate of these equipment is usually higher than that used in typical laboratory triaxial tests. For example, Boukpeti et al. (2012a) showed that the operative shear strain rate for standard field vane is ~0.05 s^{-1} and for T-bar and ball penetration is 0.15 s^{-1}, although it depends upon rotation and penetration speed. On the other hand, $\dot{\gamma}$ is in the range of 3 to 14×10^{-6} s^{-1} in typical laboratory triaxial tests. Using $\dot{\gamma}_{ref} = 0.06\,s^{-1}$, they also showed that the strain rate dependent models reasonably fit their test data. As T-bar, ball and vanes are widely used in offshore geotechnical investigation, a reference shear strain of 0.05 s^{-1} is used in the present study, and s_{u0} represents the strength at $\dot{\gamma}_{ref}$.

The thick dashed line in Fig. 4.4 shows the variation of s_u/s_{u0} with $\dot{\gamma}$ for c_1=0.4 s^n using Eq. (5). As shown, Eq. (5) fits the test data better than the power law models for $\dot{\gamma} \geq \dot{\gamma}_{ref}$. Different relationships between c_1 and s_{uc} and also the variation of n might fit individual set of test results better. However, such attempt is not taken in this study considering other uncertainties in deepwater geotechnical characterization. Equation (5) is used to calculate f_1 for $\dot{\gamma} \geq \dot{\gamma}_{ref}$.

For $\dot{\gamma} < \dot{\gamma}_{ref}$, Eq. (5) calculates higher undrained shear strength (see Fig. 4.4) than test data and power law model. Not only the experimental results shown in this figure, a large number of previous studies showed that the power law can model reasonably s_u in this range of $\dot{\gamma}$. Therefore, the power law model (Eq. 6)

$$s_u / s_{u0} = \left(\dot{\gamma} / \dot{\gamma}_{\text{ref}}\right)^{\beta} \tag{6}$$

is used to calculate f_1 with β=0.06 for $\dot{\gamma} < \dot{\gamma}_{ref}$.

The performance of the combined model with power law and Eq. (5) is shown by the thick dashed line in Fig. 4.4, which shows that the proposed combined model fits the test results better than only the power law or Herschel-Bulkley model for a wide range of $\dot{\gamma}$.

4.7 Degradation of shear strength

The shear strength of clay sediments around the riser decreases during penetration and uplift due to strain softening. The degradation of undrained shear strength depends on remoulded sensitivity of the soil. Attempts have been taken in the past to model such complex process of degradation. Einav and Randolph (2005) proposed a simple model for undrained shear strength degradation as a function of plastic shear strain. This model has been used by various authors to simulate pipeline penetration in the seabed (Chatterjee et al. 2012; Wang et al. 2010). Similarly, Hodder et al. (2010) proposed a simplified model for progressive loss of shear strength using a triangular damage influence function, avoiding complete analysis of the zone of influence. While this method is very useful for modeling cyclic response, the variation of undrained shear strength with radial distance from the pipe is not incorporated.

For better visualization of the effects of strength degradation on uplift resistance and suction, a simple degradation model shown in Fig. 4.5 is used where the degradation is defined using three zones. The location of the riser at the end of maximum penetration depth (0.5*D*) is shown in this figure. The extent of soil failure mechanism from the riser and the variation of $f_2 = \left[s_u / s_{u0}\right]_{f_1=1}$ with distance are considered.

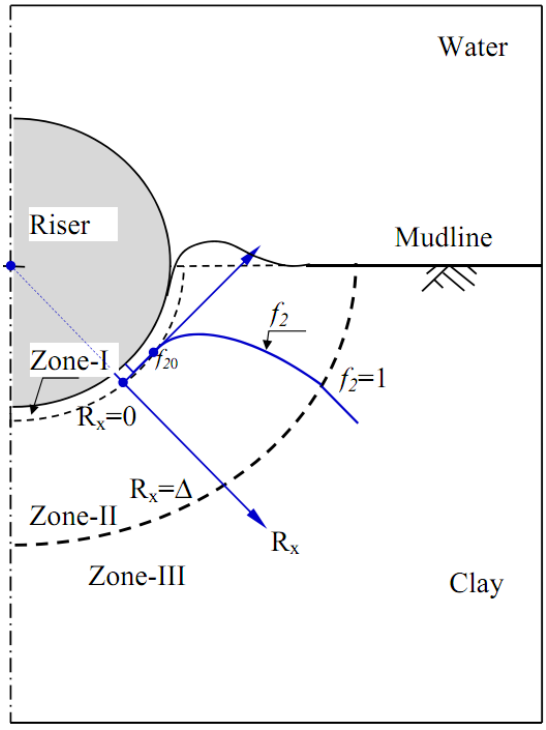

Figure 4.5: Degradation of undrained shear strength used in CFX model

A reduced shear strength is prescribed to a thin layer of soil (10 mm) near the riser (Zone-I), which can be considered as finite thickness interface elements. Note that finite thickness interface elements have been successfully used in previous studies to calculate the pullout capacity of suction caissons (Supachawarote et al. 2004) and also in slope stability analysis (Jostad and Andresen 2004). The interface shear strength is generally obtained by multiplying the undrained shear strength of soil by a factor α, where $0 \leq \alpha \leq 1.0$. In this study, a constant undrained shear strength s_{u_int}=0.4 kPa is used in this thin zone, which is then multiplied by strain rate effect f_1 to calculate mobilized s_u. As the size of the mesh does not change in the inner subdomain (Fig. 4.3), this shear strength could be easily assigned to the elements just outside the riser surface when the soil is in contact with the riser. Note that, the thickness of the first row of elements near the riser is

10 mm. When the soil is not in contact with the riser (e.g. at the level of mudline in Fig. 4.5), the face of the clay is identified using the clay volume fraction, and from that face to a distance of 10 mm an undrained shear strength of 0.4 kPa is assigned. After 10 mm radial distance, the value of $f_2$is increased using a parabolic function $f_2^2 = aR_x^2 + b$ and reached to f_2=1 (no degradation) at a distance of R_x=Δ. Using the boundary conditions f_2=f_{20} at R_x=0, and f_2=1 at R_x=Δ, the constants $a = (1 - f_{20}^2)/\Delta^2$ and $b = f_{20}^2$ are obtained. Now inserting *a* and *b* in the parabolic equation, $f_2 = \sqrt{(1 - f_{20}^2)(R_x/\Delta)^2 + f_{20}^2}$ is obtained. For simplicity, the average value $f_2 = (1 + f_{20})/2$ is used in the berm. Analyses are also performed with 15 mm and 20 mm thickness of Zone-I and no significant difference in penetration or uplift resistance is found.

In summary, this simple model shows that the maximum degradation occurs near the riser and the shear strength reaches to the original value at R_x=Δ. The location of the outer surface of the degraded shear strength zone (thick dashed line) remains constant during uplift and therefore the value of Δ is updated with each time increment during the analysis. The value of Δ=1.0*D* at the start of uplift (*w*=0.5*D*) is assumed for the "base case." However, the parametric study for different values of Δ is also conducted. For simplicity, the outer surface of Zone-II is assumed to be circular. The value of f_{20} depends on number of penetration-uplift cycles. After a number of cycles of loading-unloading it could be reduced to $1/S_t$, where S_t is the remoulded sensitivity. As only one cycle is simulated in this study, a value of f_{20}=0.45 is assumed based on numerical simulation of Dutta et al. (2014).

The large deformation FE analyses under monotonic loading show that the influence of shear strength degradation on penetration resistance is not very significant (Chatterjee et al. 2012, Dutta et al. 2012a & b). As in this study only one penetration-uplift cycle is simulated, the shear strength degradation effects during penetration is neglected. Detailed discussions on penetration behaviour are available in Dutta et al. (2014) and also in Chapter 3.

It is recognized that an improved model considering possible factors related to degradation might better simulate the response. However, with the proposed simple degradation model the advantages of CFD approach for modeling suction and uplift resistance are shown.

4.8 Soil parameters

Table 3.1 shows the parameters used in base case analysis, which are selected from a critical review of previous laboratory tests and proposed models for very soft clays in deepwater (e.g. Biscontin and Pestana 2001; Zhu and Randolph 2011; Boukpeti et al. 2012a; Abelev and Valent 2013).

4.9 Numerical results

The penetration and uplift resistances are presented in normalized form as $N_{pu}=F/s_{uN}D_eL$, where F is the penetration or uplift resistance, s_{uN} is the undrained shear strength used for normalization, D_e is the effective pipe diameter and L is the length of riser section (=10 mm). The undrained shear strength depends on mode of shearing (e.g. triaxial or simple shear), strain rate and depth (in linear s_{u0}). One should interpret the value of normalized

resistance carefully because s_{uN} at different conditions has been used in previous studies (e.g. Langford and Aubeny 2008; Zhu and Randolph 2010; Wang et al. 2010; Bridge 2005). In the present study, considering triaxial compression mode as the reference, s_{u0} at the invert of the riser ($s_{u0(i)}$) in triaxial compression stress condition at $\dot{\gamma}_{ref}$ is used for s_{uN}. Using Tresca hexagon in the deviatoric plane it can be shown that $s_{uN} = \frac{2}{\sqrt{3}} s_{u0(i)}$ (Smith and Griffiths 2004; Sousa et al. 2011; Tho et al. 2013). Following the concept of Gui and Bolton (1998) and assuming that the failure is occurred at a distance of half of the element size from the outer surface of the riser, the value of D_e can be calculated as 360 mm (=350 mm+2×10 mm/2) for 10 mm element size just outside the riser. If D (=350 mm) is used instead of D_e, the normalized penetration resistance will be increased by only 2.8%. In this study D_e is used. The depth of embedment is normalized as $\hat{w} = w/D_e$.

4.9.1 Performance of CFX modeling

In order to show the performance of the present CFX modeling, the base case is considered first. In this case, the riser is moved downward through water and penetrated into the seabed sediment of linearly increasing s_{u0} as s_{u0} (kPa)=2.3+3.6y'(in m) to a depth of 0.5D and then uplifted. A constant velocity of 20 mm/s is maintained in both penetration and uplift. The normalized penetration and uplift resistance curves are shown in Fig. 4.6.Details of Fig. 4.6 are provided in the following sections.

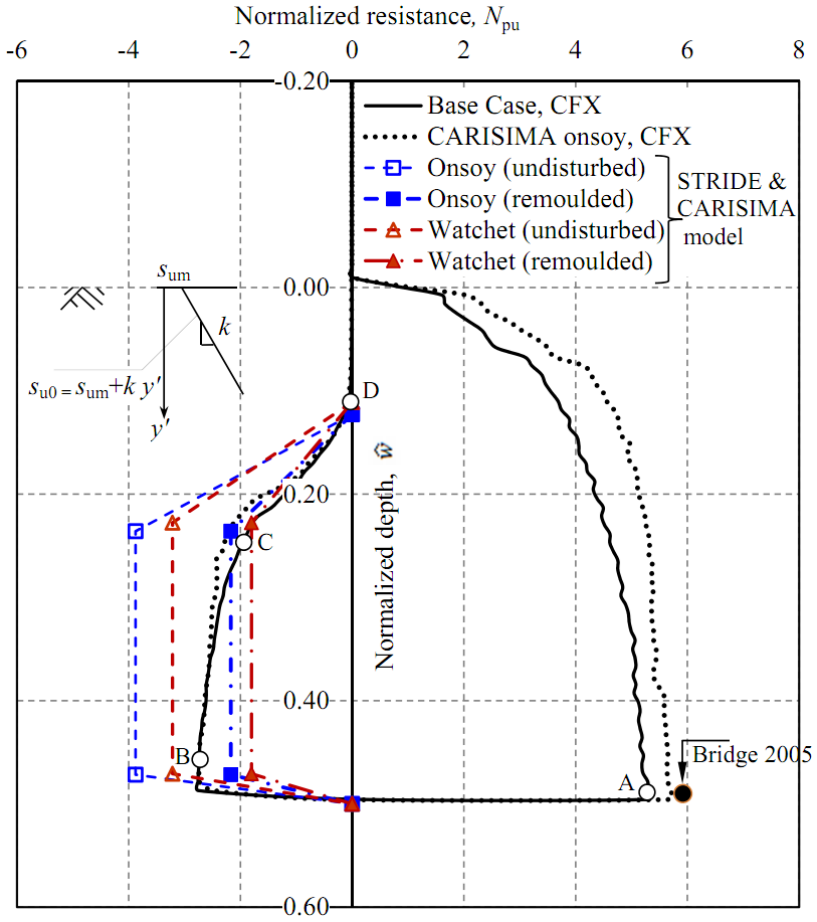

Figure 4.6: Normalized penetration and uplift resistance with depth for base case

4.9.2 Implementation of s_{u0} in CFX

As discussed in previous chapter, a special technique in CFX has been developed such that the soil elements carry the initial values of s_{u0} although they move through the mesh as Eulerian material. Figure 4.7(a) shows the contour of s_{u0} at w=0.48D during uplift.

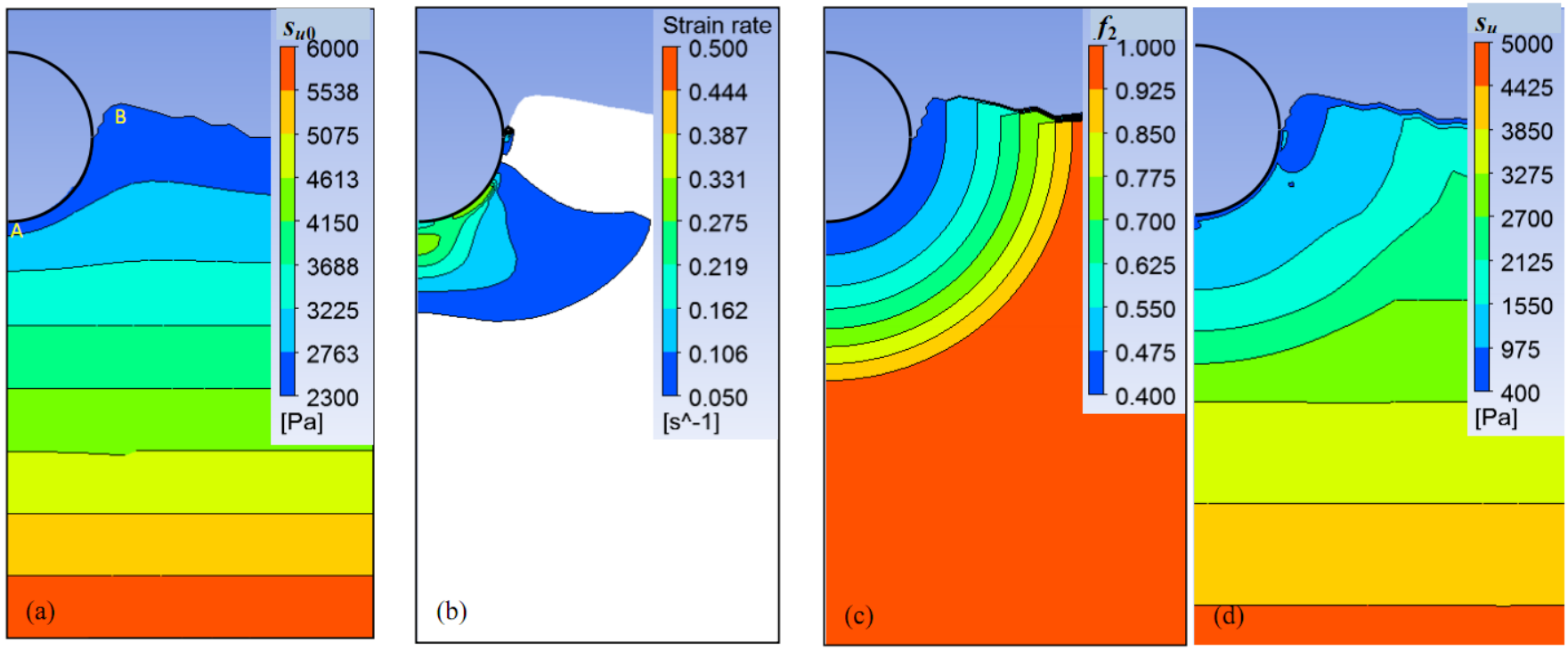

Figure 4.7: Undrained shear strength model implementation: (a) s_{u0}, (b) strain rate, (c) shear strength degradation, (d) mobilize s_u at w=0.48D during uplift

As shown, the displaced soil elements carry the initial value of s_{u0}. For example, the soil elements which were initially near the mudline are pushed under the pipe at point A or in the berm at point B still have the same value of s_{u0} although they are displaced to different locations. The mobilized s_u at a particular time is calculated with this s_{u0} using Eq. (2).

The variation of $\dot{\gamma}$ at w=0.48D during uplift is shown in Fig. 4.7(b). Note that this figure shows $\dot{\gamma}$ at this particular time. One soil element might have significant strain, but $\dot{\gamma}$ could be very small at this stage. For example, the soil element near or in the berm might have significant strain accumulation but at the current instance $\dot{\gamma}$ is negligible. Once the value of $\dot{\gamma}$ is known, f_1 is calculated using Eq. 5 or 6. Figure 4.7(c) shows the contour of strength degradation factor f_2 (≤1.0) in Zone-II. Outside Zone-II f_2=1.0, meaning that no shear strength degradation occurs in Zone-III. Once the values of f_1 and f_2 are known, the mobilized s_u is calculated using Eq. (2). As shown in Fig. 4.7(d), s_u is different from s_{u0} especially near the riser. Figures 4.7(a-d) show that the proposed model of undrained shear strength is properly implemented in CFX.

4.9.3 Uplift resistance

Upon displacement reversal at w=0.5D, the resistance is reduced and then become negative (Fig. 4.6). The negative value represents the uplift resistance. In this case, the maximum normalized uplift resistance is 2.8, which is 53% of the maximum penetration resistance. In previous studies (e.g. Randolph and Quiggin 2009, Shiri and Randolph 2010, Li and Low 2011) used an empirical factor named as ‘suction ratio’, which is the ratio of the maximum uplift and penetration resistance. They performed analyses with

suction ratio of 0.1-0.6 and also with 1.0 (extreme cases) recognizing the fact that the suction ratio depends on various factors.

As shown in Fig.4. 7 that even at w=0.48D the soil is not in contact with the riser above the springline. Therefore, the main sources of uplift resistance in Fig. 4.6are the suction and interface resistance between soil and bottom half of the riser. Figure 4.6 also shows that the uplift resistance slowly decreases from point B to point C with vertical upward displacement. The uplift resistance decreases quickly after point C ($\hat{w} \approx 0.25$) and become zero at point D ($\hat{w} \approx 0.1$). The separation of the bottom of the riser from clay occurs very quickly during the upward displacement from C to D, and the riser completely separates from clay at point D leaving a trench of approximately 0.1D depth.

The performance of the proposed model and numerical simulations are verified using model test results. Based on extensive laboratory experiment results in various conditions, Bridge et al. (2004) proposed an empirical model to calculate soil suction during uplift. According to this model the ratio between the maximum suction and ultimate penetration resistance (f_{suc}) can be calculated as

$$f_{suc} = -k_C k_V k_T \qquad (7)$$

Where k_C, k_V and k_T are dimensionless empirical factors. Bridge et al. (2004) suggested k_C=1.0, and 0.56 for undisturbed and remoulded undrained shear strength condition. The constant k_V is related to v/D as $k_V = k_F(v/D)^{n_F}$, where k_F are n_F are two empirical constants.

Bridge et al. (2004) also provided a model for breakout displacement Δ_B (the vertical displacement of the riser from the maximum penetration to the point where the riser separates from the seabed).

$$\frac{\Delta_B}{D} = k_{DC}k_{DV}k_{DT} \quad (8)$$

Where k_{DC}, k_{DV} and k_{DT} are empirical constants for uplift resistance. For the first pullout, Bridge (2005) suggested k_{DC}=1.0 Moreover, $k_{DV} = k_D(v)^{n_D}$, where k_D are n_D are two empirical constants. As in the present study the riser is lifted immediately after the penetration, the consolidation time is zero. Therefore, k_T and k_{DT} are 0.9 and 0.8, respectively, as suggested by Bridge et al. (2004).

Analyzing extensive experimental results of the CARISIMA and STRIDE projects, Bridge et al. (2005) suggested the following values for two clays: (i) for Onsøy clay k_F=1.12, n_F=0.18, k_D=0.98, n_d=0.26 and (ii) for Watchet Harbour clay k_F=0.98, n_F=0.21, k_D=0.83, n_D=0.19.

Now using the above empirical values f_{suc} and Δ_B are calculated. Then multiplying the maximum normalized penetration resistance by f_{suc}, the normalized maximum suction is calculated.

Bridge et al. (2004) also defined the mobilization of suction using 3 linear lines. At the vertical upward displacement of $0.075\Delta_B$ the maximum suction is mobilized, which has been referred as "suction mobilization." Between $0.075\Delta_B$ and $0.7\Delta_B$ the suction remains constant at the maximum value. This zone has been referred as "suction plateau." Finally, form $0.7\Delta_B$ to Δ_B the suction force reduces from the maximum to zero, which has been referred as suction release zone.

The calculated suction profiles for the Onsøy and Watchet Harbour clays for the two limiting values of s_u (undisturbed and remoulded) are shown in Fig. 4.6. As partial degradation of s_u occurs (cf. Fig. 4.5), the suction profile obtained from the present CFX model lies in between these two limits. Calculated suction and its mobilization are comparable with experimental results because Bridge et al. (2004) developed their model from an extensive test results. This also implies that the simple degradation model (Fig. 4.5), together with the model parameters (Table 3.1), can simulate the trend of suction force as observed in model test results.

In order to show direct comparison, simulation are also performed with the shear strength profile of Onsøy clay (s_{u0} (kPa)=1.5+12.5y' (in m), Bridge 2005). The calculated normalized resistance is slightly higher than that of the base case, but again comparable with the empirical model developed from experimental results. Further discussions on the effects of soil profile are presented in the following sections.

Based on upper bound solution for rough pipe in constant s_u profile (Murff et al. 1989), Bridge (2005) recommended the maximum normalized penetration resistance of 5.92 at 0.5D penetration, which is shown by a circle in Fig. 4.6. Numerical investigation of penetration resistance of offshore pipelines has been presented in Chapter 3. Therefore, instead of repeating, the main focus of the following sections is given to the uplift resistance and suction.

4.9.4 Suction

The negative pressure contours in clay around the riser during upward displacement are shown in Fig. 4.8. The negative values of pressure represent the suction. Figure 4.8(a)

shows that a considerable suction is developed in clay under the riser and its extent is almost a diameter of the riser. The maximum suction is generated below the invert of the riser, and it gradually decreased with radial distance. The suction in soil elements in the berm or near the mudline is not very significant. When the pipe is displaced up at w=0.3D (Fig. 4.8b), the zone of suction becomes smaller. Figure 4.8(c) shows that there is a very small zone of suction near the pipe invert at w=0.2D. A considerable length of pipe surface under the springline separates from clay and formed a channel for water to flow through. Because of this separation, the uplift resistance decreases quickly in this phase of upward movement (c.f. Fig. 4.6). Figure 4.8(d) shows no suction under the pipe at w=0.1D. A larger channel is formed through which water flows almost to the invert of the riser. The uplift resistance is almost zero at this stage (Fig. 4.6). A trench of 0.1D maximum depth is formed. The riser left the seabed with this trench with further upward displacement.

The instantaneous velocity vectors of soil and water are also shown in Figs. 4.8a-d. Figure 4.8(a) shows that the soil elements move towards the invert of the pipe because of high suction. At this stage, the water particles above the top half of the pipe move mainly in the upward direction. At w=0.3D (Fig. 4.8b), the water particles near the springline move downward towards the bottom of the pipe. The velocity of water particle increases when the riser separates from clay and a channel is formed as shown in Fig. 4.8c. The flow of water under the riser increases further when the channel becomes wider as shown in Fig. 4.8d.

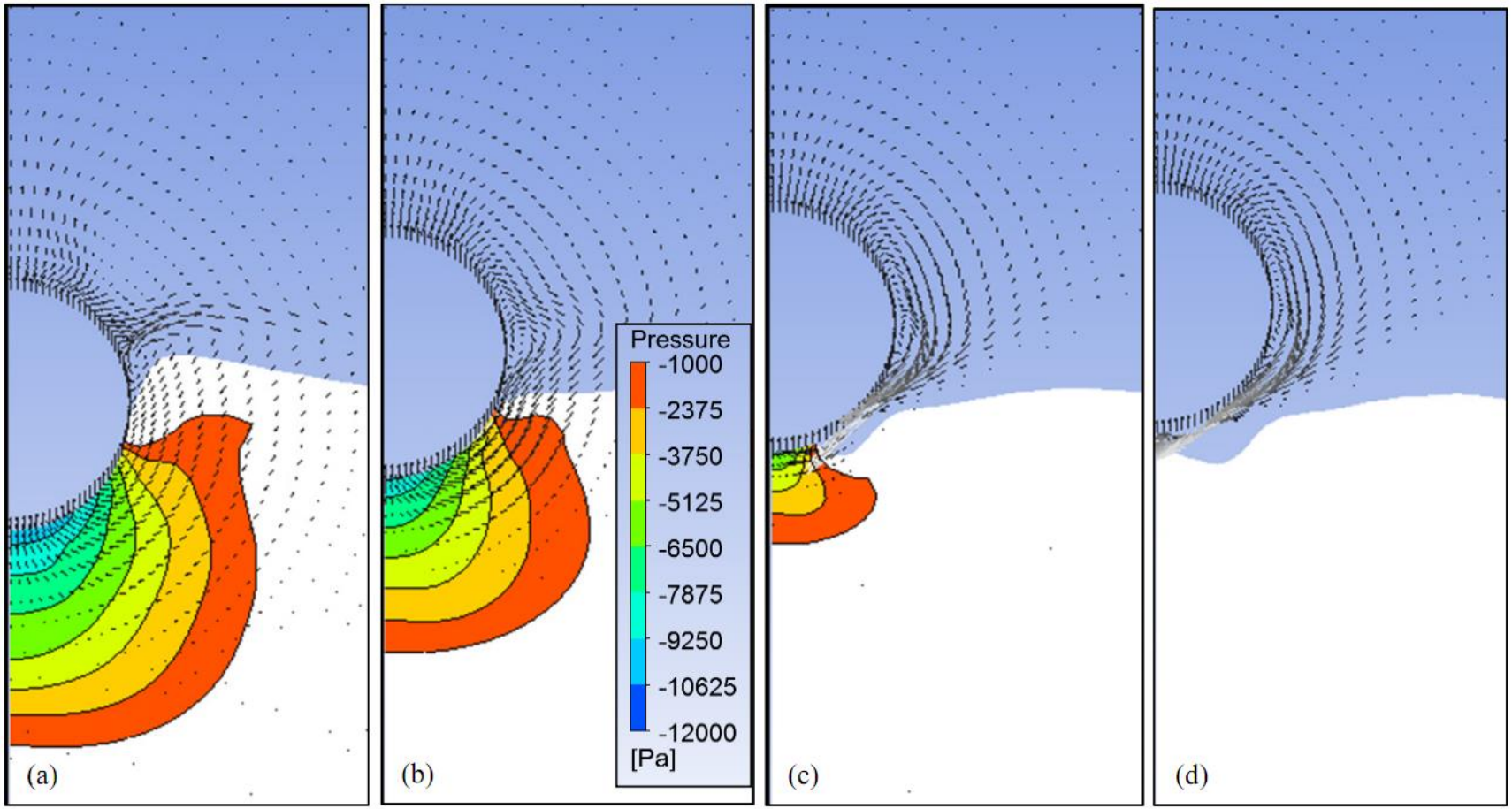

Figure 4.8: Suction and velocity vectors during uplift: (a) *w*=0.49*D*, (b) *w*=0.3*D*, (c) *w*=0.2*D*, (d) *w*=0.1*D* (-ve pressure means suction)

4.9.5 Computational time

The present CFX simulation is computationally very efficient as discussed in chapter 3. The simulation shown in Fig. 4.6 takes only18minutes with a 3.2 GHz Intel Core i5 processor and 8 GB RAM. The comparison of computational times only for penetration to 0.5*D* shows that the present CFX simulation is significantly faster than large deformation FE analyses using Abaqus CEL of similar problem (Dutta et al. 2014). As shown in Fig. 4.3, the finer mesh in the subdomain moves with the riser and therefore the present CFX model requires less number of elements as compared to CEL, because the mesh in CEL is fixed and finer mesh is required to be created over a large area where considerable soil deformation occurs.

In summary, in the numerical modeling of uplift, at least three key aspects should be considered: large deformation, suction, and riser-seabed-water interaction. The available FE techniques cannot simulate properly all of them together. For example, the advanced Abaqus CEL FE technique can simulate large deformation but cannot simulate the suction properly. However, the present CFX model can successfully simulate this behavior. Moreover, it is computationally very efficient.

4.10 Parametric study

Experimental evidences show that the uplift behavior depends on a number of factors such as undrained shear strength of soil, upward velocity and shear strength degradation (Giertsen et al. 2004; Bridge 2005; Hu 2010). A parametric study is conducted using the

above CFX model in which only one parameter is varied while the other parameters are kept constant as listed in Table 3.1, unless otherwise mentioned.

4.10.1 Mudline shear strength (s_{um}) in linear s_{u0} profile

Figure 4.9 shows the penetration and uplift resistance for four different values of s_{um} with k=4 kPa/m. At a given $\hat{w}$, the normalized penetration resistance increases with decrease in s_{um}. For s_{um}=0.2 kPa, a very small increase in normalized penetration resistance with depth is found for $\hat{w}$ greater than 0.15. The penetration resistance in this case increases almost linearly with depth from $\hat{w}$=0.15 and as it is normalized by $s_{u0(i)}$ that also increases linearly with depth, the normalized penetration resistance is almost constant with $\hat{w}$. From centrifuge tests with s_{um}=0, Hu (2010) showed that the penetration resistance increases almost linearly with depth. On the other hand, for s_{um}=2.3 kPa, the centrifuge test results in Dingle et al. (2008) show the normalized penetration resistance very similar to other four penetration curves in Fig. 4.9. In summary, the normalized penetration resistance depends on s_{um}, and it can be calculated using the present CFX model.

The effect of s_{um} on uplift resistance is different from that of on penetration resistance. For s_{um}≥1.0 kPa, the normalized uplift resistance gradually decreases with upward displacement, and from $\hat{w}$≈0.27 it decreases quickly and the complete breakout occurs at $\hat{w}$=0.08-0.15. However, the normalized uplift resistance is almost constant for s_{um}=0.2 kPa until $\hat{w}$=0.2. The uplift resistance decreases almost linearly with depth in this range, and as it is normalized by linearly increasing $s_{u0(i)}$, the normalized uplift resistance remains almost constant. The complete breakout in this case occurs above the mudline.

As the shear strength of clay near the mudline is very low, the soil can easily follow the riser due to the suction developed under it. Dragging of soil above the mudline was observed in model tests including Test-2 of CARISIMA model tests (Fig. 4.1) for high speeds. The present numerical analyses show that it could also occur in clay with very low mudline shear strength. However, it is not possible if the shear strength of clay is high near the mudline, and therefore breakout occurs before the invert of the riser reaches the mudline. That means, the higher the value of s_{um}, the higher the depth of trench.

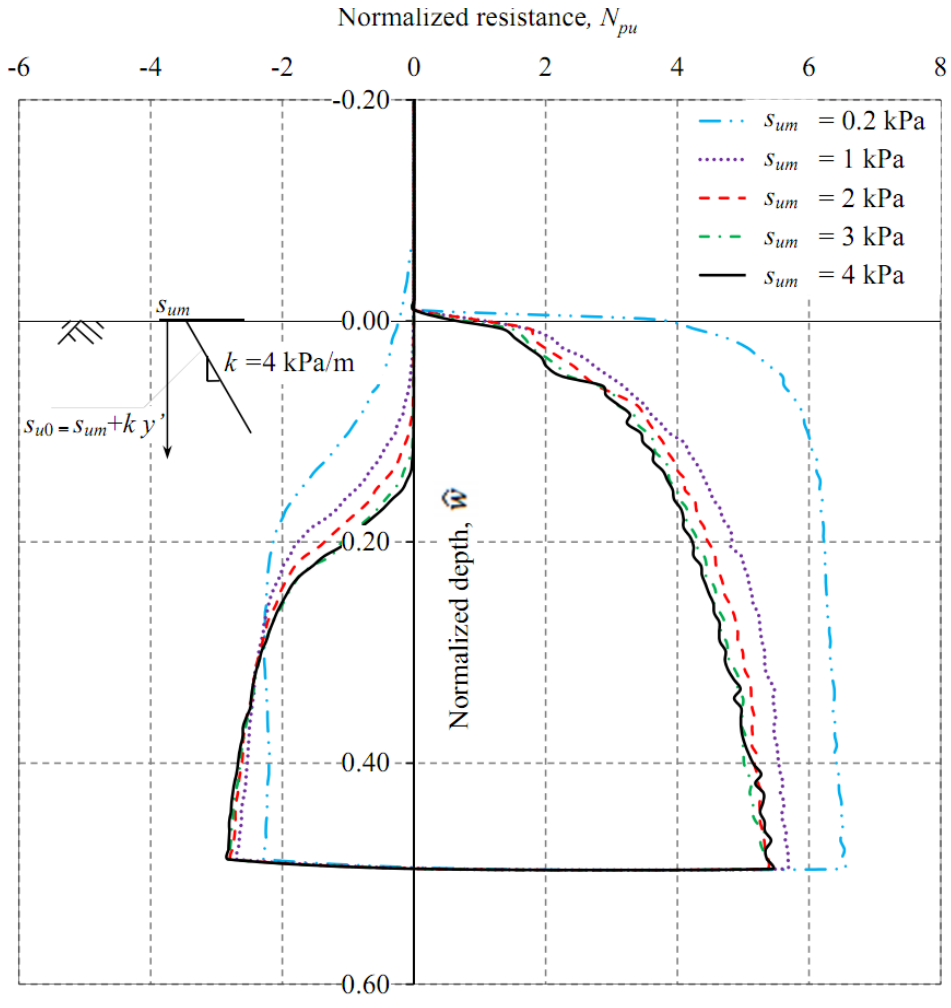

Figure 4.9: Effect of mudline shear strength

4.10.2 Shear strength gradient (k) in linear s_{u0} profile

Keeping the value of s_{um} constant (=2.3 kPa), the analyses are performed for four different values of k (=0 (uniform), 1.5, 3.0 and 4.5 kPa/m). Figure 4.10 shows that the normalized penetration resistance slightly increases with increase in k for this range of embedments.

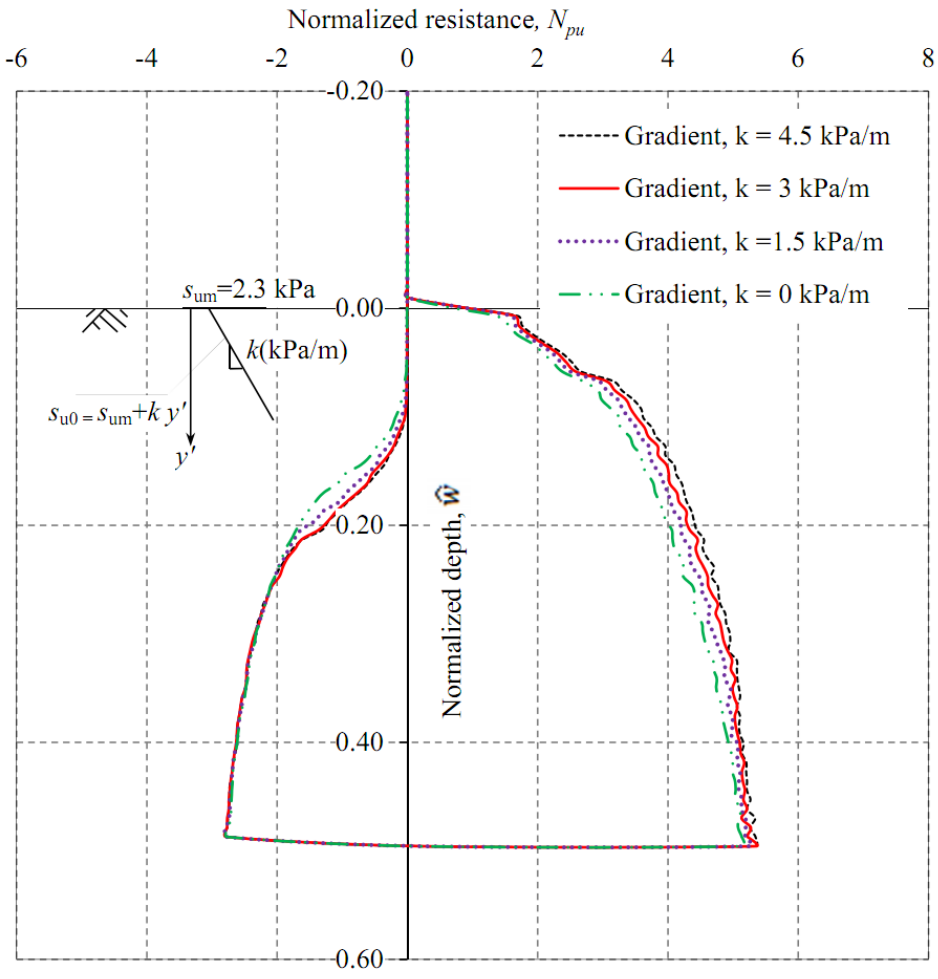

Figure 4.10: Effect of undrained shear strength gradient (*k*)

Negligible variation in the maximum normalized uplift resistance is calculated for the cases analyzed. Faster suction decay occurs in the suction release phase if k is increased. Therefore, the uplift resistance curve for higher k (e.g. 4.5 kPa/m) is under the curves with lower k (e.g. k=1.5 kPa/m). At a given embedment in the suction release phase, the shear strength of clay below the riser is higher for higher k value. The suction under the riser cannot pull this soil easily and therefore suction release occurs quickly for higher values of k. Overall, k values of this range does not have significant influence on N_{pu} for these embedments.

4.10.3 Uniform s_{u0} profile

In the above sections, the simulations for linearly increasing s_{u0} profile are presented. Figure 4.11 shows the simulations for five different uniform s_{u0} (i.e. k=0). The normalized penetration resistance increases with decrease in s_{u0}. Using Abaqus CEL, without any effect of $\dot{\gamma}$, Tho et al. (2012) also showed that the normalized penetration resistance increases with decrease in s_{u0}. Note that, the effects of $\dot{\gamma}$ on s_u during penetration are considered in the present study. An opposite trend, although not very significant, is found in the maximum uplift resistance, which decreases with decrease in s_{u0}. Moreover, with increase in s_{u0} faster suction release is occurred resulting in larger trench depths. The possible mechanisms involved in such variation of uplift resistance with s_{u0} are similar to that discussed in previous sections for linearly increasing s_{u0}.

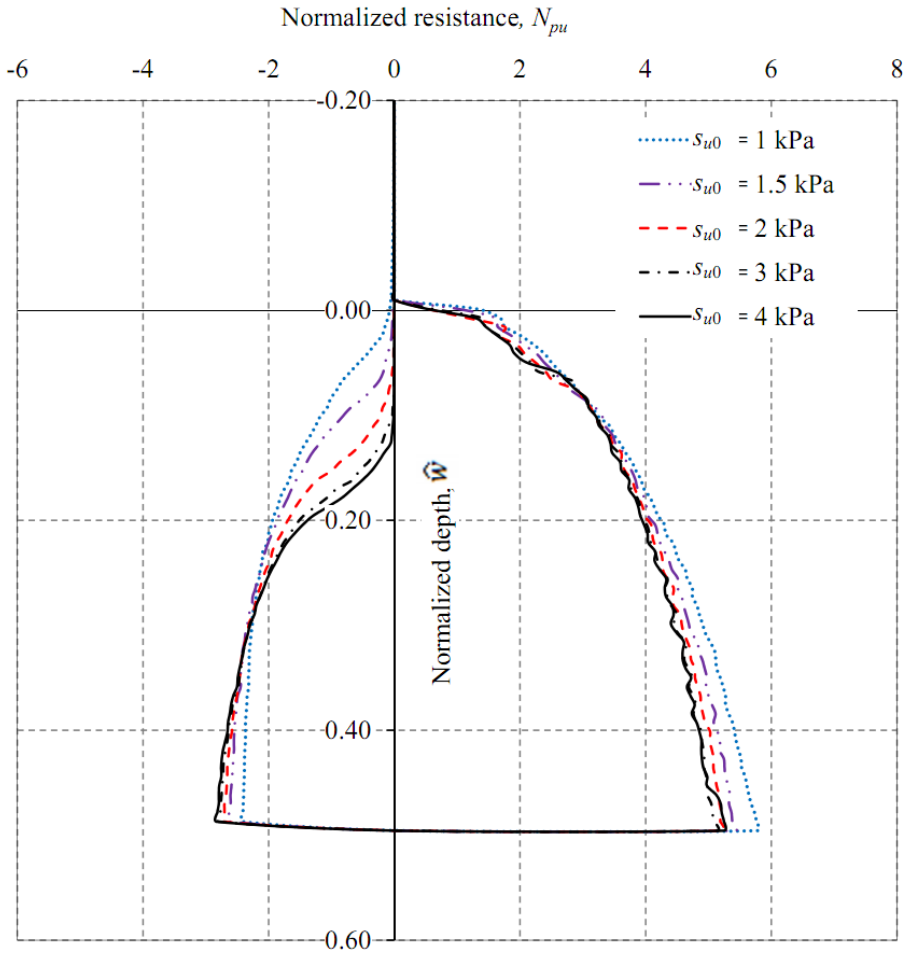

Figure 4.11: Effect of variation of uniform s_{u0}

4.10.4 Zone of strength degradation

In the analysis presented in previous sections, the extent of shear strength degradation zone is defined by $\Delta=D$ (Fig. 4.5). In order to examine the effects of Δ on uplift resistance, analyses are performed for 8 different values of Δ(Fig. 4.12). As soil strength degradation is not incorporated during penetration, the penetration resistance is same for all 8 cases. The maximum uplift resistance decreases with increase in Δ. Initially the depth of trench increases slightly with increase in Δ for $0.25D \geq \Delta \geq 1.0D$.

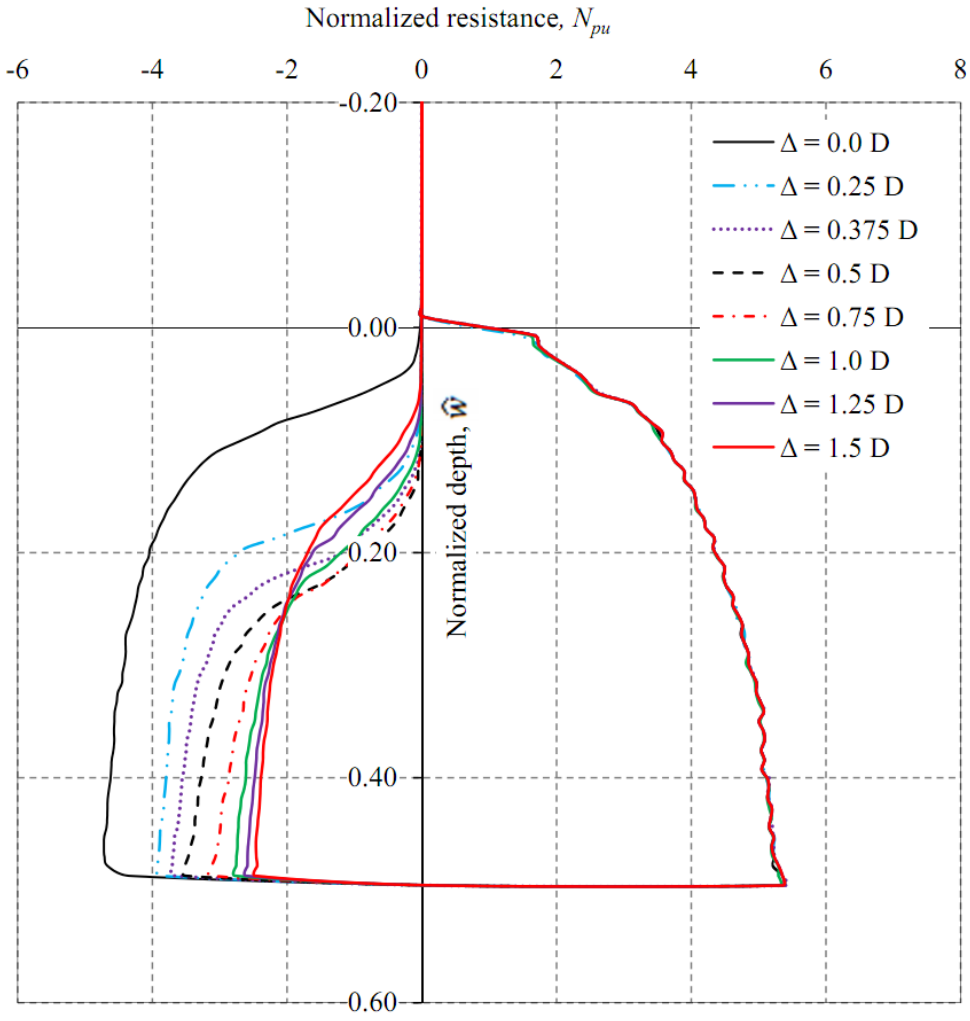

Figure 4.12: Effect of shear strength degradation zone

The increase in size of degradation zone reduces the shear strength over a larger area around the riser and therefore gives lower uplift resistance. For large values of Δ (=1.25*D* and 1.5*D*), the clay in a large area near the riser becomes soft which can move easily with the riser, and therefore the complete breakout occurs at shallow depths with large suction plateaus. For Δ=0, the ratio between the maximum uplift and penetration resistance is 0.89, and a very large suction plateau is obtained. In summary, the extent of shear strength degradation has a significant influence on suction and trench formation.

4.10.5 Pullout velocity

The pullout velocity is one of the key parameters that significantly influence the uplift resistance. A total of 54 analyses are performed for uniform and linearly increasing s_{u0}. For uniform s_{u0}, analyses are performed for three different s_{u0} (=1, 3 and 5 kPa) and five velocities (10, 20, 50, 100, 200 and 300 mm/s). For brevity, the maximum uplift resistance is presented in Figs. 4.13, which shows that the normalized maximum uplift resistance increases with v/D_e in a semi-log plot. One of the reasons is that the increase in v increases $\dot{\gamma}$ and shear strength (c.f. Fig. 4.4). Note that, the rate of increase in maximum uplift resistance with v depends on model parameters β, c_1 and n. The present simulation results are consistent with CARISIMA and STRIDE 2D model test results (Bridge 2005). Assume that the riser separates from clay when the normalized uplift resistance in the suction decay phase first reaches to a very small value (<0.2). The embedment at this stage gives the depth of trench. The maximum depth of trench of 0.15D is obtained when s_{u0} is high (5 kPa) and v is low (10 mm/s), although the variation in trench depth is not significant for $v \leq 50$ mm/s. For a low s_{u0} (1 kPa) and high velocities (200 or 300 mm/s), uplift resistance is calculated even above the mudline, which is consistent with Test 2 of Fig. 4.1.

Simulations are also performed for linearly increasing s_{u0}. Figure 4.14(a) shows the variation of the maximum normalized uplift resistance for three different values of s_{um}. Similar to Fig. 4.13, the maximum uplift resistance increases with v. The maximum depth of trench of 0.17D is obtained when s_{um}=5 kPa and v=10 mm/s. Unlike uniform s_{u0}, for s_{um}=1 kPa, the separation of the riser occurs below the mudline with trench depths

between 0.05D to 0.08D. This is because, s_{u0} increases with depth in this case and therefore clay does not move easily with the riser as compared to uniform s_{u0}=1 kPa. Therefore, it can be concluded that trench depth depends on not only the velocity but also shear strength profile.

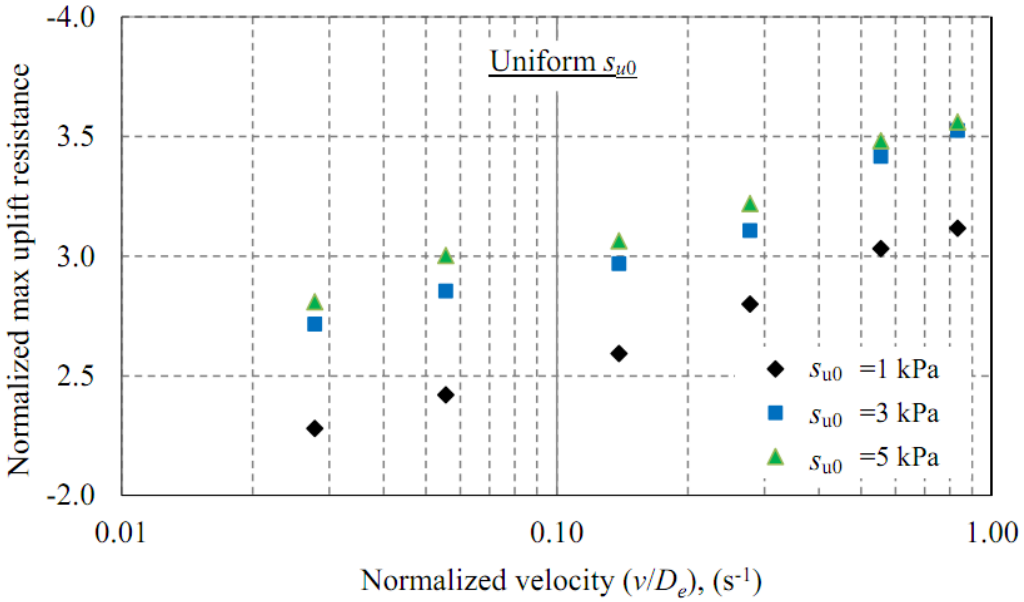

Figure 4.13: Effect of velocity for different uniform s_{u0} on maximum uplift resistance

Finally, the analyses are performed to investigate the effects of shear strength gradient k for a linearly increasing s_{u0} (=2.3+ky') profile. Figure 4.14(b) shows that the maximum uplift resistance increases with v. Small variation in trench depth, in the range of 0.08D to 0.12D, is obtained for these values of k and v.

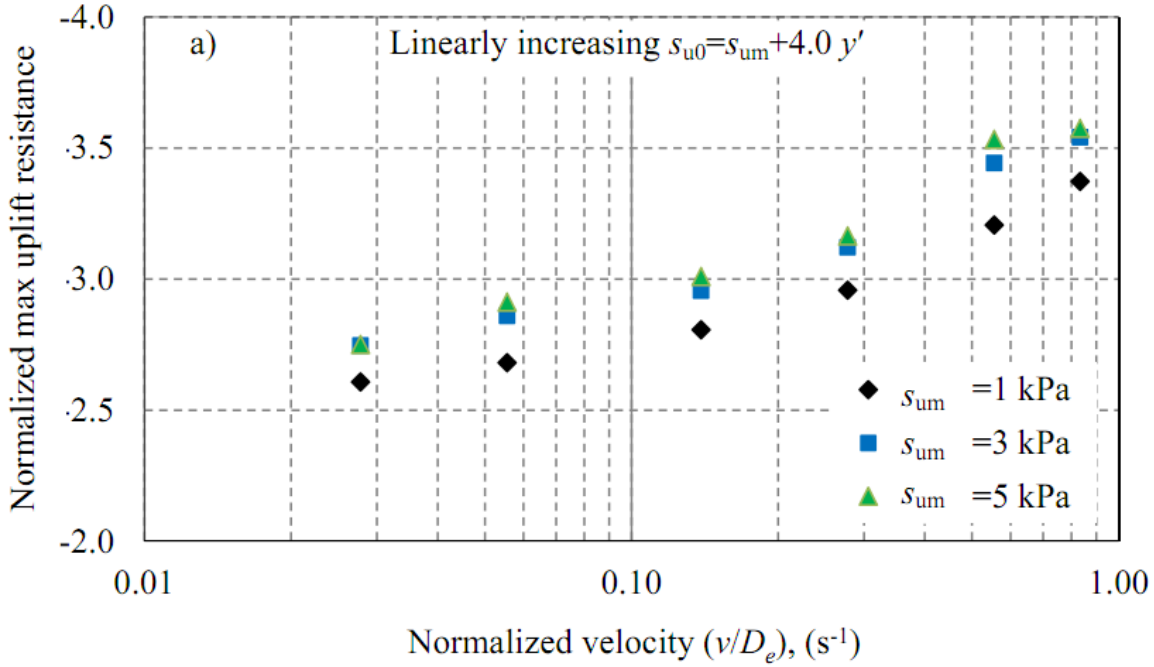

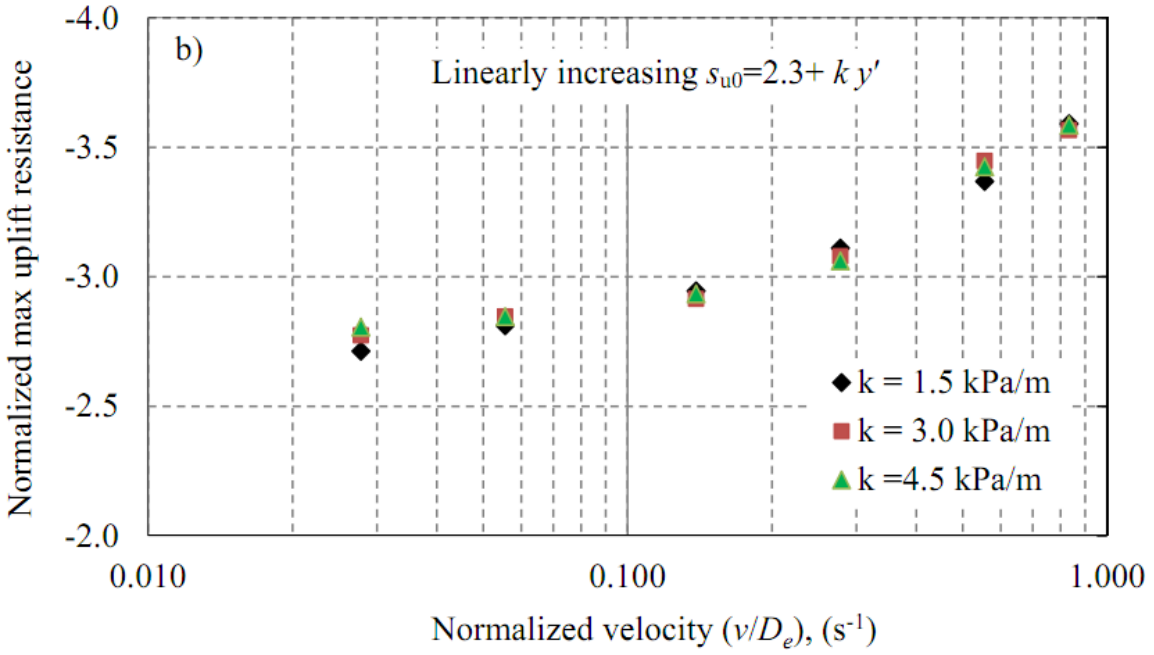

Figure 4.14: Effect of velocity for linearly increasing s_{u0} on maximum uplift resistance (a) s_{um} effect (b) k effect

4.11 Chapter summary

In this chapter both penetration and uplift behaviour are simulated using computational fluid dynamics (CFD) approach. The simulation results for penetration are presented in Chapter 3. In this chapter, CFD simulations of uplift resistance, suction and trench formation using ANSYS CFX are discussed. A new model for undrained shear strength of soft clay is proposed that is applicable to a wide range of shear strain rates. The effects of strain rate and strength degradation are incorporated properly in ANSYS CFX and simulations are performed for one penetration-uplift cycle. Comparing with empirical models developed from experimental results it is shown that the present CFX model can simulate the suction and uplift resistance. Moreover, the CFX model developed in this study using the subdomain approach is computationally very efficient. The suction under the riser is the main source of uplift resistance for shallow embedments. The parametric study shows that the maximum uplift resistance and depth of trench depend on uplift velocity and undrained shear strength of clay.

Chapter 5

Conclusions and Recommendations for Future Research

5.1 Introduction

Steel catenary risers (SCR) are widely used in deepwater oil and gas production. The riser-seabed-water interaction near the touchdown zone is one of the main concerns in the design of fatigue life of SCR. However, fatigue assessment of SCR is a major engineering challenge mainly because of lack of proper understanding of the force displacement response in the touchdown zone. In order to understand the mechanisms better, numerical modeling has been conducted in the present study for vertical penetration and uplift of a section of a riser.

During upward displacement of the riser, suction might be developed under the riser and a trench might be formed when it separates from the seabed near the touchdown point (TDP). In the subsequent downward movement, the riser penetrates through this trench to the seabed. Therefore, modeling of suction and trench formation is very important. In the existing models available in the literature for uplift resistance, these factors are incorporated using empirical relationships.

5.2 Conclusions on penetration of riser

The penetration of riser in soft clay seabed is fundamentally a large deformation problem. In addition to physical modeling, various numerical modeling techniques have been developed in the past to simulate this. Among them the RITSS and Abaqus CEL are the

two FE approaches used by a number of researchers. Both of these techniques are computationally very expensive and cannot simulate suction properly. In this study (Chapter 3), computational fluid dynamic approach is used to simulate the load-penetration response of a riser. The numerical simulations cover a wide range of embedments (up to 5*D*). The failure mechanisms in the 'transition zone' where they change from 'shallow' to 'deep' failure mechanisms are critically examined. The following conclusions can be drawn from the numerical simulations presented in Chapter 3 on penetration behaviour:

i) ANSYS CFX can successfully simulate the penetration resistance.

ii) The depth of transition zone and shape of the trench depend on magnitude and variation of undrained shear strength of clay with depth. A cavity is formed above the crown when the two faces of the trench touch each other. The negative pressure in the hydraulically isolated cavity increases the penetration resistance and it could enhance the initiation of deep failure mechanisms. These processes can be simulated by CFX modeling.

iii) The proposed CFX Model-III with a subdomain is computationally very efficient.

iv) The present CFX model can successfully simulate the influence of water on penetration behavior which could not be done properly using the large deformation FE modeling.

5.3 Conclusions on uplift resistance

Similar to penetration behaviour, the uplift resistance in the touchdown zone significantly influences the fatigue life of steel catenary risers (Thethi and Moros 2001). For shallow embedments, the uplift resistance primarily depends on suction under the riser. The modeling of trench formation due to uplift, especially near the touchdown point, is equally important in the simulation of response under cyclic loading. In the present study (Chapter 4), a new numerical modeling approach is developed in ANSYS CFX software to simulate suction, trench formation and uplift resistance. A new unified model for the effects of strain rate on undrained shear strength is proposed, which is valid for a wide range of strain rate. Combining strain rate effects with a simplified model for strength degradation the undrained shear strength is calculated. The soil model is implemented properly in ANSYS CFX software. The analyses are performed for uniform and linearly increasing shear strength profiles for one cycle of loading-unloading. The following conclusions can be drawn from the numerical simulations presented in Chapter 4.

a) The undrained shear strength increases with the increase in strain rate. While the power law model can be used for low strain rates, the proposed model is a better option for a wide range of strain rates.
b) The present CFX model with a subdomain is computationally very efficient as compared to large deformation FE analysis.
c) The present CFX model can simulate the suction under the riser during uplift. The suction is high at the start of upward displacement, gradually decreases to zero when the riser separates from the seabed.

d) The breakout distance and depth of trench depend on soil shear strength and uplift velocity. The depth of trench decreases with increase in uplift velocity and/or decrease in undrained shear strength of clay near the mudline.

e) The parametric study shows that the soil strength degradation has a significant influence on uplift resistance. The suction effects might exacerbate the strength degradation process in multiple cyclic loading although only one cycle is simulated in the present study.

5.4 Recommendations for future research

Although an excellent performance of CFX modeling is shown, there are some limitations in this study which could be addressed in future research.

a) Strain softening and strain rate effects on undrained shear strength are not considered in modeling of penetration behaviour.

b) A simplified model is used for soil strength degradation to show the effects without introducing a complex model. A better strength degradation model might improve the simulation results.

c) Although a parametric study is performed, some other factors, such as trench shape, consolidation time and depth of penetration might have effects on uplift resistance.

d) Only one loading cycle is simulated in this study. However, simulation is required for many loading cycles as encountered in the field.

e) Only vertical displacement is applied; however, in the field lateral displacement might be also significant.

f) Simulation is performed only for plane strain condition using a rigid riser section. Coupled three-dimensional simulation with realistic material properties of the riser will provide a complete picture, although it will be computationally intensive.

References

Abelev, A., and Valent, P. (2013). "Strain-rate dependence of strengh of the Gulf of Mexico soft sediments." *IEEE Journal of Oceanic Engineering*, 38(1), 25–31.

AGA, P. (1992). "Weight coating design for submarine pipeline on-bottom stability." *Final Report Comparing TAMU Test to SINTEF Model*, American Gas Association .

ANSYS CFX. (2013). "CFX Solver Modeling Guide." CFX-Program (version13.0) Physical Modelling Documentation, ANSYS Inc.

Aubeny, C. P., and Biscontin, G. (2009). "Seafloor-riser interaction model." *International Journal of Geomechanics*, 9(3), 133–141.

Aubeny, C. P., Shi, H., and Murff, J. D. (2005). "Collapse loads for a cylinder embedded in trench in cohesive soil." *International Journal of Geomechanics*, 5(4), 320–325.

Aubeny, C., and Biscontin, G. (2008). "Interaction model for steel compliant riser on soft seabed."*Offshore Technology Conference*, OTC19493, 8p.

Aubeny, C.P, Gaudin, C., and Randolph, M. (2008). "Cyclic tests of model pipe in kaolin." *Society of Petroleum Engineers*, 3(04), 1–6.

Bai, Y., and Bai, Q. (2005). " Subsea Pipelines and Riser." Elsevier, 812p.

Barbosa-Cruz, E. R., and Randolph, M. F. (2005). "Bearing capacity and large penetration of a cylindrical object at shallow embedment." *Proc. of the 1st International Symposium on Frontiers in Offshore Geotechnics (ISFOG) 2005*, 615–621.

Biscontin, G., and Pestana, J. M. (2001). "Influence of peripheral velocity on vane shear strength of an artificial clay." *Geotech. Test. J.*, 24(4), 423–429.

Bostrom, B., Svano, G., Eiksund, G., Leira, B.J. and Bjorset, A. (1998) "Response Effects of Riser-soil Interaction Modelling." *Proc. 17th Int Conf on Offshore Mechanics and Artic Engineering*, OMAE98.

Boukpeti, N., White, D. J. and Randolph, M. F. (2012b). "Analytical modelling of the steady flow of a submarine slide andconsequent loading on a pipeline." *Géotechnique*, 62(2), 137–146.

Boukpeti, N., White, D. J., Randolph, M. F., and Low, H. E. (2012a). "Strength of fine-grained soils at the solid-fluid transition." *Géotechnique*, 62(3), 213–226.

Bransby, M. F., Zajac, P., Amman, S. (2008). "Finite element analysis of the vertical penetration of on-bottom' pipelines in clay." *Proc. of the 18th International Offshore and Polar Engineering Conference, ISOPE 2008,* July 6, 2008 – July 11, 245–249.

Bridge, C. (2005). "Effects of Seabed Interaction on Steel Catenary Risers." PhD. Thesis, University of Surrey, UK.

Bridge, C., and Wills, N. (2002). “Steel Catenary Risers – Results and Conclusions from Large Scale Simulations of Seabed Interaction.” *Proceedings of International Conference on Deep Offshore Technology*, PennWell, DOT02. 15p.

Bridge, C., Howells, H., Toy, N., Parke, G., and Woods, R. (2003). “Full scale model test of steel catenary riser.” *International Conference on Fluid Structure Interaction*, Cadiz, Spain .

Bridge,C., Laver,K., and Clukey,E. (2004). “Steel catenary riser touchdown point interaction models.” *Proc. Offshore Technology Conference*, OTC 16628.

Cardoso, O. C., and Silveira, M. S. R. (2010). “Pipe-soil interaction behaviour for pipelines under large displacements on clay soils – A model for lateral residual friction factor.” *Proc. Offshore Technology Conference*, OTC 20767.

Cathie, D. N., Jaeck, C., Ballard, J. C., Wintgens, J. F. (2005). “Pipeline geotechnics-state-of-the-art.”*Frontiers in Offshore Geotechnics: ISFOG* 2005, London.

Chatterjee, S., Randolph, M. F., White, D. J. (2012a). “The effects of penetration rate and strain softening on the *vertical* penetration resistance of seabed pipelines.” *Géotechnique*, 62(7), 573–582.

Chatterjee, S., White, D. J., Randolph, M. F. (2012b). “Numerical simulation of pipe-soil interaction during lateral movements on *clay*.” *Géotechnique*, 62(8), 693–705.

Cheuk, C. Y., Take, W. A., Bolton, M. D. and Oliveira, J.R.M.S. (2007). "Soil restraint on buckling oil and gas pipelines buried in lumpy clay fill." *Engineering Structures*, 29, 973–982

Clukey, E. C., Tognarelli, M. A., Li, G., Ghosh, R., Phillips, R., Zakeri, A., Elliot, B. J., and Bhattacharyya, A. (2011). "Simulation of SCR behaviour at touch down zone- part-ii: testing of a sectional scr model in a geotechnical centrifuge." *Offshore Technology Conference*, OTC 22569.

Davis, E. H. and Booker, J. R. (1973). "The effect of increasing strength with depth on the bearing capacity of clays."*Geotechnique*, 23(4), 551–563.

De Blasio, F. V., Elverhi, A., Issler, D., Harbitz, C. B., Bryn, P., and Lien, R. (2005)."On the dynamics of subaqueous clay rich gravity mass flows – the giant Storegga Slide, Norway." Mar. Pet. Geol., 22(1–2), 179–186.

De Blasio, F. V., Elverhi, A., Issler, D., Harbitz, C. B., Bryn, P., and Lien, R. (2004a). "Flow models of natural debris flows originating from overconsolidated clay materials." *Mar. Geol.*, 213(1–4), 439–455.

De Blasio, F. V., Engvik, L., Harbitz, C. B., and Elverhoi, A. (2004b). "Hydroplaning and submarine debris flows." *Journal of Geophysical Research*, 109(C1), 1978–2012.

Dickin, E. A. (1994). "Uplift resistance of buried pipelines in sand." *Soils and Foundations*, 34(2), 41-48.

Dingle, H. R. C., White, D. J., and Gaudin, C. (2008). "Mechanisms of pipe embedment and lateral breakout on soft clay." *Canadian Geotechnical Journal*, 45(5), 636–652.

DNV (2010). Riser Fatigue, DNV-RP-F204, 36p

Dunlap, W. A., Bhojanala, R. P., and Morris, D. V. (1990). "Burial of vertically loaded offshore pipelines in weak sediments." *Proc. Offshore Technology Conference*, OTC 6375.

Dutta, S. (2012c). "Large deformation finite element analysis of partially embedded offshore pipelines for vertical and lateral motion at seabed."MEng.Thesis, Memorial University of Newfoundland, Canada.

Dutta, S., Hawlader, B., and Phillips, R. (2012a). "Finite element modeling of vertical penetration of offshore pipelines using coupled eulerian lagrangian approach." *Proc. 22nd International Offshore and Polar Engineering Conference*, Rhodes, Greece, 343–348.

Dutta, S., Hawlader, B., and Phillips, R. (2012b). "Strain softening and rate effects on soil shear strength in modeling of vertical penetration of offshore pipelines." *Proc. 9th International Pipeline Conference*, September 24–28, Calgary, Alberta, Canada, 1–8.

Dutta, S., Hawlader, B., and Phillips, R. (2013). "Numerical investigation of dynamic embedment of offshore pipelines."*Proc. 18th International Conference on Soil Mechanics and Geotechnical Engineering*, Paris, France, 1–4.

Dutta, S., Hawlader, B., and Phillips, R. (2014). “Finite element modelling of partially embedded pipelines in clay seabed using Coupled Eulerian Lagrangian method” *Canadian Geotechnical Journal*. 51. 10.1139/cgj-2014-00451.

Einav, I., and Randolph, M. F. (2005). “Combining upper bound and strain path methods for evaluating penetration resistance.” *Int. J. Numer. Methods. Eng.*, 63(14), 1991–2016.

Elliott, B. J., Zakeri, A., Barrett, J., Hawlader, B., Li, G., and Clukey, E. C. (2013b). “Centrifuge modeling of steel catenary risers at touchdown zone Part II: Assessment of centrifuge test results using kaolin clay.”*Ocean Engineering*, 60(1), 208–218.

Elliott, B. J., Zakeri, A., Macneill, A., Phillips, R., Clukey, E. C., and Li, G. (2013a). “Centrifuge modeling of steel catenary risers at touchdown zone Part I: Development of novel centrifuge experimental apparatus.”*Ocean Engineering*, 60(1), 200–207.

Elliott, B., Phillips, R., Macneill, A., and Piercey, G. (2014). “Physical modelling of SCR in the touchdown zone under three axis motions.” *Proc. 8th International Conference on Physical Modelling in Geotechnics*, January 14 – 17, 265–270.

Foda, M. A. (1983). “Breakout theory for offshore structure seated on sea-bed.” *e-book, Offshore Engineering Practice*, 288–299.

Fugro, L. (1999). “STRIDE JIP – touchdown point behaviour of steel catenary risers, Phase II – Riser/soil response curve development study.” *Report no*. 93819–1.

Gauer, P., Elverhoi, A., Issler, D., and DeBlasio, F. V. (2006). "On numerical simulations of sub aqueous slides: back calculations of laboratory experiments of clay-rich slides." *Norwegian Journal of Geology*, 86(3), 295–300.

Gauer, P., Kvalstad, T. J., Forsberg, C. F., Bryn, P., and Berg, K. (2005). "The last phase of the Storegga slide: Simulation of retrogressive slide dynamics and comparison with slide-scar morphology." *Marine and Petroleum Geology*, 22(1–2), 171–178.

Giertsen, E., Verley, R., Schrder, K. (2004). "CARISIMA a catenary riser/soil interaction model for global riser analysis." *Proc. 23rd International Conference on Offshore Mechanics and Arctic Engineering*, June 20– 25, 633–640.

Gui, M. W., and Bolton, M. D. (1998). "Geometry and scale effects in CPT and pile design." *Geotechnical Site Characterization*, 1063–1068.

Har. C. G. (2007). "Modeling and analysis of riser-seabed interaction" M Eng. Thesis, National University of Singapore. 129p.

Harbitz, C. B., Parker, G., Elverhøi, A., Marr, J. G., Mohrig, D., and Harff, P. A. (2003). "Hydroplaning of subaqueous debris flows and glide blocks: analytical solutions and discussion."*Journal of Geophysical Research*, 108(B7), EPM - 1-EPM - 17.

Hodder, M. S., and Byrne, B. W. (2010). "3D experiments investigating the interaction of a model scr with the seabed."*Appl. Ocean Res.*, 32(2), 146–157.

Hodder, M. S., White, D. J. and Cassidy, M. J. (2010). "Analysis of soil strength degradation during episodes ofcyclic loading, illustrated by the T-Bar penetration test." *InternationalJournal of Geomechanics,* 10(3), 117–123.

Hu, H. J. E. (2010). "Pipeline/riser soil interaction analysis." PhD Thesis, National University of Singapore, Singapore, 282p .

Hu, H. J. E., Leung, C. F., Chow, Y. K., and Palmer, A. C. (2011). "Centrifuge modelling of SCR vertical motion at touchdown zone." *Ocean Engineering*, 38(7), 888–899.

Hu, Y., and Randolph, M. F. (1998)."Deep penetration of shallow foundations on non-homogenous soil."*Soils and Foundations,* 38(1), 241–246.

Jeanjean, P. (2002). "Innovative design method for deepwater surface casing."SPE 77357, 13p.

Jostad, H. P. and Anderson, L. (2004). "Modeling of shear band propagation in clays using interface elements with finite thickness."*Proc. Of the 9th International Symposium on Numerical Models in Geomechanics*-NUMOG IX, Ottawa, Canada, 121–128

Langford, T. E., and Aubeny, C. P. (2008b). "Large scale soil-riser model testing on high plasticity clay." *Proc. 18th International Offshore and Polar Engineering Conference*, July 6 –11, 80–86.

Langford, T., and Aubeny, C. (2008). "Model tests for steel catenary riser in marine clay." *Offshore Technology Conference*, OTC 19495.

Li, F. Z., and Low, Y. M. (2011). “Fatigue reliability analysis of a steel catenary riser at the touchdown point incorporating soil model uncertainties.” *Applied Ocean Research*, 38, 100–110.

Lunne, T. & Andersen, K. H., Low, H. E, Randolph, M. F. and Sjursen, M. (2011). “Guidelines for offshore in situ testing andinterpretation in deepwater soft clays.” *Canadian Geotechnical Journal*, 48, 543–556.

Lunne, T. and Andersen, K. H. (2007). “Soft clay shear strengthparameters for deepwater geotechnical design, Keynote Address.” *Proc. 6th Internatonal Offshore Site Investigation and Geotechnics Confernce: Confronting New Challenges and Sharing Knowledge*, London, 151–176.

Major, J. J., and Pierson, T. C. (1992). “Debris flow rheology: Experimental analysis of fine-grained slurries.”*Water Resources Research,* 28(3), 841–857.

Marintek (2000a) “CARISMA, Soil Parameters”, *Report No.700039.00.02*, Trondheim, Norway.

Marintek (2000b) “CARISMA, Interpetation of Suction Test Results”, *Report No.700039.00.03,* Trondheim, Norway.

Martin, C. M., and Randolph, M. F. (2006). “Upper-Bound analysis of lateral pile capacity in cohesive soil.” *Géotechnique*, 56(2), 141–145.

Martin, C., and White, D. (2012). “Limit analysis of the undrained bearing capacity of offshore pipelines.” *Géotechnique*, 62(9), 847–863.

Merifield, R. S., Lyamin, A. V., Sloan, S. W., and Yu, H. S. (2003). “Three-dimensional lower bound solutions for stability of plate anchors in clay.” *J. Geotech. Geoenviron. Eng.*, 129(3), 243–253.

Merifield, R. S., Sloan, S. W., and Yu, H. S. (2001). “Stability of plate anchors in undrained clay.”*Géotechnique*, 51(2), 141–153.

Merifield, R. S., White, D. J., and Randolph, M. F. (2009). “Effect of surface heave on response of partially embedded pipelines on clay.” *J. Geotech. Geoenviron. Eng.*, 135(6), 819–829.

MMS (2008). “Deepwater Gulf of Mexico 2008: Ameica’s offshore energy future.” *OCS Report* MMS 2008–013.

Morrow, D. R., and Bransby, M. F. (2010). “Pipe-soil interaction on clay with a variable shear strength profile.” *Proc. 2nd International Symposium on Frontiers in Offshore Geotechnics*, Nov. 8–10, 821–826.

Murff, J. D., Wagner, D. A., and Randolph, M. F. (1989). “Pipe penetration in cohesive soil.” *Géotechnique*, 39(2), 213–229.

Nakhaee, A., and Zhang, J. (2010). “Trenching effects on dynamic behavior of a steel catenary riser.” *Ocean Eng.*, 37(2–3), 277–288.

O'Brien, J. S., and Julien, P. Y. (1988). "Laboratory analysis of mudflow properties." *J. Hydraul. Eng.*, 114(8), 877–887.

Pike, K., Duan, G., Sun, J., Jukes, P. (2010). "Comprehensive FEA of thermal mitigation buoyancy module (TMBM)-soil interaction using the Coupled Eulerian Lagrangian (CEL) method." *Proc. 29th InternationalConference on Ocean, Offshore and Arctic Engineering*, June 6–11, Shanghai, China.

Puech, A., Orozco-Calderon, M., and Foray, P. (2010). "Mini T-bar testing at shallow penetration."*Proc., 2nd International Symposium on Frontiers in Offshore Geotechnics*, ISFOG 2010, Nov. 8–10, Taylor & Francis - Balkema, 305–310.

Randolph, M. F., and Houlsby, G. T. (1984). "Limiting pressure on a circular pile loaded laterally in cohesive soil." *Géotechnique*, 34(4), 613–623.

Randolph, M., and Quiggin, P. (2009). "Non-linear hysteretic seabed model for catenary pipeline contact." *Proc. 28th International Conference on Ocean, Offshore and Arctic Engineering*, May 31– June 5,145–154.

Sheahan, T. C., Ladd, C. C., Germaine, J. T. (1996). "Rate-dependent undrained shear behavior of saturated clay."*J. Geotech. Geoenviron. Eng*., 122(2), 99–108.

Shi, H., Sun, J., Hossain, K., Eltaher, A., Jukes, P. (2011). "Offshore pipeline embedment in cohesive soil – a comparison between existing and CEL solutions." *Proc. of the ASME*

2011 30th International Conference on Ocean, Offshore and Arctic Engineering, OMAE2011, June 19–24, Rotterdam, The Netherlands, 1–6.

Shiri,H. and Randolph, M. (2010). "The infuence of seabed response on fatigue performance of steel catenary risers in touchdown zone." *Proc. 29th International Conference on Ocean, Offshore and Arctic Engineering*, June 6–11, Shanghai, China, 1–10.

SINTEF, O. (1986a). Pipe-soil interaction test,soft clay, *STF60 F86023* .

SINTEF, O. (1986b). Pipe-soil interaction test, stiff clay.

SINTEF, O. (1987). Pipe-soil interaction test on sand and soft clay .

Sloan, S. W. (1988). "Lower bound limit analysis using finite elements and linearprogramming." *International Journal of Numerical and Analytical Methods in Geomechanics*, 12, 61-67.

Sloan, S. W., and Kleeman, P. W. (1995). "Upper bound limit analysis using discontinuous velocity fields." *Computer Methods in Applied Mechanics and Engineering*, 127, 293-314.

Small, S. W., Tamburello, R. D., and Piaseckyj, P. J. (1972). "Submarine pipeline support by marine sediments." *Journal of Petroleum Technology*, 24, 317–322.

Smith, I. M., and Griffiths, D. V. (2004). “Programming the finite Element Method.” *4th Ed., John Wiley & Sons*, West Sussex, England.

Sousa, J. R.M., Porto, E.C., Foppa, D., Aguiar, C. S., Ellwanger, G. B. and Medeiros, C.J. Jr. (2011). “Undrained load capacity of torpedo anchors embedded in cohesive soils.” *Journal of Offshore Mechanics and Arctic Engineering*, v133(2), 12p

Supachawarote, C., Randolph, M. and Gourvenec, S. (2004). "Inclined pull-out capacityof suction caissons."*Proc*.9, Copyright © 2015 by ASME, 14th *International Offshore and Polar Engineering Conference*, Toulon, France, 500-506.

Terzaghi, K. (1943). “ Theoretical soil mechanics.” *John Wiley & Sons, Inc*.

Thethi, R. and Moros, T. (2001). “Soil interaction effects on simple catenary riser response.” *Proc., Deepwater Pipeline and Riser Technology Conference*, March 2001, Houston, Texas, USA.

Tho, K. K., Leung, C. F., Chow, Y. K., and Palmer, A. C. (2012). “Deep cavity flow mechanism of pipe penetration in clay.” *Canadian Geotechnical Journal*, 49(1), 59–69.

Tho, K. K., Leung, C. F., Chow, Y. K., and Swaddiwudhipong, S. (2013). “Eulerain finite element simulation of spudcan-pile interaction.”*Canadian Geotechnical Journal*, 50(6), 595–608.

Thorne, C. P., Wang, C. X., Carter, J. P. (2004). “Uplift capacity of rapidly loaded strip anchors in uniform strength clay.” *Géotechnique*, 54(8), 507–517.

Ting, I. H. Y., Kimiaei, M. and Randolph, M. F. (2011). "Advanced nonlinear hysteretic seabed model for dynamic fatigue analysis of steel catenary risers."*Proc.2nd International Symposium on Frontiers in Offshore Geotechnics*, Nov. 8–10, Taylor & Francis - Balkema, 833–838.

Verley, R and Lund, K.M. (1995)."A Soil Resistance model for Pipelines Placed on Clay Soils."*OMAE*, Vol. 5, Pipeline Technology, ASME.

Wang, D., White, D. J., and Randolph, M. F. (2010). "Large-deformation finite element analysis of pipe penetration and large-amplitude lateral displacement." *Canadian Geotechnical Journal*, 47(8), 842–856.

Wang, L, Zhang, J., Yuan, F. and Li, K. (2014). "Interaction between catenary riser and soft seabed: Large-scale indoor tests." *Applied Ocean Research*, 45, 10–21.

White, D. J., and Dingle, H. R. C. (2011). "The mechanism of steady friction between seabed pipelines and clay soils." *Géotechnique*, 61(12), 1035–1041.

White, D. J., Gaudin, C., Boylan, N., and Zhou, H. (2010). "Interpretation of T-Bar penetrometer tests at shallow embedment and in very soft soils." *Canadian Geotechnical Journal*, 47(2), 218–229.

Wills, N., and West, P. T. J. (2001). "Interaction between deepwater catenary risers and a soft seabed: large scale sea trials." *Offshore Technology Conference*, OTC-13113-MS.

Woodworth-Lynas, C., Nixon, D., Phillips, R., Palmer, A. (1996).“Subgouge deformations and the security of Arctic marine pipelines.”*Proc. Offshore Technology Conference*, May 6–9, Texas, Houston, USA.

Zakeri, A. (2009). “Submarine debris flow impact on suspended (free-span) pipelines: Normal and longitudinal drag forces.”*Ocean Eng.*, 36(6–7), 489–499.

Zakeri, A., and Hawlader, B. (2013). “Drag forces caused by submarine glide block or out-runner block impact on suspended (free-span) pipelines - Numerical analysis.”*Ocean Eng.*, 67, 89–99.

Zakeri, A., Høeg, K., and Nadim, F. (2009a). “Submarine debris Flow Impact on Pipelines - Part II: Numerical Analysis.” *Coastal Engineering*, 56(1), 1–10.

Zhao, B., Gao, F., Kang, R. (2010). “Numerical investigation on bearing capacity of a pipeline on clayey soils.” *Proc. of the* ASME *2010 29th International Conference on Ocean, Offshore and Arctic Engineering*, OMAE2010, June 6–11, 2010, Shanghai, China.

Zhao, B., Gao, F., Liu, J., Wu, Y. (2009). “Vertical bearing capacity of a partially-embedded pipeline on tresca soils.” *Pro. 9th International Offshore and Polar Engineering Conference* Osaka, Japan, June 21–26.

Zhou, H., and Randolph, M. F. (2007). "Computational techniques and shear band development for cylindrical and spherical penetrometers in strain-softening clay." *International Journal of Geomechanics*, 7(4), 287–295.

Zhu, H. and Randolph, M.F. (2010). "Large deformation finite-element analysis of submarine landslide interaction with embeded pipelines." *Int. J. Geomech.*, 10(4), 145–152.

Zhu, H. and Randolph, M.F. (2011). "Numerical analysis of a cylinder moving through rate depedent undrained soil." *Ocean Eng*. 38, 943–953.